UNIVERSITY OF CALIFORNIA,
IRVINE

Toxoplasma gondii interactions with vascular endothelium under fluidic shear stress

DISSERTATION

submitted in partial satisfaction of the requirements
for the degree of

DOCTOR OF PHILOSOPHY

in Biological Sciences

by

Katherine Snyder Harker

Dissertation Committee:
Assistant Professor Melissa B. Lodoen, Chair
Professor Michael J. Buchmeier
Professor Christopher Hughes
Associate Professor Naomi Morrissette
Professor Andrea J. Tenner

2014

TABLE OF CONTENTS

LIST OF FIGURES

ACKNOWLEDGMENTS

I would like to thank my thesis advisor and mentor, Dr. Melissa Lodoen, for her unwavering support and guidance throughout my graduate studies. Working with her has been a privilege and I will leave not only a better researcher, writer, and scientific thinker, but also a better person. Her influence has been substantial and this dissertation work could not have been completed without her assistance along the way. I am proud to become an alumnus of the Lodoen Lab.

I would also like to thank my committee members, Drs. Michael Buchmeier, Christopher Hughes, Andrea Tenner and Naomi Morrissette. I greatly appreciate all your guidance whether it pertained to experiments or career planning. Each of you has pushed me to be a better researcher, thinker, and scientific professional and I am so grateful for all of your direction in completing my dissertation.

To my lab family, Nori, Lanny, Pedro, Datta and Elizabeth, I could not have done it without you. You all make coming to work a pleasure everyday. Your lightheartedness keeps the lab a happy place and there are not enough pages for me to list all the skills I have learned from each of you! Completing my graduate studies by your side has been a privilege and a joy.

Thank you to our many collaborators who have worked with us over the last few years on these projects. I thank the laboratory of Wendy Liu with whom we collaborated to develop the fluidics system. I greatly appreciate the hard work of Dr. Tingting Wang for developing the original fluidic channel design discussed in Chapters Two and Three and Frances McWhorter for redesigning the system to reach the micro-scale as discussed in Chapters Two and Four. The work presented in Chapter Three was completed with the help of many, but I would like to extend a deep appreciation to my co-first author Dr. Norikiyo Ueno for his work examining integrin clustering and Dr. Cyrille Bonhomme for his training and troubleshooting on the

microscope. For the work presented in Chapter Four, I would like to thank my undergraduate researcher, Elizabeth Jivan, for all her help running experiments and analyzing data.

I would also like to thank the Molecular Biology and Biochemistry department administrative staff for all of their assistance over the last few years. They have always been happy to help by answering questions, filing paperwork, and booking conference rooms. Their aid is essential and I greatly appreciate all of their help.

To my husband, Tim, I would like to extend my deepest gratitude for your support. You have heard about every experiment, every lab meeting, every seminar, and every paper. I could not have completed this work without your constant encouragement. You're my biggest cheerleader and I can't thank you enough for your unconditional love, patience, and support.

To my parents, Nancy and Ross, thank you for your love and support throughout this process. You have always answered my calls and provided guidance when I needed it most. Your encouragement has kept me going and helped me push forward when I needed to.

I would like to send a big "thank you" to the entire Snyder and Harker families. To my brother Jim and his fiancé Tani, you guys have continued to keep me grounded and laughing over the last few years. Your good humor reminds me to focus on what matters most and your support has been essential. To the Harker clan: Grandpa Milt and Grandma Pat; Joan and Chuck; Uncle Jim and Aunt Pat; Uncle Jerome and Aunt Diane; Jamie; Chris, Amber and Braxton, thank you for all your support and encouragement. I could not have married into a better family. I appreciate all your understanding as I pursued my graduate degree. On many occasions I have had to leave early or come late to family gatherings, to fit in a trip to the lab, and you have always understood. Thank you for all your love and support.

To my best friends, Jenna, Helen and Jennie, and their wonderful spouses, thank you for all of your support. Even though we don't live close, our regular telephone calls and ladies brunches have been so crucial for my success in graduate school and I could not have made it this far without you. Thank you for always being a shoulder to lean on when I needed it.

I would also like to thank all the new friends I have made along the way. Graduate studies can be difficult and having friends that understand the struggle has helped me to survive the process. I could not have done it without my graduate school buddies, so thank you.

Lastly, I thank the Society of Leukocyte Biology for permission to include Chapter Three of my dissertation, which was originally published in the *Journal of Leukocyte Biology*, as well as the American Society for Microbiology for permission to include Chapter Four of my dissertation, which was originally published in *mBio*. Financial support for my studies was provided by the University of California, Irvine, Brython-Davis Fellowship, and the NIH Immunology Training Grant T32 AI60573.

CURRICULUM VITAE

EDUCATION

Doctor of Philosophy	University of California, Irvine
September 2010 – August 2014	Thesis Advisor: Melissa B. Lodoen, PhD
Bachelor of Science	California Lutheran University
August 2004 – May 2008	Mentor: Dennis Revie, PhD

RESEARCH AND WORK EXPERIENCE

2011 – 2014	Ph.D. candidate in the laboratory of Dr. Melissa B. Lodoen at University of California, Irvine
2010 – 2011	Rotation student in the laboratories of Dr. Bert Semler, Dr. Rozanne Sandri-Goldin, and Dr. Melissa Lodoen at University of California, Irvine
2009 – 2010	Research associate IV, Cell Biology department of One Lambda, Inc.
2008 – 2009	Temporary research associate, Protein Department, Amgen.
2007	Summer undergraduate research student in the laboratory of Dr. Karl Munger at Harvard Medical School
2006 – 2008	Undergraduate research student in the laboratory of Dr. Dennis Revie at California Lutheran University in collaboration with Dr. Syed Z. Salahuddin at the California Institute of Molecular Medicine.

AWARDS AND PROFESSIONAL HONORS

2013-2014	Graduate Fellow Award, HHMI-UCI Teaching Fellows Program
2013-2014	Predoctoral appointment, NIH Immunology Training Grant
2013	Best Talk Award, 17th Annual Woods Hole Immunoparasitology meeting
2013	UCI Brython-Davis Fellowship
2012	1st place speaker, 10th Annual UCI Immunology Fair
2008	Graduated summa cum laude
2006	Swenson Summer Undergraduate Research Fellowship
2004 – 2008	California Lutheran University Dean's list (every semester)

TEACHING ASSISTANCE

2013	HHMI-UCI Teaching Fellows Program, *DNA to Organisms*
2013	Teaching assistant, *Microbiology Lecture* and *Microbiology Laboratory*
2012	Teaching assistant, *Microbiology Lecture* and *Microbiology Laboratory*
2007 – 2008	Teaching assistant, *Molecular Biology Laboratory*
2007	Chemistry departmental assistant

PUBLICATIONS

Salahuddin SZ, **Snyder KA**, Godwin A, Grewal R, Prichard JG, Kelley AS, Revie D (2007) The simultaneous presence and expression of human hepatitis C virus (HCV), human herpesvirus-6 (HHV-6), and human immunodeficiency virus-1 (HIV-1) in a single human T cell. Virol J. 4:106.

Harker KS, Ueno N, Wang T, Bonhomme C, Liu W, Lodoen MB. (2013) *Toxoplasma gondii* modulates the dynamics of human monocyte adhesion to vascular endothelium under fluidic shear stress. *J Leukocyte Biol.* 93: 789-800.

Ueno N, **Harker KS**, Clarke E, McWhorter FY, Liu W, Tenner AJ, Lodoen MB. (2014). Real-time dynamic imaging reveals Mac-1-mediated transmigration of *Toxoplasma gondii*-infected human monocytes across endothelial barriers. *Cell Microbiol.* 16: 580-595.

Harker KS, Jivian E, McWhorter FY, Liu W, Lodoen MB. (2014). Shear forces enhance *Toxoplasma gondii* tachyzoite motility on vascular endothelium. *mBio*. *5*(2), e01111–13–e01111–13. doi:10.1130/mBio.01111-13

Morgado P, Sudarshana D, Gov L, **Harker KS**, Lam T, Casali P, Lodoen MB. (2014) Type II Toxoplasma gondii induction of CD40 on infected macrophages enhances IL-12 responses. In Press.

SCIENTIFIC CONFERENCE PRESENTATIONS

2011 University of California, Irvine, Institute for Immunology 9th Annual Immunology Fair, Irvine, California, USA
"*Toxoplasma gondii* Modulation of Monocyte-Endothelial Cell Interactions" Poster.

2012 La Jolla Immunology Conference, La Jolla, California, USA
"Imaging *T. gondii*-Infected Human Monocytes on Vascular Endothelium Reveals Parasite Modulation of Leukocyte Adhesion" Poster.

2012 Southern California Eukaryotic Pathogen Symposium, Riverside, California, USA
"*Toxoplasma gondii* Modulates Human Monocyte Adhesion to Vascular Endothelium under Fluidic Shear Stress" Talk.

2012 University of California, Irvine, Institute for Immunology 10th Annual Immunology Fair, Irvine, California, USA
"*Toxoplasma gondii* Modulates Human Monocyte Adhesion to Vascular Endothelium under Fluidic Shear Stress" Talk.

2013 24th Annual Orange County Graduate Women in Science Spring Conference, Orange, California, USA
"Imaging *T. gondii*-Infected Human Monocytes on Vascular Endothelium Reveals Parasite Modulation of Leukocyte Adhesion" Poster.

2013 17th Annual Woods Hole Immunoparasitology Meeting, Woods Hole, MA, USA
"*Toxoplasma gondii* Modulates the Dynamics of Human Monocyte Adhesion to Vascular Endothelium under Fluidic Shear Stress" Talk.

2013 12th International Congress on Toxoplasmosis, Student and Postdoc Workshop, Oxford, UK
"A Fluidic and Time-Lapse Fluorescence Microscopy System for Examining the Effect of *Toxoplasma gondii* Infection on Human Monocyte Adhesion to Vascular Endothelium" Talk.

2013 12th International Congress on Toxoplasmosis, Oxford, UK
"*Toxoplasma gondii* Interactions with Vascular Endothelium in Conditions of Fluidic Shear Stress" Poster.

2013 Southern California Eukaryotic Pathogen Symposium, Riverside, California, USA
"*Toxoplasma gondii* Interactions with Vascular Endothelium in Conditions of Fluidic Shear Stress" Poster.

2013 University of California, Irvine, Institute for Immunology 11th Annual Immunology Fair, Irvine, California, USA
"*Toxoplasma gondii* Interactions with Vascular Endothelium in Conditions of Fluidic Shear Stress" Poster.

2014 25th Annual Orange County Graduate Women in Science Spring Conference, Irvine, California, USA
"Shear Forces Enhance *Toxoplasma gondii* tachyzoite motility on vascular endothelium"
Talk

2014 Gordon Research Conference on Host-Parasite Interactions, Newport, Rhode Island, USA
"Shear Forces Enhance *Toxoplasma gondii* tachyzoite motility on vascular endothelium"
Talk

ABSTRACT OF THE DISSERTATION

***Toxoplasma gondii* interactions with vascular endothelium under fluidic shear stress**

by

Katherine Snyder Harker

Doctor of Philosophy in Biological Sciences

University of California, Irvine, 2014

Assistant Professor Melissa B. Lodoen, Chair

Toxoplasma gondii is a highly successful parasite that infects approximately one-third of the human population and can cause fatal disease in immunocompromised individuals. Systemic parasite dissemination to organs such as the brain and eye is critical to disease pathogenesis. *T. gondii* can disseminate via the circulation, and both intracellular and extracellular modes of transport have been proposed. To examine the dynamics of both of these dissemination mechanisms we have developed a fluidic system combined with time-lapse fluorescence microscopy. Using this approach, we showed that *T. gondii*-infected primary human monocytes and THP-1 cells exhibited altered adhesion dynamics compared to uninfected monocytes: infected cells rolled at significantly higher velocities (2.5 to 4.6-fold) and over greater distances (2.6 to 4.8-fold) than uninfected monocytes before firmly adhering. Since infected monocytes appeared delayed in their transition to firm adhesion, we examined the effects of infection on integrin expression and function. *T. gondii* did not affect the expression of LFA-1, VLA-4, or MAC-1 or the ability of Mn^{2+} to activate these integrins. However, *T. gondii* infection impaired LFA-1 and VLA-4 clustering and pseudopod extension in response to integrin ligands.

We then applied this same fluidic system to questions of extracellular parasite adhesion to endothelium and showed that shear force influenced parasite adhesion and motility dynamics and the outcome of parasite interactions with endothelium. Extracellular parasites were capable of adhesion to primary human endothelium in shear stress conditions, and interestingly, shear stress enhanced *T. gondii* helical gliding, resulting in a significantly greater displacement. In addition, shear stress increased the percentage of tachyzoites that invaded or migrated across the endothelium. By examining *T. gondii* deficient in the adhesion protein MIC2, we found that MIC2 contributed to initial adhesion but was not required for adhesion strengthening. These data suggest that in fluidic conditions, *T. gondii* adhesion to endothelium may be mediated by a multistep cascade of interactions that is governed by unique combinations of adhesion molecules.

This dissertation work has led to a better understanding of the mechanisms by which *T. gondii* interacts with and migrates across endothelium into tissues, where the parasites ultimately cause disease.

CHAPTER 1

INTRODUCTION TO *TOXOPLASMA GONDII* AND MECHANISMS OF DISSEMINATION

T. gondii biology and life cycle

Toxoplasma gondii is a eukaryotic protozoan pathogen belonging to the phylum Apicomplexa, subclass coccidia. This subclass contains a diverse group of unicellular parasitic organisms distinguished by their motile and invasive life stages, obligate intracellular niche and ability to form spores (1). Many human and animal pathogens belong to the phylum Apicomplexa, including *Plasmodium*, *Crytopsporidium, Sarcocystis,* and *Babesia*, which are the causative agents of malaria, cryptosporidiosis, sarcosporidiosis, and babesiosis, respectively. *T. gondii* is globally distributed and has a complex population structure. Genetic analysis of European and North American isolates of *T. gondii* indicates the presence of three stable multilocus genotypes (strain types I-III) that show low levels of divergence at the DNA sequence level (2). However, isolates from South and Central America, Africa, and Asia have much greater genetic diversity and have been classified into haplogroups IV-XII (3).

T. gondii is an obligate intracellular parasite capable of infecting nearly any nucleated cell in any warm-blooded animal (1). In its asexual stages *T. gondii* has a haploid genome that is comprised of approximately 8×10^7 base pairs (4). The population structure in North America and Europe is remarkably clonal, consisting of three dominant linages, types I, II, and III, that differ in their virulence by host. Type I is recognized as being the most virulent in mice, whereas type II is more commonly associated with human disease, and type III with disease in livestock (1, 5). Sexual replication of all *T. gondii* strain types occurs in the gut of infected felids, making them the parasite's definitive host. A single infected cat can shed millions of oocysts in their feces into the environment over the course of several weeks (6). Upon sporulation, which occurs between 1-21 days, oocysts containing sporozoites are highly infective and can be ingested by a secondary host, which can include humans, livestock, poultry, and rodents, among others. Transmission of oocysts typically occurs via contaminated water or vegetation and following ingestion there is a conversion to the tachyzoite life stage in the gut of the newly infected host.

Tachyzoites are crescent in shape and approximately 2 x 8 μm in size. They have a polar morphology with an apical conoid ring and apical secretory organelles from which they secrete proteins involved in motility and invasion (7). Tachyzoites invade nucleated host cells by active penetration (8) and establish a non-fusogenic vacuole (9) within which they rapidly replicate by endodyogeny. During this life stage, the parasite readily invades, replicates within, and then ruptures host cells. Ultimately, tachyzoites will enter the circulation and disseminate to secondary tissues. The tissue damage associated with the primary infection induces a strong inflammatory response from the host (10). It is thought that this immune response in addition to parasite-specific stress responses contributes to the following life stage conversion to the bradyzoite.

Bradyzoites reside in tissue cysts in host cells for the life of the host and are characterized as multiplying very slowly and having a quiescent metabolic program (11). Additionally, bradyzoites express stage specific genes and are antigenically distinct from those expressed by tachyzoites (12). Recrudescent infection can occur if the immune status of the host is comprised, resulting in stage conversion back to the rapidly replicating and destructive tachyzoite. Bradyzoite-containing tissues cyst also represent a secondary means of transmission, as the tissue of chronically infected secondary hosts can be ingested by another intermediate host, which includes other carnivorous mammals, or a felid, completing the life cycle.

Clinical outcomes and the immune response to *T. gondii*

Human infection with *T. gondii* is predominantly the result of the ingestion of parasite cysts. This could be ingestion of infected tissue from another intermediate host containing bradyzoites or the ingestion of oocysts from the environment; in either case there is a stage conversion to the tachyzoite in the gut. Additionally, humans can become infected by organ transplantation or blood transfusion from an infected donor, or the parasite can be transmitted

vertically from mother to child when there is a primary material infection during or immediately prior to pregnancy.

The immune response to *T. gondii* infection, acute or recrudescent, is dominated by a strong pro-inflammatory response and skewing toward a T-helper-1 adaptive program. Innate immune cells, such as monocytes, neutrophils, and dendritic cells (DCs), are recruited to the primary site of infection where they sense the pathogen via Toll-like receptors (TLRs) and express and secrete interleukin-12 (IL-12) (13, 14). IL-12 then induces the production of interferon-gamma (IFN-γ) by natural killer (NK) cells and T cells (15, 16). These responses largely serve to control parasite burden. Within two weeks after infection the humoral response has been initiated and antibodies can be detected in sera. These antibodies have many protective roles including opsonization for phagocytosis, blocking invasion, and activating the classical complement cascade (17, 18). Ultimately, the majority of tachyzoites are cleared from the host; however, a fraction disseminate to secondary sites where they differentiate into bradyzoites and establish latent infection as tissue cysts. It is the dissemination of parasites into tissues that leads to the development of disease in the immunocompromised host or results in the potential to develop disease later in life in the immunocompetent host.

In humans, infection is typically asymptomatic and results in the establishment of life-long latent infection. Symptomatic disease (called toxoplasmosis) occurs in specific populations including the congenitally infected fetus and newborn, and in immune compromised individuals by either acute infection or reactivation of latent infection. The clinical manifestations of disease are influenced by the parasite strain type, host genetic background and host immune status, among other factors. In the immunocompetent, primary infection with *T. gondii* is generally asymptomatic, however in a minority of cases it can be associated with fever and mild flu-like symptoms (19). The most common manifestation of disease is asymptomatic cervical lymphadenopathy; however, *T. gondii* infection is associated with 3-7% of clinically significant lymphadenopathys (20). In immunocompromised patients, toxoplasmosis is typically associated

with recrudescent infection and often presents in the central nervous system (CNS) as encephalitis, an inflammation of the brain. These patients can suffer initially from minor focal neurological deficits, most often difficulty with speech, and can then progress to more severe symptoms including focal motor deficits and seizures (1). Immunocompromised patients may also show signs of ocular toxoplasmosis, which commonly presents as acute chorioretinitis, an inflammation of the choroid and the retina. Patients have difficulty with vision and typically present with active retinal lesions (21). In the case of congenital infection, disease can manifest in either the brain or the eye, or both. Neonatal manifestations of toxoplasmosis include hydrocephalus, an abnormal accumulation of cerebral spinal fluid around the brain, intracranial calcifications, chorioretinitis and sometimes blindness (1). Congenital, ocular and CNS infection are of particular interest because they each require dissemination of the parasite to distinct tissue sites: invasion of the uterus during pregnancy and breaching of the blood-brain and blood-retinal barriers, respectively. These topics will be discussed in further detail below.

Primary infection of pregnant women with *T. gondii* is typically asymptomatic for the mother, but it can result in transmission of parasites to the fetus. The placenta is the primary natural barrier to congenital infection; however, tachyzoites can invade and replicate within the trophoblast layer, which is a layer of specialized epithelial cells separating the mother and fetus (22). TORCH syndrome is a diverse group of congenitally acquired infections that include toxoplasmosis. The acronym stands for the following: Toxoplasmosis*,* Other (a category that includes Sypilius, Varacella-Zoster Virus infection, and Human Immunodeficiency Virus infection, among others), Rubella, Cytomegalovirus, and Herpes Simplex Virus infection. The causative agents of these perinatal infections are quite diverse, however they share many clinical features including targeting of the CNS, leading in many cases to microcephaly and intracranial calcification (23). During pregnancy the barrier integrity of the placenta is inversely proportional to gestational age, which may contribute to the increased likelihood of *T. gondii* transmission as pregnancy progresses (23). Transmission of *T. gondii* during weeks 10-24

results in more severe clinical disease, whereas transmission during weeks 24-40 usually results in subclinical infection or disease manifesting later in life (24). If left untreated, 85% of children with a subclinical infection will ultimately develop signs and symptoms of toxoplasmosis, in most cases as ocular disease (25). Infection of the fetus results in the development of necrotic foci and severe inflammation in the brain and eye as a result of rapid tachyzoite replication (19). Ultimately this can lead to a myriad of clinical outcomes associated with ocular and cerebral toxoplasmosis, which are discussed below.

Ocular toxoplasmosis is most commonly associated with postnatal acquired infection; however, congenital infection can result in chronic and recrudescent disease (26). In either case, the clinical and morphological appearance of ocular toxoplasmosis is variable, and distinguishing the type of infection after the onset of symptoms is difficult. Disease in the eye tissue typically presents as necrotizing chorioretinitis, though this is variable and can also extend to neighboring tissues beyond the choroid (21). Recurrent chorioretinitis is common and patients often present with clustered retinal lesions near old hyperpigmented scars that were the result of earlier retinal pigment epithelium destruction caused by infection (21). In some cases, parasites have been identified in an active retina lesion within or near the focus of inflammation by immuno-histopathology (27). However, disease is variable, and mouse models suggest a possible autoimmune component, as parasite cysts are not always in close proximity to the focus of inflammatory infiltrates and tissue destruction (28). In addition, in congenitally acquired ocular toxoplasmosis, the location of the lesion within the eye does not appear to be random. Cysts tend to localize centrally in the macular region, and it has been suggested that this localization is influenced by the developing vascular architecture and microenvironment (29). Ocular disease in congenitally infected newborns is more frequently associated with legal blindness than postnatally acquired infection (21); however there can be a significant delay in the onset of symptoms, up to several years after birth, making diagnosis with congenital ocular toxoplasmosis difficult.

Infection of the CNS also occurs in both congenital infection and recrudescent infection in immunocompromised patients. In the context of recrudescent infection, tissue cysts are predominantly found in the neurons of the cerebral cortex, hippocampus, basal ganglia and the amygdala (30). Latent infection is typically characterized as asymptomatic, though it has been associated with mental disorders, such as schizophrenia (31). Immunosuppression of the chronically infected host, as in the case of transplantation or AIDS, can result in excystation of parasites from the tissue cyst. Subsequently an acute inflammatory immune response ensues that includes the increased expression of IL-12 and IFN-γ, recruitment of monocytes, dendritic cells, and $CD4^+$ and $CD8^+$ T cells, and the activation of resident microglia (32, 33). In AIDs patients, cerebral toxoplasmosis is the most common CNS pathology and is associated with encephalitis (34). Other associated clinical features include headache, incoordination, dementia and seizures, and in 75% of cerebral toxoplasmosis cases there is an onset of focal neurological abnormalities such as hemiparesis, weakness on one side of the body, or aphasia, difficulty with language comprehension (35). Congenital infection of the fetal brain is distinct and is associated with psychomotor or mental retardation, hydrocephalus, microcephalus (reduced brain growth), intracranial calcifications, deafness, and epilepsy (19). It should be noted however, that the severity of disease is greatest when infection occurs early during pregnancy, before week 20 (36).

Mechanisms of *T. gondii* dissemination

Upon primary infection *T. gondii* spread rapidly to tissues distant from the initial site of infection (37). It is in these tissue sites that the parasite will encyst and establish a chronic, life-long infection of the host. The reactivation of these encysted parasites later in life contributes substantially to severe disease pathology in the immunocompromised host, as described above. How *T. gondii* spreads to these secondary tissue locations via the circulation is not well understood. There are three proposed mechanisms the parasite is thought to use to

disseminate in the host: 1) The parasite may invade a motile immune cell population and exploit these cells for leukocyte-assisted transfer from the primary site of infection to secondary locations and across biological barriers (38-40). In addition to the protection from both innate and humoral immune responses provided by intracellular transport, parasites may also gain access to a variety of otherwise inaccessible tissues due to the inherent migratory functions of the immune cells they hijack. 2) Extracellular parasites circulating in the blood may directly adhere to and migrate across endothelium. In acutely infected mice, extracellular *T. gondii* are found in the blood, and free tachyzoites injected directly into the blood can disseminate to distant sites (38, 39). 3) A combined strategy using both intracellular transport and extracellular adhesion and motility may also be used. In this scenario the invaded leukocyte circulates in the blood, shuttling the parasite away from the primary site of infection to a secondary location where the parasites may then egress and transmigrate across the cellular barrier under their own power by either a transcellular or paracellular route (41). Little is known about the molecular mechanisms required for *T. gondii* to disseminate away from the primary site of infection to reach secondary locations. The mechanisms of leukocyte assisted transfer and extracellular parasite adhesion and motility will be discussed in further detail below.

Leukocyte-assisted transfer

One potential mechanism of parasite dissemination is through the exploitation of motile immune cells. Migratory leukocytes are an ideal target for pathogen dissemination due to their innate homing and migratory behavior. *T. gondii* infection of DCs enhances their migratory capacity in a parasite strain-specific manner (39, 42). This hypermotile phenotype coincides with actin cytoskeletal rearrangement, morphological changes, and a redistribution of integrins at the cell surface (43). Infection of macrophages reduces the expression of the integrins αL, α4, and α5 and adhesion to the extracellular matrix components, fibronectin, laminin and collagen IV (44). Additionally, *T. gondii*-infected macrophages show an enhanced transmigratory capacity in

transwell assays (40). These data suggest that the dysregulation of actin assembly, integrin expression and localization, and subsequent loss of adhesiveness in leukocytes enhances their migratory capacity. In addition to DCs and macrophages, other immune cell types have also been implicated as potential 'Trojan horses' for *T. gondii*, including neutrophils (45), T cells (46), NK cells (47), and monocytes (38, 48).

Other pathogenic microorganisms have similarly been shown to hijack immune cells as a means to disseminate throughout their host. *Theileria*, another member of the phylum Apicomplexa, has been shown to transform infected mononuclear phagocytes and induce migration into distant non-lymphoid tissues including the brain and heart (49). Additionally, *Theileria annulata* infection of macrophages alters actin dynamics and establishes a polarized morphology in a Src-kinase dependent manner (50). These properties promote dissemination of *Theileria*-infected cells and are thought to contribute to disease pathogenesis (51). *Neisseria gonorrhea* adhere to the uropod of recruited neutrophils via a type IV pilus, avoid phagocytosis, and 'hitchhike' as a means to facilitate their spread throughout the epithelial cell layer (52). During *Listeria* infection, a subset of monocytes are infected with the bacteria and have been shown to transport *L. monocytogenes* into the brain of infected mice (53). A precedent for leukocyte-assisted transfer as a mechanism for dissemination among microorganisms is clearly evident.

A likely target for *T. gondii* leukocyte-assisted transfer in the blood is the monocyte, since these cells circulate in the bloodstream and interact with the endothelium homeostatically. Monocytes are mononuclear leukocytes of hematopoietic origin. They are derived from monoblasts residing in the bone marrow and are the precursors to mononuclear phagocytes in various tissues such as lung alveolar macrophages, liver Kupffer cells, peritoneal macrophages, and a large variety of DC populations (54). Monocytes are defined by the surface expression of CD11b and CD14 or CD16 in humans, and CD11b, F4/80, and an absence of B cell, T cell, DC, and NK cell markers in mice (55). However, it is important to note that monocytes are a

phenotypically heterogeneous and diverse group of leukocytes that can be further classified into two broad groups. In humans, the expression of CD16 (FcγRIII), the Fractalkine receptor and adhesion molecule CX_3CR1, and the chemokine receptors CCR2 and CCR5 distinguish classical ($CD14^{hi}CD16^{-}CX_3CR1^{low}CCR2^{+}$) monocytes from non-classical or resident monocytes ($CD14^{lo}CD16^{+}CX_3CR1^{hi}CCR5^{hi}$) (56). Similarly, in mice, classical or inflammatory ($Ly6C/Gr1^{hi}$ $CX_3CR1^{+}CCR2^{+}$) monocytes are distinguished from resident ($Ly6C/Gr1^{low}CX_3CR1^{hi}CCR2^{low}$) monocytes by the expression of lymphocyte antigen 6 complex (Ly6C), also called Gr1, CX_3CR1 and CCR2 (57). These two classes of monocytes in either species can be further distinguished by their expression of adhesion molecules, suggesting different tissue trafficking patterns. In general, classical monocytes are thought to be short-lived and selectively recruited to sites of inflammation or to lymph nodes where they differentiate into DCs or other tissue specific phagocytes. Classical monocytes represent 90-95% of the total monocyte population in circulation in humans, whereas in mice they only represent about 50% (57). Non-classical or resident monocytes are longer-lived, are found in both resting and inflamed tissues, and appear to have patrolling behavior that helps to initiate an early immune response to infection in mice (58).

Either of these monocyte populations may be parasitized during *T. gondii* infection. Where this infection takes place remains controversial. Infection of monocytes in the gut has been shown in mice (45); however, whether these infected monocytes are in fact carrying parasites into the circulation and ultimately to secondary tissues is unclear. Monocytes represent an attractive target for dissemination via the circulation since they homeostatically interact with the endothelium and have the potential to extravasate into tissues. Additionally, *T. gondii* has been shown to preferentially infect monocytes over other peripheral blood leukocytes (PBLs) (59), and monocytes are found to harbor the parasites in acutely infected individuals (60). *T.* gondii-infected monocytes can transmigrate across a blood-brain barrier model *in vitro* (48) and have been shown to shuttle the parasite into the brain in mice (38). Monocytes,

therefore, appear to function as a key 'Trojan horse' for parasite spread in the blood.

Monocyte extravasation occurs through a dynamic multi-step cascade of receptor-ligand interactions, culminating in diapedesis. Monocytes are captured out of the blood flow by the interaction of selectins on endothelium with their monocyte-selectin ligands, which are a heterogeneous group of glycoproteins and glycolipids previously shown to participate in leukocyte capture and/or rolling with varying affinities for particular selectins (61). This adhesion initiates rolling movement, which allows the monocyte chemokine receptors to contact their chemokine ligands on the surface of the endothelium (62), initiating G-protein coupled receptor (GPCR) signaling events, and resulting in the 'inside-out' activation of integrins. Integrins are heterodimeric transmembrane cell receptors that mediate rolling and firm adhesion. The 'activated' integrins will bind their endothelial ligands with both high affinity, in which the conformation state of the extracellular domain results in the strongest receptor-ligand binding, and valency, referring to the number of the those binding events. This binding will induce further integrin clustering and 'outside-in' signaling leading to focal adhesion formation, cell spreading, and sustained cell adhesion (63). Firmly adherent leukocytes can then crawl toward endothelial cell junctions where they transmigrate and exit the circulation.

How *T. gondii*-infected human monocytes interact with vascular endothelium prior to transmigration in the dynamic shear-stress conditions of blood flow remains poorly characterized. Investigation of parasite dissemination strategies has largely been limited to static tissue culture systems (40, 42, 44, 48, 64-66) or end-point analysis *in vivo* (38-40, 42, 44). Modeling the dynamic environment of the circulation in an adaptable *in vitro* system that includes shear force as an experimental parameter is critical for investigating the mechanisms by which *T. gondii* manipulates monocyte-endothelial cell interactions. Such systems have been used to examine selectin-mediated leukocyte tethering (67), Ca^{2+} signaling during neutrophil rolling (68) and the contributions of integrins to rolling adhesion under physiological shear flow (69). The design and development of our *in vitro* microfluidic system will be discussed in greater

detail in Chapter 2. The application of this system to investigate the interaction of *T. gondii*-infected human monocytes with vascular endothelium in physiological shear stress is detailed in Chapter 3.

Extracellular parasite adhesion and motility

Another potential mechanism of parasite dissemination from the blood into tissues is via direct adhesion and motility of extracellular parasites to endothelium. In the circulation *T. gondii* are found both as extracellular parasites (70) as well as within blood leukocytes (60). Extracellular tachyzoites can adhere to and transmigrate through mouse ileum (64) and across human retinal cultures *ex vivo*, in which the retina was freed from the choroid and was cultured for several weeks until it presented as a mat of retinal glial cells supporting retinal neurons (71). Additionally, extracellular tachyzoites have been shown to cross polarized epithelial monolayers (64, 72) and human retinal endothelial cell monolayers (66) *in vitro*. Type I parasites are associated with a stronger migratory capacity (64) and localize to intercellular junctions during *in vitro* transmigration assays, suggesting a paracellular route of transmigration (72).

Extracellular mechanisms of dissemination through the vasculature have been described for many pathogenic microorganisms. Amino *et al.* have shown that *Plasmodium* injected into the skin can migrate through the tissue and enter capillaries where they then circulate (73). *Cryptococcus neoformans* has been observed adhering to and transmigrating across brain microvasculature in a urease dependent manner *in vivo* (74). Moreover, intravital imaging has revealed a complex multi-step adhesion cascade for *Borrelia burgdorferi* culminating in extravasation out of the vasculature *in vivo* (75, 76). These data suggest that an extracellular mechanism of dissemination could similarly be used by *T. gondii* to exit the circulation and disseminate into tissues.

The majority of Apicomplexan zoites are motile organisms, though many do not have cilia or flagella with which to propel themselves in solution. Rather, they rely on a form of gliding

motility to move across surfaces and invade host cells without modification to their overall shape, as is used in amoeboid movement (77). *T. gondii* secretes adhesion molecules from apical secretory organelles called the micronemes. These adhesins bind to stationary substrates and are subsequently translocated via an actomyosin motor complex to the posterior end of the parasite where they are cleaved, producing the net forward movement of the parasite body relative the gliding surface (7). In the late 1990s Håkansson *et al*. defined classes of movement for the *T. gondii* tachyzoite using video microscopy, and these modes of motility have since been adopted by the field (78). These modes include helical and circular gliding, which produce net forward movement, and twirling, which does not. Gliding motility of this type has also been observed for the zoites of *Plasmodium* (77)*, Babesia* (79) and *Cryptosporidium* (80). The molecular mechanisms of parasite adhesion and motility are discussed in further detail in Chapter 4.

More recent work has focused on identifying the parasite adhesins that participate in *T. gondii* motility and host invasion. Studies using genetically deficient parasites have identified several microneme proteins (MICs) with roles in adhesion, motility, invasion and virulence in mice (81-83). The most well characterized microneme protein associated with adhesion and motility is microneme protein 2 (MIC2). MIC2 is conserved in apicomplexans and belongs to a family of adhesins originally described in *Plasmodium* as thrombospondin-related anonymous proteins (TRAPs) (84). TRAPs play a critical role in *Plasmodium* attachment and invasion (85). MIC2 contains two extracellular adhesive domains, an N-terminal integrin-like A/I domain and six thrombospondin type I repeats (86). The A/I domain of MIC2, like the A/I domain of integrins LFA-1 and MAC-1, binds Intracellular Adhesion Molecule 1 (ICAM-1), and this interaction has been shown to facilitate transmigration across polarized epithelium and human retinal endothelium (66, 72). Under static assay conditions on protein substrates, MIC2 was found to contribute to parasite adhesion, helical gliding and twirling movement (81).

Extracellular *T. gondii* adhesion and motility on vascular endothelium in conditions of

shear stress remain unknown. Chapter 4 will describe the use of an *in vitro* fluidic system combined with time-lapse fluorescence microscopy to characterize parasite adhesion and motility to a cellular substrate under conditions of shear flow and the contributions of MIC2 to these processes.

Concluding remarks

T. gondii is a global pathogen of great health and economic importance. The dissemination of tachyzoites throughout the host via the circulation underlies the development of chronic infection and significantly contributes to pathogenesis. This dissertation describes the development and application of an *in vitro* live-cell microfluidic and time-lapse fluorescence microscopy system to investigate the effects of physiological shear flow on the interactions of both infected human monocytes and extracellular tachyzoites with primary human endothelial cells. Understanding how tachyzoites and infected monocytes interact with vascular endothelium in shear flow conditions will fill a key knowledge gap in understanding how parasites both exploit motile immune cells and mediate their own dissemination in the infected host to cause disease.

CHAPTER 2

APPLICATION OF FLUIDICS FOR STUDYING THE DYNAMICS OF CELL ADHESION TO VASCULAR ENDOTHELIUM

Reproducing the dynamic microenvironment of the human vasculature is critical to understanding the mechanisms of pathogen dissemination via the circulatory system. Traditional *in vitro* culture systems are static. They do not include many of the parameters present in a natural vascular microenvironment, including fluid shear stress and a multitude of cell-cell interactions. The goal for developing *in vitro* flow-based adhesion assays was to design systems that mimicked the complex *in vivo* conditions of the vasculature in such a way that cellular and molecular interactions could be examined under clearly defined flow conditions.

The parallel plate flow chamber and modern fluidics for mimicking the vasculature *in vitro*

The parallel-plate flow chamber was developed in the early 20th century by Burrows (87) and was later adapted to study leukocyte adhesion in flow conditions during the mid-1980s by Forrester and Lackie (88). Parallel-plate flow chambers have been used to define many of the cellular and molecular interactions in the leukocyte adhesion cascade (69, 89-93). In addition, they have been used to examine the adhesion and movement of many disseminating pathogens, including *Candida albicans* (94) and *Plasmodium berghei* (95). In the early 2000s Brown and Larson (96) introduced an improved design in which the scale of the device had been drastically reduced. This design included a polymeric gasket held between two glass plates by a vacuum. Over the last decade advances in microfabrication have permitted the application of microfluidic technology for modeling dynamic cellular events in the vasculature. This has led to the development of systems similar in principle to the parallel plate flow chamber; however, these microfluidic devices are less expensive to produce, customizable, relatively easy to assemble and handle, and can be used in conjunction with traditional experimental techniques (97).

In vitro fluidic devices create tunable microenvironments in which to examine cell-cell interactions in a more physiological setting. They can be made from metal, glass, or polymer-

based materials. Most devices, including those employed in our research, are made from glass and polydimethylsiloxane (PDMS), a silicon-based organic polymer. These types of materials are favored because they are inexpensive, biocompatible, and optically transparent. PDMS-based devices are produced using soft lithography to generate an elastic replica of a solid, reusable mold of the desired channel geometry. The negative relief mold of the channel is typically produced by laser-cutting poly(methyl methacrylate) (PMMA). A mixture of the PDMS polymer is poured over the master mold, solidified by crosslinking, and then pealed off. Holes can be manually punched to produce inlet and outlet ports to the channel. These molds are then UV or plasma bonded to glass slides, generating leak-proof fluidic channels with tubing access. The hand-made nature of these devices allows for control and customization of surface chemistry, channel geometry and mechanical forces, making these systems highly adaptable.

The transition away from parallel plate flow chambers to modern fluidic devices affords many practical advantages, one of which is a reduced reagent burden. Within a fluidic channel the shear stress is proportional to the flow rate and inversely proportional to the channel dimensions. As a result, in a small channel only a very low flow rate is required to generate physiologically relevant shear stress. In addition, because of the reduced dimensions, fluid flow in the channel is entirely laminar and devoid of turbulent mixing. The wall shear stress, t, is a function of flow rate (Q), the channel dimensions (height h and width w), and fluid viscosity (m), and can be calculated as follows:

$$t = 6 \bullet Q \bullet m / (w \bullet h^2)$$

Small adjustments to the flow rate can produce substantial changes in shear stress within the channel, meaning that only a limited amount of cells and culture media are required even when the shear force being examined is high. This is particularly advantageous for the analysis of rare primary human cells.

We are interested in addressing questions about how *T. gondii*-infected cells and extracellular tachyzoites interact with the vascular endothelium. We aim to define the

mechanisms by which parasites in the circulation interact with the vasculature and ultimately leave the circulation and enter into tissues. To date, most of the research on *T. gondii* dissemination has utilized either static *in vitro* assay systems (40, 42, 44, 48, 64-66) or long-term *in vivo* dissemination studies (38-40, 42, 44). The application of fluidics allows us to incorporate the mechanical forces of blood flow and better recapitulate the *in vivo* environment while still retaining the control and flexibility of an *in vitro* system. Similar systems have been recently been applied to questions of pathogenesis for other species and have improved our understanding of cytoadhesion of *Plasmodium*-infected erythrocytes to brain microvascular endothelium (98) and the adhesion and motility of *Pseudomonas aeruginosa* in conditions of shear flow (99).

By using fluidic systems we can observe cell-cell interactions in real-time and determine the molecules that mediate these interactions. Mechanisms found to be important *in vitro* can then be tested in an *in vivo* model. Ultimately, we are interested in the effects of the dynamic fluid-shear environment of the circulation, which can range from shear forces lower than 0.5 dyn/cm^2 in large veins to over 50 dyn/cm^2 in arterioles (100), on the cellular and molecular interactions that mediate parasite dissemination. Fluidics provides the necessary tool to address this question.

Fluidic systems for studying *T. gondii* interactions with vascular endothelium

To investigate the dynamics of infected leukocyte and extracellular tachyzoite adhesion to vascular endothelium in shear stress conditions, we developed fluidic chambers in collaboration with the Liu Lab in the department of Biomedical Engineering at the University of California, Irvine. Our open-loop flow systems consist of a fluidic channel connected via polyethylene tubing to a syringe pump on one end and a reservoir on the other end (Fig. 2.1). The fluidic chambers are comprised of a PDMS channel mold bonded to glass, as described above. For our purposes the glass bottom of the fluidic channel is coated with fibronectin, an

extracellular matrix protein, and seeded with primary human umbilical vein endothelial cells (HUVEC). The fibronectin coating provides a surface that promotes the adhesion of endothelial cells through the binding of the fibronectin receptor $\alpha_5\beta_1$; however it should be noted that this coating is not neutral and activation of signaling downstream of this integrin in endothelial cells influences endothelial cell migration and fibronectin matrix assembly (101).

We were interested in modeling the adhesive dynamics of both *T. gondii*-infected monocytes and free tachyzoites with vascular endothelium. These dynamics include capture and tether events, high velocity and long-range movement (for example: cell rolling), low velocity and short-range movement (for example: cell crawling, parasite gliding), and ultimately transmigration across the endothelium. Observing this array of movements required the development of distinct systems.

The first fluidic channel we developed was designed on the milli-scale (Fig. 2.1A). The shear stress in the device is determined by the flow rate and channel dimensions (H 0.8 mm, W 3 mm, L 20 mm). A flow rate of 1 ml/minute (min) results in a 0.5 dyn/cm^2 shear stress at the surface of the channel. This shear force is within the range of forces found in larger veins (<0.5-5 dyn/cm^2) (100). There are many advantages to using the milli-scale fluidic chamber. The first of which is that the ratio of media volume to surface area is close to that of traditional tissue-culture systems. As a result, primary human endothelial cells can be seeded and maintained with relative ease within the chamber. Secondly, the larger channel dimensions make for a channel that is less sensitive to air-bubbles during live-cell imaging. This also allows for hand-perfusion, when necessary, to clear the channel of media or to remove air gaps without disruption of the monolayer due to excessive force within the channel. Lastly, these benefits permitted the development of a “flow/switch” system that employs a Y-connector with a stopcock and dual syringe pumps (Fig. 2.1A). Using this system, we can introduce flow to the channel using one syringe pump and then switch to perfusion on the second pump at the same flow rate without a disruption to flow. We have used the flow/switch system to examine long-

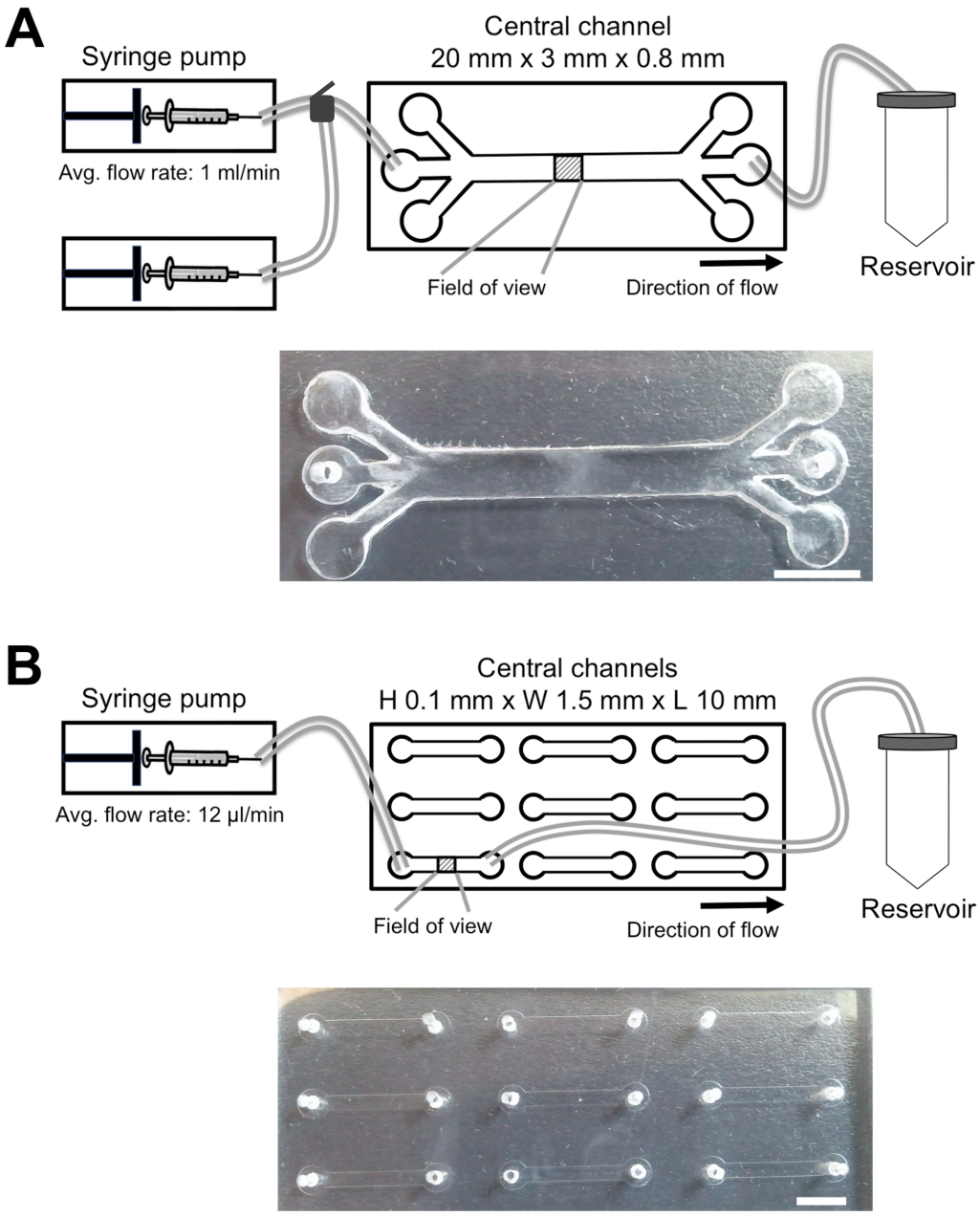

Figure 2.1: Schematics of fluidic systems.
HUVEC are seeded into the central channel on fibronectin. *T. gondii*-infected monocytes or extracellular tachyzoites are perfused through channels by a syringe pump. Shown are schematics (not to scale) and photographs of the (A) milli-scale system with Y-connector for dual syringe pump flow and (B) micro-scale system. Scale bars are 5 mm.

term interactions of infected leukocytes with HUVEC in shear stress (102). We have also used this system to perfuse formaledehyde through the channel to fix adherent cells while in flow conditions and then perform immunofluorescence microscopy within the channel (103).

Associated with the many advantages of this milli-scale system are several disadvantages. The greatest disadvantage is that the high flow rate required to achieve even a relatively low shear force of 0.5 dyn/cm^2 (1 ml/min) requires processing a large number of parasites and leukocytes (on the order of tens of millions) to achieve a reasonable density of adherent cells for live-cell imaging. Furthermore, this poses a limit on the length of time of perfusion with a single pump and the magnitude of shear force that can be examined. Finally, due to the height of this channel, a large fraction of the infected cells or parasites that are flowed through the device never come into contact with the endothelial surface at the base of the channel. Since the average diameter of a primary human monocyte is 8-10 μm, and *T. gondii* tachyzoites are approximately 2 x 8 μm in size, these interactions occur in the bottom 5-10% of an 800 μm tall fluidic channel, and over 90% of the cells that are processed for live-cell imaging never reach the field of view. Additionally, the dimensions of the milli-scale fluidic chambers make it difficult to include more than one channel/slide, producing a manufacturing burden. Ultimately, the milli-scale fluidic chambers are best suited to experiments requiring large fields of view, low shear forces, and the capacity to connect to the flow/switch set-up.

The second fluidic channel that we developed was a micro-scale chamber (Figure 2.1B). The micro-scale channels are significantly smaller in size (H 0.1 mm, W 1.5 mm, L 10 mm); in particular the height of the channel was reduced 8-fold. The reduced dimensions led to a drastically lower flow rate requirement (12 μl/min) to produce a shear force of 0.5 dyn/cm^2. Moreover, the reduced scale allowed us to fabricate 9 micro-scale channels within the dimensions of a standard glass slide. The primary advantage to perfusion in the microchannels is the reduced flow rate. This allows us to experiment with much higher shear forces and to

perfuse with a single syringe pump for significantly longer time periods than is feasible at the milli-scale. Using the microchannels we can easily reach 10 dyn/cm^2 shear force, replicating fluidic conditions in venules and arteries, or much higher (> 15 dyn/cm^2), to represent conditions is arterioles. For example, to produce 10 dyn/cm^2 of shear force requires a flow rate of only 228 μl/min. At the micro-scale we can perfuse at the same shear force for over 80-times as long as can be achieved at the milli-scale, with the same density and volume of cells. Consequently, the number of cells and parasites that need to be grown and processed for live-cell imaging is substantially reduced, and the time allotted for live-cell imaging can be significantly extended. In particular, the reduction in channel height has increased the fraction of cells that come into contact with the HUVEC (the bottom 40% of the channel volume). Another clear advantage to the micro-scale fluidic chambers is the reduced manufacturing burden, since a single device contains 9 channels.

The significant advantages of the micro-scale fluidic chamber design do, unfortunately, come with a few disadvantages, the first of which is the low media volume to surface area within the channel. Seeding primary human cells and maintaining adequate culture conditions to ensure their health is more difficult in the micro-scale channels. However, we have been able to overcome this obstacle and establish protocols for the continuous maintenance of healthy monolayers of both primary human umbilical vein and brain microvascular endothelium for up to 72 hours within the microchannels. These protocols require regular monitoring and changing of culture media to establish a healthy and intact endothelial cell monolayer for live-cell imaging.

Secondly, the micro-scale channels are significantly more sensitive to air bubbles during perfusion. The clearing of air gaps from tubing prior to perfusion is critical to preserving endothelial cell monolayer integrity during live-cell imaging. Furthermore, the reduced scale and increased sensitivity to changes in flow rate makes hand perfusion particularly challenging. To address this we employ the use of empty, unseeded channels to connect our system and ensure the removal of air gaps prior to connection to HUVEC seeded channels. Finally, the

micro-scale fluidic chambers are ideal for experiments that require long time frames, high shear forces and the processing of limited primary cells.

Future Directions: Improving our system

In its current design our fluidic systems are ideal for mimicking laminar flow at various flow rates through a rigid rectangular channel. Myriad questions regarding parasite and infect-cell adhesion and transmigration dynamics can be answered using these systems. However, additional modifications can be applied to better recapitulate other key factors that influence the vascular microenvironment. These factors include the addition of chemical signals, alteration of channel geometry and most importantly, though challenging, the development of layered and/or co-culture systems.

Many of the adhesion interactions we have investigated using our system may be influenced by soluble factors, such as cytokines and chemokines. It is quite possible that invasion of leukocytes by *T. gondii* no only alters the function of adhesion molecules, like integrins, but also potentially affects receptors important for sensing cytokine and chemokine gradients that influence adhesion and the direction of migration. Various strategies can be implemented to address the effects of these components on adhesion, movement and transmigration within a fluidic system. One method would be to pre-layer a gradient of chemokine below the surface of the endothelium. This strategy has been used to study the effects of CXCL12 on the adhesion of metastatic breast cancer cells on endothelium (104). This type of system would allow us to determine whether *T. gondii*-infected leukocytes can detect and respond efficiently to various chemokine signals. Alternatively, parallel laminar flow could be used to introduce various biochemical factors with both temporal and spatial control during live cell imaging. Using perfusion, a gradient of cytokine or chemokine could be established, and the migration of parasites or infected-cells could be assayed, as was done for examining T cell chemotaxis in fluidic shear stress (105). A simple, three-armed channel similar to our milli-scale

device was used to examine endothelial cell migration in response to gradients of vascular endothelial cell growth factor (VEGF) (106). More complex systems that rely on a multitude of serpentine, or zigzagging, channels to establish multiple gradients in a single channel have also been developed and used to examine both neutrophil (107) and dendritic cell (108) migration in response to chemokine gradients in shear flow. These types of systems would allow us to examine the effects of multiple chemical signals and determine which host signaling networks, if any, are potentially disrupted by infection and what affect that has on infected leukocyte adhesion and migration.

In addition to the cellular and chemical components of the vasculature, the varying geometry and non-uniform flow patterns through the vascular tree can greatly influence the adhesion and movement of flowing cells. Our current fluidic systems are comprised of single channels of uniform geometry. Modifications could be made to introduce varying channel width and bifurcations, or branch points, to better replicate circulatory dynamics and their effects on parasite and infected cell adhesion and migration. By drastically reducing channel width to model the circulation in pulmonary capillaries, Yap *et al*. found that human neutrophils transiently reduce their mechanical stiffness and extend pseudopods when forced through thin microchannels in a macrofluidic gravity-based flow system (109). Moreover, these types of modifications to channel geometry have also been influential in better understanding the cytoadhesion of *Plasmodium*-infected red blood cells. In a single study, microfluidic modeling was used to describe cytoadhesion in constricted channels under constant shear force, under varying degrees of shear stress within channels of defined widths, and in bifurcations, all by altering channel geometry and flow rate (110).

Incorporating chemical signals and more diverse channel geometries help to better recapitulate the vascular microenvironment at the endothelial cell surface; however we are ultimately most interested in how parasites transmigrate out of vessels and into tissues. Traditionally, Boyden chambers (111), also referred to as transwells, were used to assay

transmigration in static conditions (112-114). In our current system we can visualize transmigration events based on changes in light reflectance by differential interference contrast (DIC) microscopy. However, since our endothelium is seeded onto a thin layer of fibronectin coated onto a hard glass surface, transmigrating cells are ultimately constrained in the z-direction. A combination of microfluidic technology and transwell systems similar to the Boyden chamber would allow for clearer resolution of transmigration events. Such a system was used by Schreiber *et al*., to investigate the integration of chemokine signaling in T cell migration across an endothelial monolayer in shear flow conditions (115). Similarly, this type of layered system could also be used to co-culture vascular support cells, such as stromal and smooth muscle cells, with endothelial cells. Using this type of system stromal cells were found to influence neutrophil and lymphocyte transmigration in shear flow (116).

An ideal *in vitro* fluidic system accurately recapitulates the vascular microenvironment while still retaining flexibility and control of experiment parameters. Our systems, in their current state, are powerful tools that allow us to accurately replicate the shear force conditions at various points throughout the vascular network and precisely quantify the effects of this force on adhesion, movement, and transmigration of *T. gondii*-infected cells and tachyzoites across endothelium. The aforementioned modifications will improve our ability to model other aspects of the vascular microenvironment, including the influence of soluble factors, varied vessel geometries and multi-cell interactions. The addition of these parameters to our current system will improve our ability to model parasite interactions with human vasculature *in vitro*, leading to a better understanding of the mechanisms of parasite dissemination that can then be tested *in vivo*.

CHAPTER 3

TOXOPLASMA GONDII MODULATES THE DYNAMICS OF HUMAN MONOCYTE ADHESION TO VASCULAR ENDOTHELIUM UNDER FLUIDIC SHEAR STRESS

Introduction

Monocytes circulate in the bloodstream and homeostatically leave the circulation to seed the macrophage and DC populations in tissues; they are also recruited to sites of inflammation (57, 117). These important physiological processes can be hijacked by pathogens to travel in the bloodstream and to gain entry into new sites in the body. Bacteria, viruses, and parasites have evolved a variety of strategies to disseminate to distant tissues in their hosts while eluding immune detection. *T. gondii* is a highly successful intracellular parasite that infects approximately one-third of the human population worldwide and can cause fatal disease in immunocompromised individuals (3). *T. gondii* typically infects individuals who ingest food or water contaminated with parasite cysts or by vertical transmission from mother to fetus (118). In the intestine, the parasites differentiate into a rapidly dividing form, called the tachyzoite, which disseminates from the intestine to multiple organs in the body, including the brain and the eye (119).

Dissemination underpins pathogenesis, and *T. gondii* likely uses multiple mechanisms to spread from the intestine. Bioluminescent imaging of infected mice reveals a characteristic dissemination pattern from the abdomen, extending to the thorax and then ultimately reaching the brain between 10-14 days after infection (39, 120), where the parasites establish a persistent infection in the form of tissue cysts. In mice infected via intragastric inoculation of tissue cysts, DC and monocytes are rapidly infected, and $CD11b^+$ cells can shuttle tachyzoites into the brain (38). The transport of pathogens within migrating cells is believed to be a common mechanism of dissemination, and circulating immune cells can serve as ideal “Trojan horses” for pathogen spread (51). *T. gondii* infection of DCs (39, 42), macrophages (40, 44), and monocytes (38, 48) enhances the migration of these cells. For DCs, the hypermotility phenotype occurs in a parasite strain-specific manner, with the type II strain inducing the highest hypermigratory frequency and intensity *in vitro* (42).

In the mucosa, a population of $Gr1^+$ inflammatory monocytes plays a critical role in the control of *T. gondii* infection(121). These cells are recruited to the site of infection using the chemokine receptor CCR2 and ligand CCL2 (121). Recruited monocytes then differentiate into inflammatory macrophages and IL-12-producing DC that replace the resident mononuclear phagocytes at the site of infection and contribute to parasite control (122). In addition to providing protective immunity against *T. gondii*, monocytes are actively infected by the parasite. Among human peripheral blood cells, *T. gondii* preferentially infects and grows in monocytes (59), and in the blood of infected mice, *T. gondii* is found in monocytes(38). Moreover, monocytes can transport tachyzoites from the bloodstream into the brains of mice (38) and across a human blood-brain barrier model (48).

Monocyte extravasation occurs by a multistep recognition process that links receptor-ligand interactions on the monocyte surface with cytoskeletal changes that induce adhesion and diapedesis (123). The initial capture or “tethering” of monocytes is mediated by weak interactions between selectins on the endothelium and monocyte glycosylated surface proteins containing the sialyl-$Lewis^X$ tetrasaccharide (124). Notably, selectins form catch bonds with glycosylated ligands under conditions of fluidic stress and release their ligands in the absence of flow (67). These transient interactions facilitate rolling and bring the monocyte in close contact with the endothelial surface (125) to allow chemokine receptors on the monocyte to scan for chemokines displayed on the endothelium (62). Chemokine receptor signaling through G-proteins leads to cytoskeletal changes in the monocyte and the “inside-out” activation of integrins, which bind with high affinity to their ligands and mediate firm adhesion to endothelium (126). Integrin binding to ligand subsequently induces integrin clustering and “outside-in” signaling, which contributes to focal adhesion formation and downstream cytoskeletal changes that mediate sustained adhesion (63). The monocyte then crawls on the endothelium to a site of transmigration (127).

In mice *T. gondii*-infected monocytes have been shown to shuttle parasites into tissues where they cause disease (38, 39), and static culture assays have revealed that *T. gondii*-infected cells can traverse the endothelium (39, 65). However, how infected human monocytes tether and adhere to endothelium in conditions of shear stress remains unknown. To address this question and to investigate the dynamics of adhesion, we developed a fluidic and time-lapse fluorescence microscopy system. This system simulates the conditions found in postcapillary venules and permits the analysis of cellular and molecular factors involved in sustained adhesion. We found that *T. gondii*-infected monocytes can tether, roll, and firmly adhere to the endothelium. Notably, infected monocytes exhibited altered rolling dynamics compared to uninfected monocytes: they rolled over greater distances and at higher velocities before transitioning to firm adhesion. Since integrins are known to mediate leukocyte adhesion, we investigated the effects of infection on integrin function. Although the abundance of integrins on the monocyte surface was not altered by infection, *T. gondii* impaired integrin clustering and pseudopod extension in response to integrin ligands. This suggests that a reduced capacity for adhesion or a delayed transition to firm adhesion due these clustering defects may participate in the enhanced monocyte rolling in shear flow conditions. These studies reveal a novel pathway by which *T. gondii* alters the dynamics of human monocyte adhesion.

Results

Fluidic system allows for dynamic imaging of human monocytes on vascular endothelium

To examine the interactions of human monocytes with vascular endothelium under shear stress, we developed an open-loop flow system. Primary human monocytes or THP-1 cells, a human monocytic leukemia line, were infected with GFP-expressing *T. gondii*. Since THP-1 cells are larger than primary monocytes and can be cultured to a later time point post-infection, these cells allowed us to examine the effects of replicating parasites (and therefore, increased parasite burden) on monocyte adhesion. Infection conditions resulted in 70-80% infection

efficiency and >95% viability (Fig. 3.1A). To facilitate automated cell tracking, infected monocyte cultures were labeled with Hoechst nuclear dye, and uninfected cultures were stained with CFSE (Fig. 3.1B).

HUVEC were stained with CellTracker CMTPX, seeded in the fluidic device on fibronectin, and treated with TNF-α to upregulate adhesion molecules, including E-selectin, ICAM-1, and VCAM-1 (Fig. 3.1C). At 4 hours (hr) after treatment, the expression of P-selectin was not altered by TNF-α treatment. The infected and uninfected cultures were mixed 1:1, loaded into the syringe pump, and flowed into the device (Fig. 3.1D), which was positioned in a live-cell environmental chamber on the microscope stage. Cells that did not adhere to the endothelium in the device flowed into a collection reservoir. Since the CellTracker CMTPX produced punctate staining at the top surface of the endothelium (Appendix A Movie 1), DIC imaging was used to confirm that the HUVEC monolayer remained intact for the duration the experiments. Images in the field of view were taken before and after the fluidic runs to confirm confluence of the monolayer (Fig. 3.1E). Adherent monocytes were visible on the endothelium at the end of each experiment (Fig. 3.1E).

T. gondii-*infected monocytes exhibit an extended rolling phenotype*

Primary human monocytes were infected with *T. gondii* for 4 hr and THP-1 cells were infected for 4 or 18 hr. Infected and uninfected monocytes were flowed into the fluidic device, and time-lapse fluorescence microscopy was performed (Appendix A Movie 1). Cell traces of all infected ($GFP^+Hoechst^+$) and uninfected ($CFSE^+$) monocytes interacting with the endothelium were generated (Fig. 3.2A). In both cell types and at both time points, the traces of infected monocytes were notably longer than those of uninfected monocytes (Fig. 3.2A). A magnified series of images shows an infected cell containing two intracellular parasites traveling a greater distance than the uninfected cells in the field during the same time period (Fig. 3.2B). Imaging

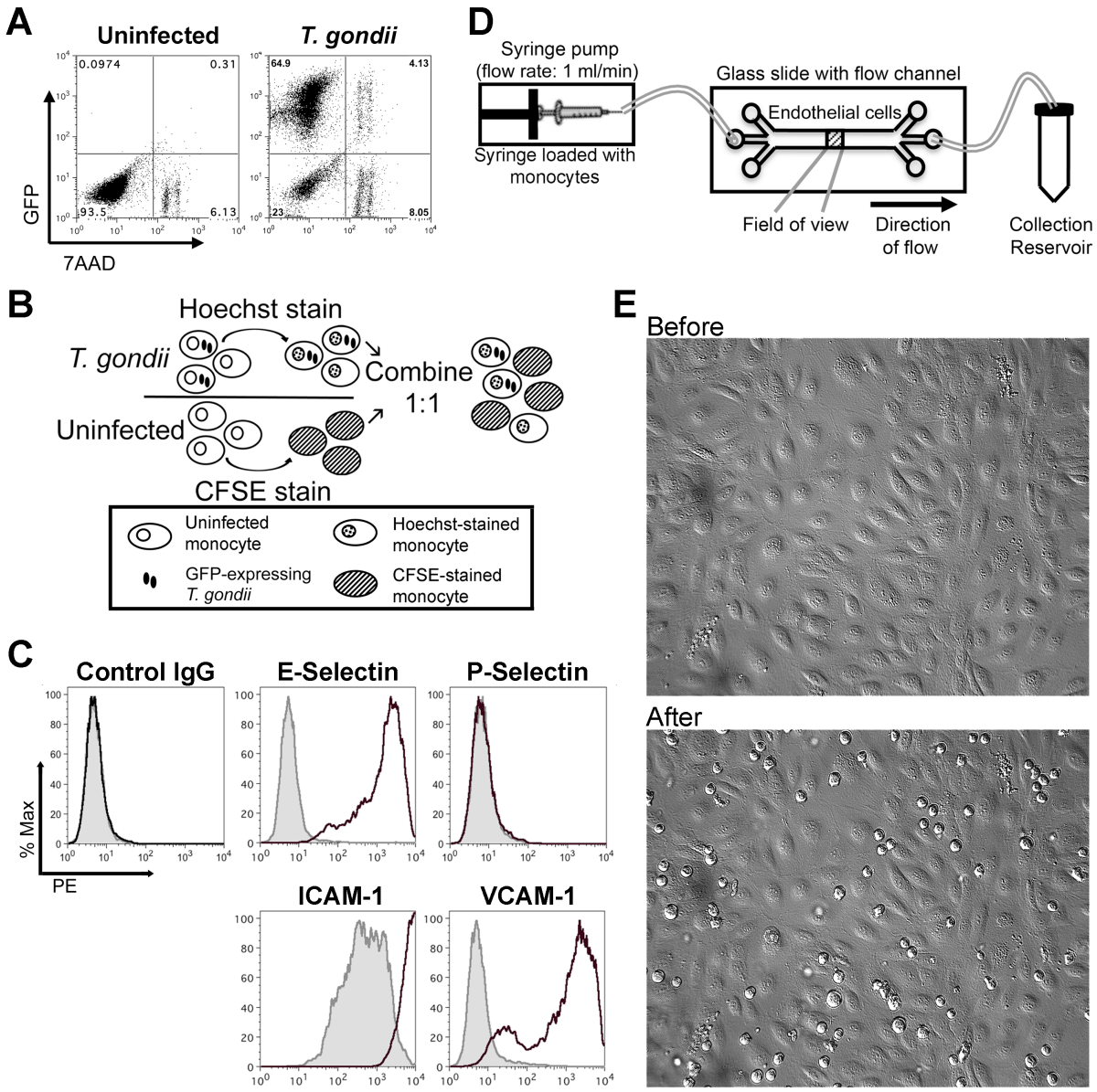

Figure 3.1: *In vitro* fluidic system for analyzing monocyte-endothelial cell interactions. (A) THP-1 cells were uninfected or infected with GFP^{+} *T. gondii*, stained with 7-AAD at 18 hpi, and analyzed by flow cytometry. (B) Infected monocytes were stained with Hoechst dye to label the nucleus and uninfected monocytes were stained with CFSE. The populations were mixed and flowed into the fluidic device. (C) HUVEC monolayers were left untreated (gray histograms) or activated with 25 ng/ml of TNF-α for 4 hrs (black histograms) and analyzed by flow cytometry for the expression of adhesion molecules. (D) Schematic of fluidics assay set-up (not to scale). HUVEC were seeded in the device on fibronectin and monocytes were introduced into the device using a syringe pump. (E) DIC images of a representative HUVEC monolayer in the fluidic chamber before and after a fluidic assay.

was performed approximately in the center of the device to minimize any potential effects of the channel walls on monocyte adhesion dynamics. There did not appear to be a bias in the adhesion of monocytes at different locations in the channel, since monocytes were found evenly distributed along the entire length of the device at the end of imaging (data not shown).

The transition of a cell from rolling to searching is marked by a decline in its instantaneous velocity below a defined threshold (128). We first examined monocytes during rolling (velocity > 0.05 μm/second (sec)). The total pathlength, maximum displacement, and average velocity of infected and uninfected primary monocytes (Fig. 3.2C) and THP-1 cells (Fig. 3.2D) were calculated. During rolling, the average velocities of uninfected primary monocytes, THP-1 cells at 4 hr, and THP-1 cells at 18 hr were 1.3 μm/sec, 0.76 μm/sec, and 2.97 μm/sec, respectively. In contrast, infected monocytes rolled at significantly higher velocities: 2.5-fold higher for primary monocytes, 4.6-fold higher for THP-1 cells at 4 hours post infection (hpi), and 4-fold higher for THP-1 cells at 18 hpi (Fig. 3.2C and D). Infected monocytes also traveled a substantially greater distance than uninfected monocytes. The average pathlengths for uninfected monocytes ranged from 32.79 μm to 114.89 μm, whereas the average pathlengths for infected monocytes ranged from 158.98 μm to 513.88 μm (Fig. 3.2C and D). This resulted in 2.6-fold, 4.8-fold, and 4.5-fold longer pathlengths for infected primary monocytes, THP-1 cells at 4 hpi, and THP-1 cells at 18 hpi, respectively, compared to uninfected cells. Although the velocity, pathlength, and displacement of uninfected THP-1 cells at 18 hr appeared greater than at 4 hr (Fig. 3.2D), these differences were not statistically significant. For each category of cells, the total pathlength and maximum displacement were similar, since most of the distance traveled during rolling was in the direction of flow (left to right). The fluorescent dyes used to stain the monocytes did not appear to alter the behavior of the cells in this system, since switching the dyes on infected and uninfected cells did not affect monocyte rolling velocity, pathlength, or displacement (Appendix A.1A). Interestingly, an increase in the number of

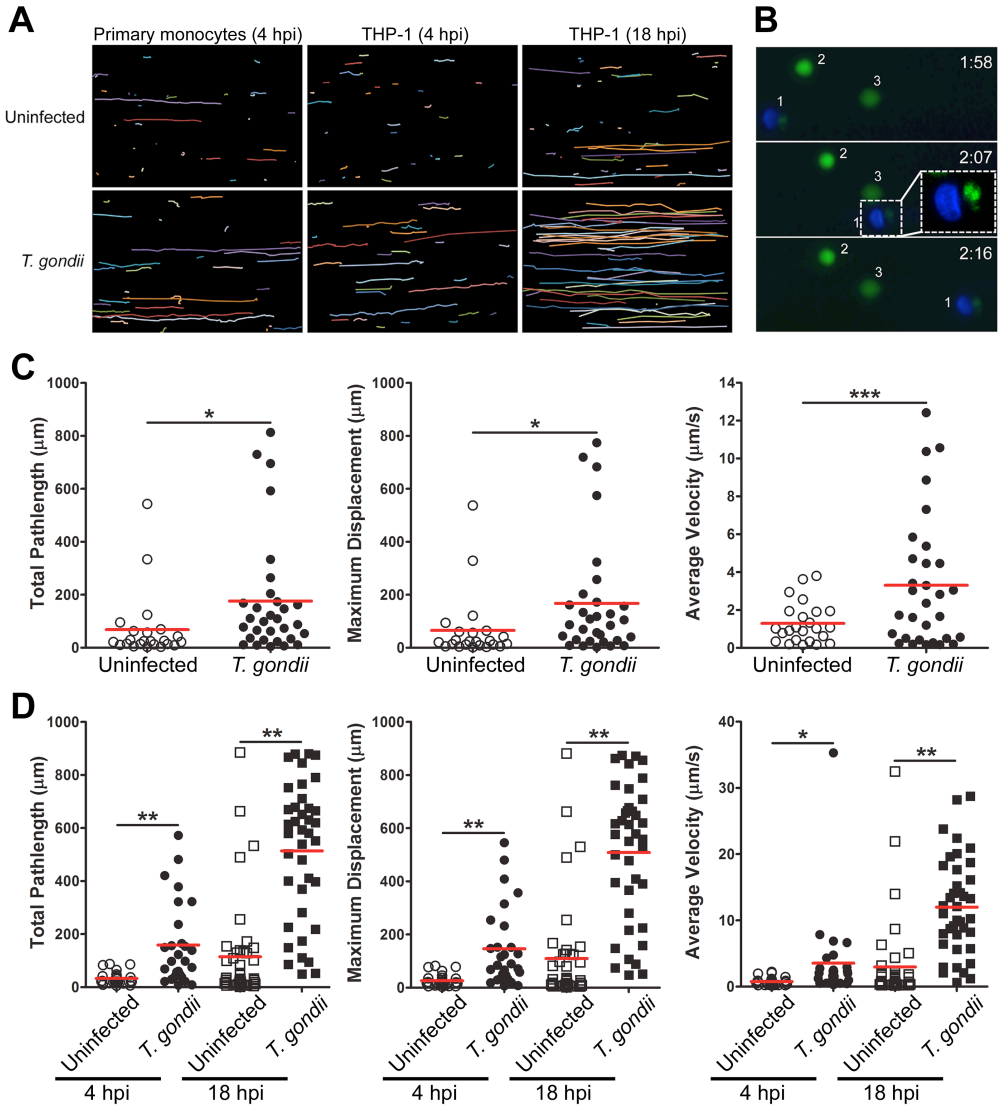

Figure 3.2: *T. gondii*-infected and uninfected monocytes during rolling.
(A) Cell traces for all uninfected or infected primary human monocytes (4 hpi) and THP-1 cells (4 hpi and 18 hpi) analyzed are shown. Each trace shows the entire path of a single cell. The following numbers of cell traces are shown: primary monocytes ($n_{uninfected}$=32, $n_{T.\ gondii}$=31), THP-1 cells at 4 hpi ($n_{uninfected}$=30, $n_{T.\ gondii}$=30), THP-1 cells at 18 hpi ($n_{uninfected}$=43, $n_{T.\ gondii}$=44). A representative series of time-lapse images is shown in Supplemental Video 1. (B) Magnified time-lapse images show that infected Cell #1 and uninfected Cell #2 appeared in the field at 1 min 58 sec. Cell #3 was already firmly adhered at this time. The inset of Cell #1 shows two GFP^+ intracellular parasites, which can be visualized with increased contrast. (C, D) Total pathlength, maximum displacement, and average velocity of uninfected and infected primary monocytes at 4 hpi (C) or THP-1 cells at 4 and 18 hpi (D). For each cell type and time point, at least three independent experiments were performed, and the data were pooled. For C and D, the following number of cells performed rolling in the field of view: primary monocytes ($n_{uninfected}$=23, $n_{T.\ gondii}$=31), THP-1 cells at 4 hpi ($n_{uninfected}$=25, $n_{T.\ gondii}$=27), THP-1 cells at 18 hpi ($n_{uninfected}$=41, $n_{T.\ gondii}$=42). The red bar shows the mean. *P < 0.01, **P< 0. 001, ***P < 0.0001.

intracellular parasites did not correlate with increases in the velocity or distance traveled by individual infected monocytes (Appendix A.1B and C). These data indicate that *T. gondii* infection profoundly alters monocyte rolling on endothelium and that a single intracellular parasite is sufficient to induce this effect.

T. gondii-*infected monocytes have "wandering" searches*

After rolling, monocytes firmly adhered and initiated searching on the endothelium. In contrast to rolling, infected and uninfected monocytes did not differ markedly in their searching. Calculations of the total pathlength, maximum displacement, and average velocity of searching monocytes revealed few statistically significant differences in these parameters and indicated that on average, most infected and uninfected cells performed similar searching (Fig. 3.3A and B). Most cells searched within a confined radius of <10 μm (Fig. 3.3C-E), and the average searching velocity of infected and uninfected cells was ~0.1 μm/sec (this average velocity exceeded the 0.05 μm/sec instantaneous velocity that marks the transition to searching, since cells frequently fluctuated above and below the instantaneous velocity threshold). Among the searching cells, we also observed a subpopulation of cells that exhibited a low velocity migration resulting in a maximum displacement greater than 10 μm from the point where they initiated searching. This "wandering" migration was predominantly in the direction of the flow (Fig. 3.3C-E). Wandering migration was more frequently observed in infected than uninfected cells: 36% of infected compared to 0% of uninfected primary monocytes; 33% of infected compared to 11% of uninfected THP-1 cells at 4 hpi; and 29% of infected compared to 3% of uninfected THP-1 cells at 18 hpi performed wandering searches (Fig. 3.3F). This resulted in a 2.5-fold increase in the maximum displacement of infected compared to uninfected primary monocytes (Fig. 3.3A). We also occasionally observed cells that initiated searching and then appeared to be picked up by flow and deposited at a distant location where they reinitiated searching. This accounted for the

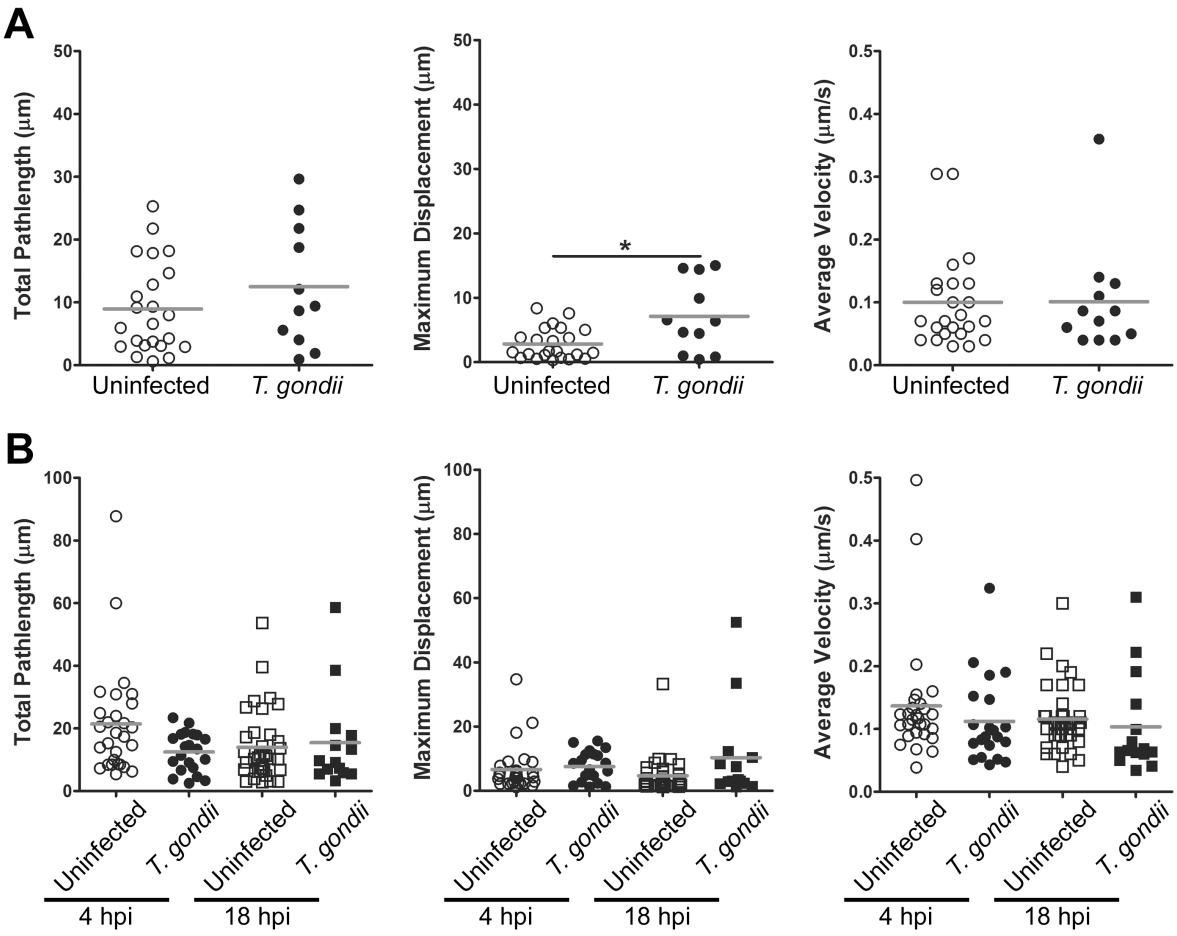

Figure 3.3: Migration of *T. gondii*-infected and uninfected monocytes during searching. (A, B) Total pathlength, maximum displacement, and average velocity of uninfected and infected primary monocytes at 4 hpi (A) and THP-1 cells at 4 hpi and 18 hpi (B). The bars indicate the mean. *P < 0.05. For A-B, the following numbers of cells performed searching in the field of view: primary monocytes ($n_{uninfected}$=23, $n_{T. gondii}$=11), THP-1 cells at 4 hpi ($n_{uninfected}$=28, $n_{T. gondii}$=21), and THP-1 cells at 18 hpi ($n_{uninfected}$=36, $n_{T. gondii}$ =14).

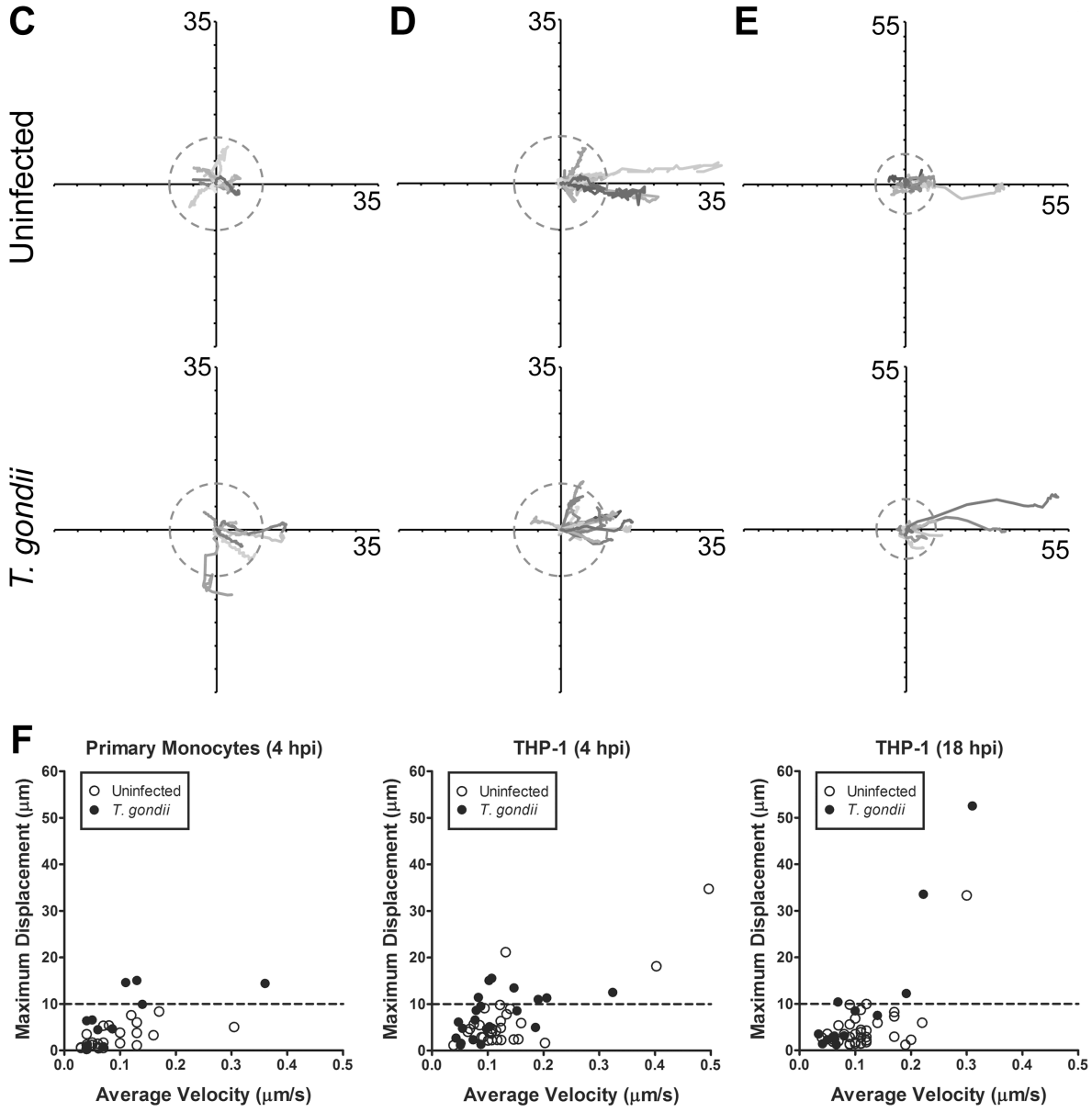

Figure 3.3: Migration of T. gondii-infected and uninfected monocytes during searching (cont.).

(C-E) Cell traces of uninfected and *T. gondii*-infected primary monocytes at 4 hpi (C), THP-1 cells at 4 hpi (D), and THP-1 cells at 18 hpi (E). Each trace begins at the origin and shows the path of a single cell during searching. The dashed circle represents a radius of 10 μm from the origin. The units on the axes are in μm. (F) Graphs showing the maximum displacement and average velocity of individual uninfected (open circles) and infected (closed circles) cells during searching. The dashed line indicates a maximum displacement of 10 μm. Cells exceeding this maximum displacement threshold were defined as performing "wandering" searching. For each cell type and time point, at least three independent experiments were performed, and the data were pooled. For C-F, the following numbers of cells performed searching in the field of view: primary monocytes ($n_{uninfected}$=23, $n_{T.\ gondii}$=11), THP-1 cells at 4 hpi ($n_{uninfected}$=28, $n_{T.\ gondii}$=21), and THP-1 cells at 18 hpi ($n_{uninfected}$=36, $n_{T.\ gondii}$ =14).

high maximum displacement and average velocity of a small number of searching cells, particularly at 18 hpi (Fig. 3.3F). These data indicate that *T. gondii* infection may impart changes in the searching of subsets of monocytes. A potential mechanism for these changes could be the reduced expression or impaired function of adhesion molecules, such as selectins or integrins, on the monocyte cell surface.

T. gondii *does not alter total integrin expression or Mn^{2+}-induced integrin activation*

To investigate the molecular basis for the phenotypes observed under shear flow, we examined the expression of monocyte adhesion molecules. Since selectins tether monocytes to the endothelium and mediate initial rolling, we determined the expression of the E-selectin ligands PSGL-1, CD15, and CD44. Infection did not alter the expression of these ligands (Appendix A.2). We then examined the expression and activation state of the major monocyte integrins. Integrins are heterodimeric receptors comprised of a and b subunits and mediate leukocyte rolling and firm adhesion. *T. gondii* infection did not dramatically change the abundance of LFA-1 (a_Lb_2), VLA-4 (a_4b_1), or MAC-1 (a_Mb_2) on the surface of monocytes at 4 or 18 hpi (Fig. 3.4A). Next, we determined whether parasite infection affects the expression of the active b_1, b_2, or a_M subunits of VLA-4, LFA-1, or MAC-1, respectively, or their ability to become activated upon stimulation with divalent cation. We also examined the expression of talin-1, a cytoskeletal protein that binds to the cytoplasmic tail of integrin b subunits and plays a central role in regulating integrin activation (91). Infection induced a slight increase in the level of active a_M (by 1.4-fold) on the cell surface without affecting active b_1 or b_2 (Fig. 3.4B). *T. gondii* did not affect the ability of Mn^{2+}, which activates integrins (129), to increase active b_1, b_2, or a_M levels (Fig. 3.4B). We observed a modest reduction in talin-1 mRNA (by 1.7-fold at 12 hpi and 1.8-fold at 18 hpi, Fig. 3.4C) and protein levels at 6, 12, and 18 hpi (Fig. 3.4D) in infected monocytes. These data suggest that although *T. gondii* slightly reduced the expression of talin-1 in

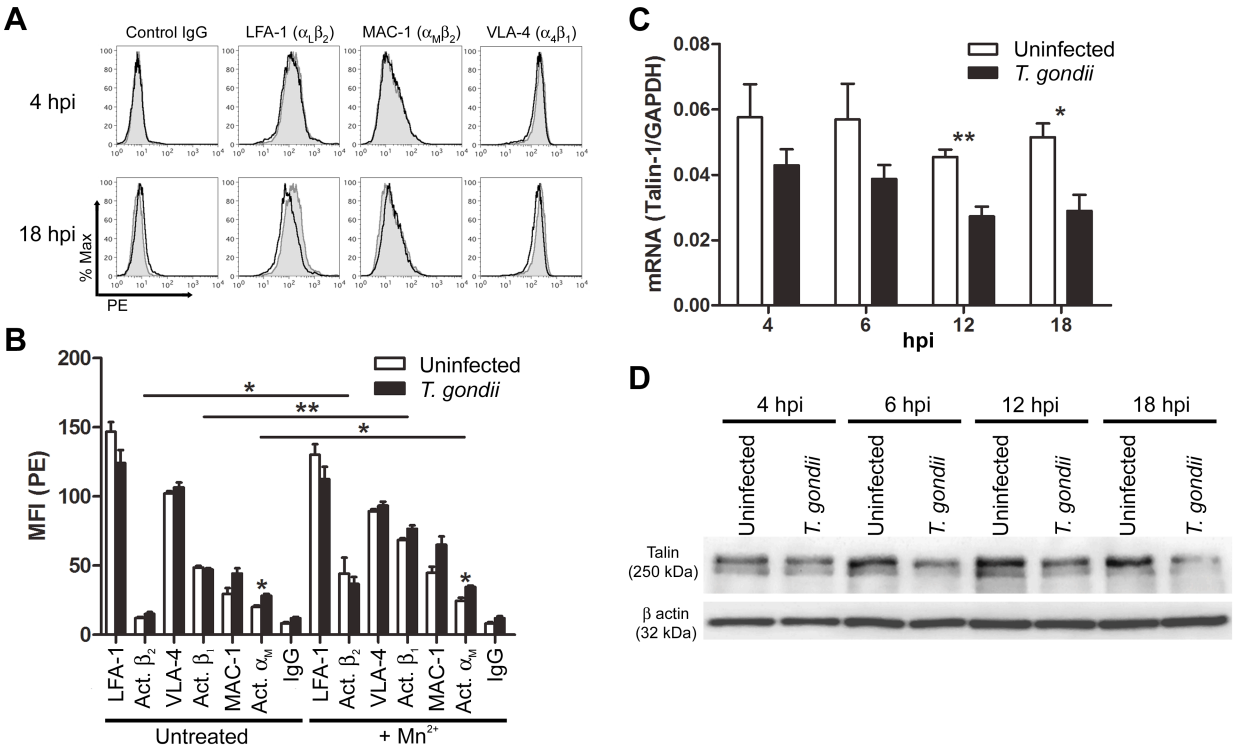

Figure 3.4: Integrin expression and activation in *T. gondii*-infected monocytes.
(A) THP-1 cells were uninfected (gray histograms) or infected with *T. gondii* (black histograms), stained with mAbs against LFA-1, MAC-1, or VLA-4, and analyzed by flow cytometry. Shown are representative plots from one of six independent experiments. (B) THP-1 cells were infected with *T. gondii*, left untreated or stimulated with Mn^{2+}, and stained for LFA-1, VLA-4, MAC-1, or active b_2, β_1, or α_M integrin subunits. The average MFI ± SEM from three independent experiments is shown. *P < 0.01, **P < 0.001. (C) Talin-1 mRNA in uninfected or *T. gondii*-infected THP-1 cells at 4, 8, 12, and 18 hpi was measured by qPCR. The average values ± SEM from three independent experiments are shown. *P < 0.05, **P < 0.01. (D) Proteins from total cell lysate collected at 4, 8, 12, and 18 hpi were analyzed by Western blotting with anti-talin mAb or anti-b-actin mAb. A representative blot from one of three independent experiments is shown.

monocytes at later time-points, infection did not dramatically alter integrin expression or Mn^{2+}-dependent integrin activation.

T. gondii-*infection severely impairs integrin clustering*

Integrin function is governed not only by affinity, but also by valency (130, 131). Valency refers to the number of receptor-ligand bonds that can be made and is governed by the number of receptors expressed and the ability of those receptors to move in the membrane to facilitate clustering (123). During firm adhesion, the cytoskeleton of leukocytes becomes polarized, and cells redistribute and cluster integrins to the point of contact with the endothelium (132). To address the possibility that *T. gondii* infection alters integrin clustering, we imaged the distribution of LFA-1 and VLA-4 on monocytes by confocal microscopy. Monocytes were infected with *T. gondii* and settled onto immobilized ICAM-1/Fc or VCAM-1/Fc. The localization of LFA-1 or VLA-4 in confocal z-sections was determined by sequentially imaging the cells from the base (at the point of contact with ICAM-1 or VCAM-1) to the top surface of the cell. In uninfected cells, LFA-1 and VLA-4 clustered at the base of the cell in contact with ICAM-1 or VCAM-1, respectively (Fig. 3.5A and Appendix A.3A). In contrast, LFA-1 and VLA-4 remained distributed over the entire surface of *T. gondii*-infected cells and were not concentrated at the cell base in contact with ligand (Fig. 3.5B and Appendix A.3A). In uninfected cells, integrin clustering at the cell base positively correlated with pseudopod extension and increased surface area at the point of contact with ligand. Infected cells, however, retained a spherical morphology due to a lack of pseudopods and reduced surface area at the cell base (Fig. 3.5C and D). Monocytes were also settled onto recombinant human IgG to control for possible interactions between monocyte Fc receptors and the Fc domains of the ICAM-1/Fc or VCAM-1/Fc chimeric proteins: both infected and uninfected monocytes failed to cluster LFA-1 or VLA-4 or extend pseudopods on human IgG (Appendix A.3D), indicating that integrin clustering and cell spreading in this system were ligand-dependent. Interestingly, the closely related apicomplexan

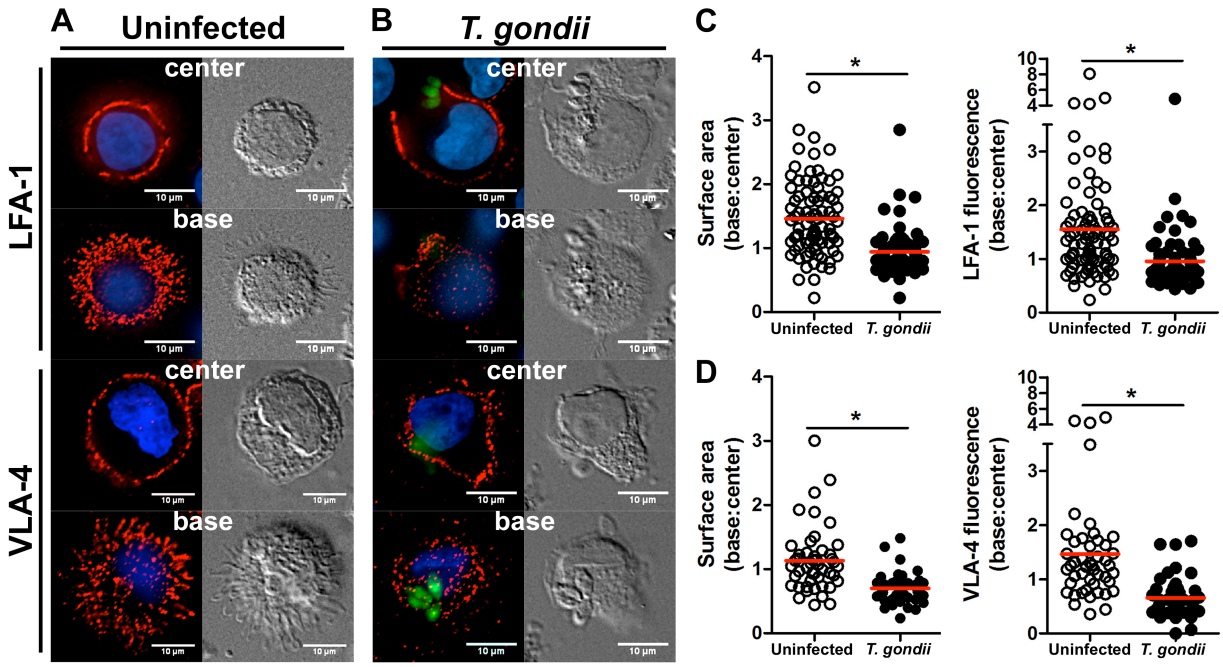

Figure 3.5: Integrin clustering and morphology of *T. gondii*-infected monocytes.
(A, B) THP-1 cells were infected with GFP^{+} *T. gondii* for 18 hr and settled onto immobilized human rICAM-1/Fc or rVCAM-1/Fc. Samples were fixed and stained to detect LFA-1 or VLA-4 for confocal microscopy. Fluorescent and DIC z-sections from the cell base and cell center of uninfected (A) and infected (B) cells are shown. Parasites are shown in green, LFA-1 or VLA-4 in red, and nuclei in blue. (C, D) Differences in surface area and LFA-1 or VLA-4 distribution on uninfected versus infected monocytes when settled onto ICAM-1 (C) or VCAM-1 (D) were quantified as ratios of their respective values at the cell base to the cell center. For C, $n_{uninfected}$=86, $n_{T.gondii}$=73 from four independent experiments. For D, $n_{uninfected}$=47, $n_{T.gondii}$=44 from three independent experiments. The red bar shows the mean. *P < 0.0001.

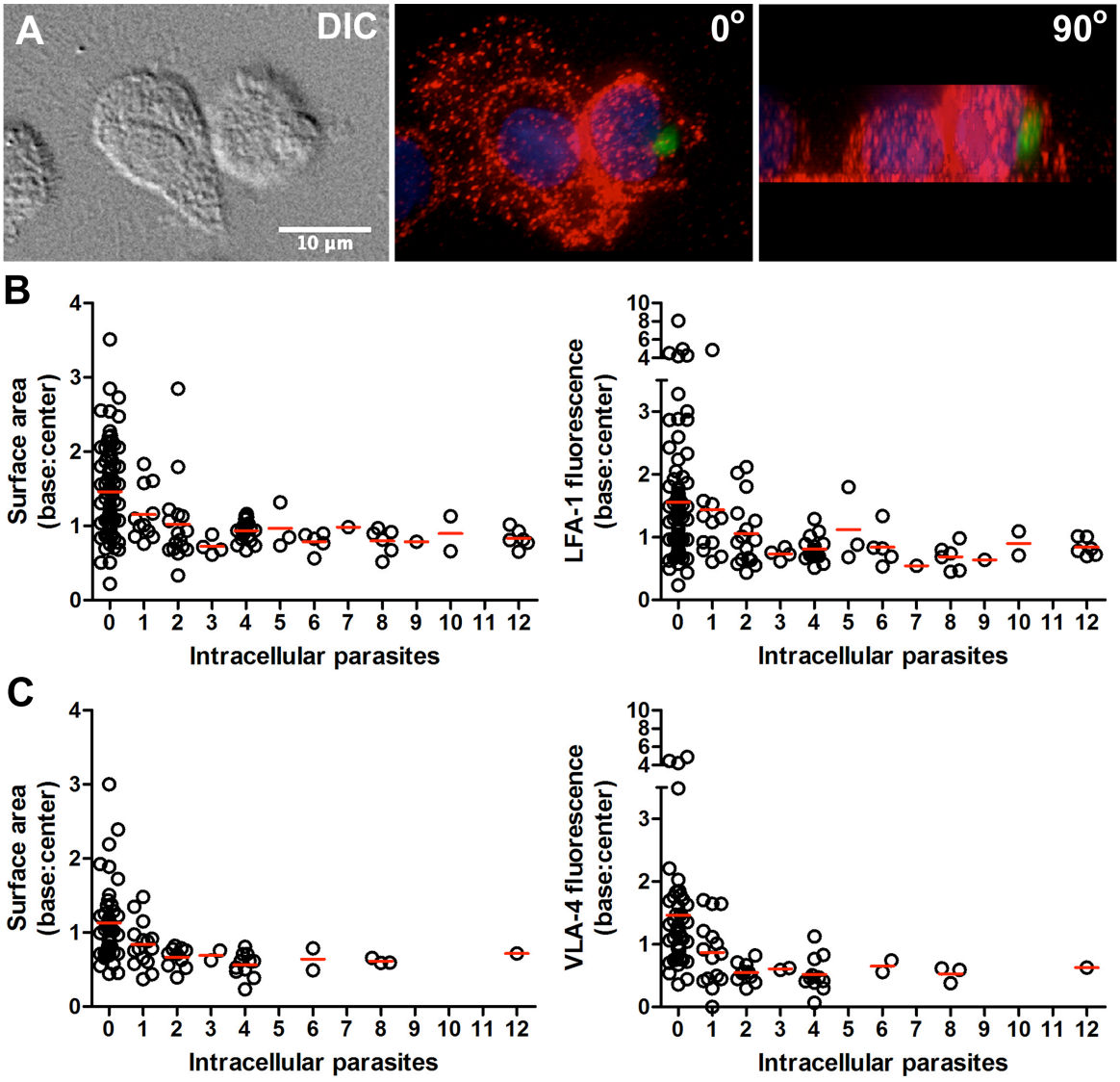

Figure 3.6: Effects of intracellular parasite burden on integrin clustering and cell morphology.
(A) 3D projections of monocytes settled onto ICAM-1 were reconstructed from z-sections. Panels from left to right: DIC micrograph of top-down view, fluorescent micrograph of top-down view (0˚ rotation), and fluorescent micrograph of orthogonal view (90˚ rotation). In each panel, the cell on the left is uninfected, and the cell on the right is infected. Parasites are shown in green, LFA-1 in red, and nuclei in blue. These cells can also be seen in Video S2. (B, C) Differences in LFA-1 or VLA-4 distribution and surface area of THP-1 cells settled onto ICAM-1 (B) or VCAM-1 (C) were plotted with respect to parasite burden. There was no significant correlation between changes in LFA-1 or VLA-4 distribution or surface area and the number of intracellular parasites, using one-way ANOVA with a Tukey comparison. The red bar shows the mean.

parasite *Neospora caninum* induced similar changes in infected monocytes (Appendix A.3B and C), suggesting that these effects are not unique to *T. gondii* and may be a shared feature of other parasitic infections.

Lastly, we examined whether the reduced integrin redistribution and pseudopod extension in infected cells correlated with parasite burden. Surprisingly, a single parasite was sufficient to inhibit both integrin clustering and cell spreading of *T. gondii*-infected monocytes (Fig. 3.6A, Appendix A Movie 2). There was no correlation between intracellular parasite number and cell spreading or integrin redistribution on either ICAM-1 (Fig. 3.6B) or VCAM-1 (Fig. 3.6C) in cells containing from one to twelve parasites (from replication and/or multiple invasion events). Therefore, we conclude that differences in LFA-1 and VLA-4 clustering and cell spreading in infected monocytes were independent of the number of intracellular parasites.

Discussion

T. gondii infection of circulating immune cells has been shown to facilitate parasite passage across endothelial barriers and migration from the bloodstream into organs including the brain (38, 39, 48). The infection of DCs, particularly with the type II strain of *T. gondii,* was shown to induce a “hypermotility” phenotype, which contributes to dissemination (39, 42). Infected DC actively transmigrated across retinal endothelium using ICAM-1, VCAM-1, and activated leukocyte cell adhesion molecule (ALCAM) (65). In addition, a recent report demonstrated that the soluble *T. gondii* dense granule protein GRA5 induces CCR7-dependent migration of human DCs (133). In a blood-brain barrier model examining infected mouse peripheral blood mononuclear cells (PBMC), infected $CD11b^+$ cells transmigrated to a greater degree than infected $CD11c^+$ cells (48). These studies all support the idea that *T. gondii*-infected cells contribute to parasite dissemination across biological barriers. What remained unknown were the dynamics of infected human monocyte adhesion to endothelium in conditions of shear stress. We have used live cell imaging to address this step upstream of transmigration.

Dynamic imaging approaches have provided valuable insights into the migration and interaction of murine immune cells during *in vivo T. gondii* infection in lymph nodes (46, 134, 135) and the brain (136-138). Our current study contributes to a growing understanding of host-parasite interactions by comparing the adhesion dynamics of infected and uninfected primary human monocytes. This approach revealed that under shear stress conditions, *T. gondii*-infected monocytes tether, roll, firmly adhere, and search/crawl. Interestingly, they roll at higher velocity and over greater distances than uninfected cells. Whether this extended rolling contributes to the long-distance migration of intracellular parasites away from the initial site of infection remains to be determined by *in vivo* experiments. A population of monocytes is known to 'patrol' resting endothelium by long-range crawling and rapidly invading damaged or infected tissues (58). Indeed, a central function of monocytes is the highly efficient homing to sites of inflammation. Infected monocytes, however, have a "cargo" of intracellular parasites that are known to modulate host cell function. Our findings indicate that parasite infection alters monocyte rolling, but ultimately, the infected cells undergo firm adhesion and searching on the endothelium. Defining the mechanisms that mediate the subsequent stage of extravasation, namely transmigration in shear stress conditions, is of great interest and under active investigation.

The extended rolling of infected monocytes suggested that *T. gondii* induced a delayed transition to firm adhesion. Although infection did not change the expression of the selectin ligands CD44, CD15, and PSGL-1 on the surface of monocytes, we cannot rule out that altered selectin function may be involved in some aspect of infected monocyte rolling. Given the critical role of integrins in mediating rolling and firm adhesion, we suspected a potential impairment in integrin function. Notably, *T. gondii* infection did not reduce the total expression of integrins on the cell surface; however, it is known that integrin activity is largely regulated by affinity conformation and valency. LFA-1 in the bent, inactive conformation binds ICAM-1 with such low affinity that it cannot mediate the transition from rolling to firm adhesion under fluidic stress (132,

139). In response to chemokines, GPCR-dependent mechanisms activate LFA-1 via “inside-out” signaling, leading to increased LFA-1 affinity for ICAM-1 (63). Mn^{2+} is a potent inducer of integrin activation and promotes ligand binding (129). Interestingly, *T. gondii* slightly reduced the expression of the adaptor protein talin-1, which is required for GPCR-dependent activation of LFA-1, but did not affect Mn^{2+}-induced integrin activation. Infection did result in an increase in the level of active a_M (MAC-1), which is involved in monocyte crawling (140). Whether the slightly increased frequency of wandering infected monocytes in our system is due to alterations in MAC-1 affinity remains to be determined.

Integrin signaling is bidirectional, such that binding to ligand induces “outside-in” signaling that increases integrin affinity and avidity and activates downstream signaling cascades (63). The redistribution of LFA-1 to ICAM-1 occurs during firm adhesion and diapedesis of neutrophils (131) and monocytes (141), and results in leukocyte polarization as high affinity integrins mobilize toward ligand. On monocytes, LFA-1 organizes into lipid raft “nanoclusters” (130) that are stabilized by extracellular Ca^{2+} (141). Studies have documented close interplay between the cytoskeleton and cell membrane plasticity in LFA-1 (142) and VLA-4 (143) redistribution. We found that *T. gondii* infection impaired the ability of monocytes to redistribute LFA-1 and VLA-4 in response to ICAM-1 and VCAM-1. To our knowledge, these findings are the first report of pathogen dysregulation of integrin clustering.

The altered adhesion dynamics of monocytes at 4 hpi indicated that the changes in adhesion caused by *T. gondii* occurred relatively early during infection (i.e., prior to parasite replication). In addition, monocytes containing one or multiple parasites exhibited similar phenotypes under fluidic stress. This is consistent with the observation that a single intracellular parasite was sufficient to dysregulate integrin clustering and cell morphology. Interestingly, *N. caninum*-infected monocytes exhibited a similar phenotype, although the effect was less dramatic. *N. caninum* and *T. gondii* are similar in size and shape, and it is possible that the impaired integrin redistribution results from constrained cytoskeletal dynamics due to the

presence of the intracellular parasites. As noted above, however, the degree of integrin clustering did not correlate with parasite burden, suggesting that these effects may not be mediated solely by the physical presence of the parasites. An alternative possibility is that *N. caninum* and *T. gondii*, which are highly related, carry effector proteins that similarly affect host cell adhesion dynamics. During invasion *T. gondii* is known to secrete proteins into host cells, which can modulate a variety of host cell processes and contribute to virulence (144-147). It has yet to be determined whether parasite-secreted proteins or events after parasite invasion and the establishment of a parasitophorous vacuole lead to integrin dysregulation. It is likely that many intracellular pathogens are capable of modulating the adhesion or migration of infected cells. The infection of red blood cells by *Plasmodium falciparum* facilitates adhesion to ICAM-1 on vascular endothelium (148), and it is believed that the sequestration of *P. falciparum*-infected red blood cells in capillary beds may lead to alterations in the microcirculation. Given the important role of adhesion proteins in a variety of intercellular interactions and cell migration processes, they may represent a common target of pathogens. By targeting the expression, activation, or regulation of adhesion molecules on host cells, pathogens may influence their trafficking in the host organism. For example, enhancing dissemination to a particular tissue site that is more hospitable or contributes to transmission.

It will be of great interest in future studies to further dissect the mechanisms by which *T. gondii* dysregulates the cell adhesion machinery. It is likely that the impact of *T. gondii* on infected monocyte migration in the vasculature is the result of a combinatorial effect, and delineating these pathways will be important for understanding parasite dissemination and ultimately disease pathogenesis.

Acknowledgments

We would like to thank all members of the Tenner, Nelson, Prescher, and Morrissette labs for helpful discussion on this project. We also thank Dr. Michael Buchmeier for the generous use of his microscope, Dr. Michael Cahalan and Milton Greenberg for help with the cell tracking analysis, Elizabeth Clarke for monocyte isolation, and Dr. Anthony James for comments on the manuscript, and Dr. Diane Campbell for help with statistical analysis.

CHAPTER 4

SHEAR FORCES ENHANCE *TOXOPLASMA GONDII* TACHYZOITE MOTILITY ON VASCULAR ENDOTHELIUM

Introduction

T. gondii is a single-celled eukaryotic parasite that is found worldwide (3). Infection predominantly occurs through the ingestion of parasite tissue cysts or oocysts from contaminated food or water (149). In immune-competent individuals, a robust cellular and humoral immune response controls the infection, and the parasite establishes a latent state. In immune-suppressed individuals, however, infection can result in severe toxoplasmosis, typically presenting as chorioretinitis in the eye (21) or cerebral infection resulting in encephalitis with associated clinical features including headache and dementia (34). These manifestations of disease can be due to reactivation of encysted parasites or to acute infection (3).

The spread of *T. gondii* from the intestine into secondary tissues is critical for pathogenesis, in that the presence of actively replicating tachyzoites in these secondary tissues contributes to tissue damage and symptomatic disease (119). Infection results in colonization of the heart, brain, eye, skeletal muscle, and kidney (149, 150). Many recent studies on *T. gondii* dissemination have focused on an intracellular mode of transport in motile leukocytes (38-40, 102, 151). However, free *T. gondii* are found in the blood of acutely infected mice (38) and humans (70), and *in vitro* assays have shown that extracellular tachyzoites can adhere to and cross polarized epithelial cell barriers (64) and retinal endothelium (66), suggesting that an extracellular mode of dissemination may also be employed, depending on the tissue or site in the body.

T. gondii uses an actomyosin motor complex to power substrate-dependent gliding motility and invasion (7). The parasite adhesion proteins are exposed extracellularly from apical secretory organelles called the micronemes. These adhesins are anchored to the parasite surface via their cytoplasmic domains, which associate with the parasite actin cytoskeleton via an aldolase bridge (152). The adhesins “treadmill” along the length of the parasite, propelling it forward, and are cleaved at the posterior end. *T. gondii* gliding motility has been largely studied *in vitro* by the examination of adhesion trails (8, 153) or by live cell microscopy (78, 154) on

protein-coated glass. Håkansson *et al*. defined three major types of parasite motility: circular and helical gliding, which produce net forward movement, and twirling, which does not (78). Similar modes of movement have also been described for other members of the phylum Apicomplexa, including *Plasmodium* (77) and *Cryptosporidium* sporozoites (80).

T. gondii dissemination in the body occurs via the circulation. To leave the bloodstream and enter tissues, the parasites must adhere to vascular endothelial cells and cross the endothelial barrier in conditions of blood flow. Whether *T. gondii* are capable of completing this processes as extracellular tachyzoites has not been examined. Using a system combining live cell microscopy with microfluidic devices we have performed an in-depth analysis of parasite adhesion and motility in conditions of physiologic shear stress. Remarkably, *T. gondii* undergo adhesion and gliding on human endothelium in flow conditions. Fluidic shear stress significantly influenced motility dynamics and the outcome of parasite interactions with endothelium. Lastly, we identified a distinct role for MIC2 in the initial adhesion events of *T. gondii* to endothelium in conditions of shear flow.

Results

Extracellular T. gondii adhere to endothelium and are motile in shear stress conditions

To examine *T. gondii* tachyzoites in conditions of fluidic shear stress, we modified our previously described fluidic system (151) to a microfluidic scale. We characterized parasite interactions with primary HUVEC and with fetal bovine serum (FBS)-coated glass, which is commonly used to examine *T. gondii* motility (78, 81, 155). *T. gondii* tachyzoites were syringe-lysed from human foreskin fibroblast (HFF) monolayers and filtrated through a 5.0 μm syringe filter to remove cellular debris. Tachyzoites were then added to wells of a chamber slide (static condition) or perfused into a microfluidic channel (flow condition) at 0.5 dyn/cm^2, and movements were tracked at the apical end of the parasite for the 30 sec after contact with either HUVEC or FBS. Interestingly, extracellular *T. gondii* were capable of adhesion and motility in

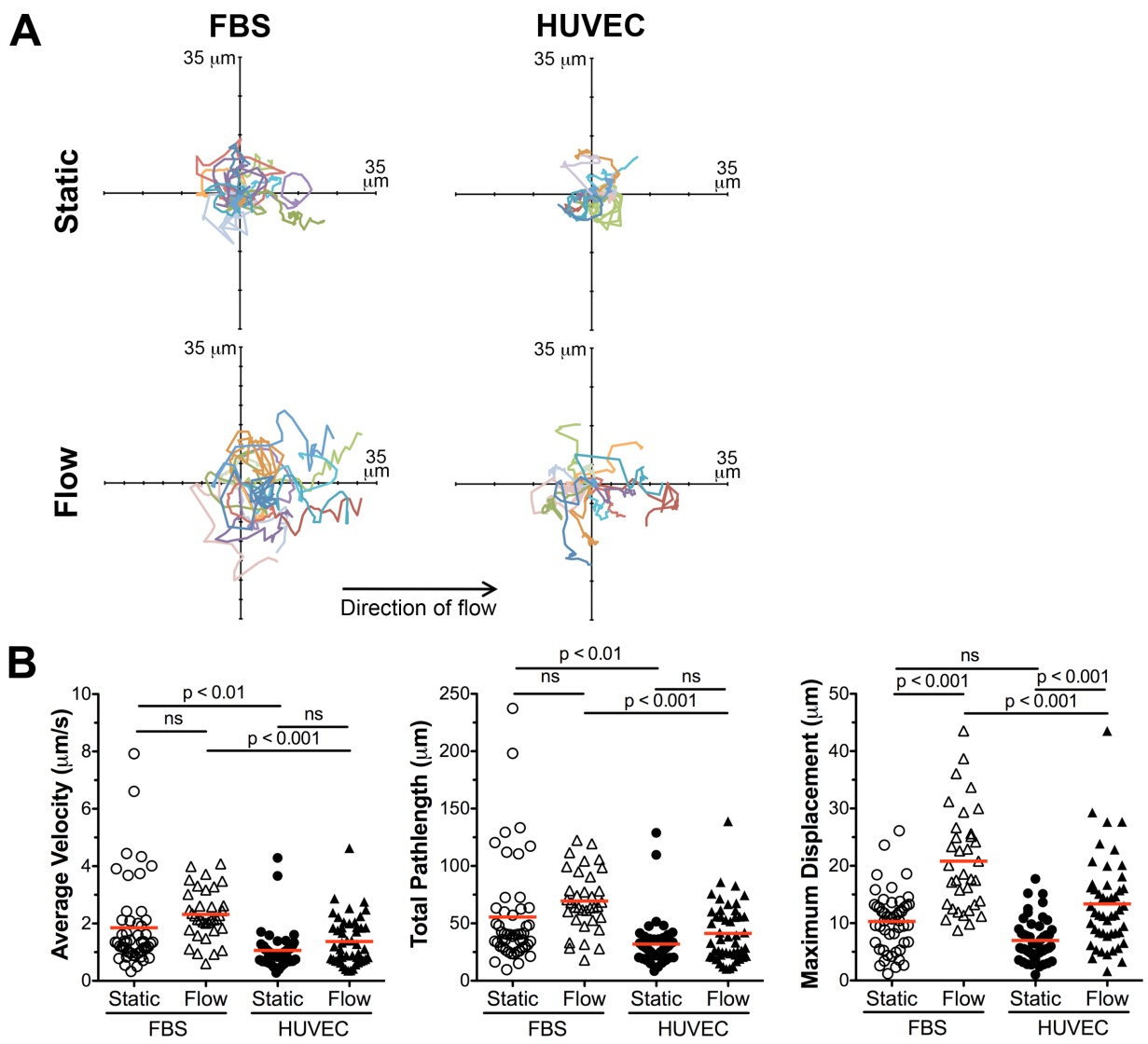

Figure 4.1: Extracellular *T. gondii* adhere to and are motile on HUVEC in static and shear stress conditions.
T. gondii tachyzoites were added to FBS-coated glass or confluent monolayers of HUVEC in either a chamber slide (static conditions) or in the microfluidic channel (flow conditions). (A) Representative cell traces of extracellular tachyzoites on FBS or HUVEC in static or flow conditions are shown. Each trace begins at the origin and shows the path of a single parasite (n=15 for all conditions). The direction of flow is from left to right. (B) The average velocity, total pathlength traveled, and maximum displacement reached by each parasite during their first 30 sec post-adhesion is shown. Each data point represents a single parasite. 3 independent experiments were performed, and the data were pooled ($n_{FBS, Static}$=50, $n_{FBS, Flow}$=35, $n_{HUVEC, Static}$=50, $n_{HUVEC, Flow}$=49). The red bar indicates the mean for the group. ANOVA with a Tukey comparison of all means was used to compare multiple means.

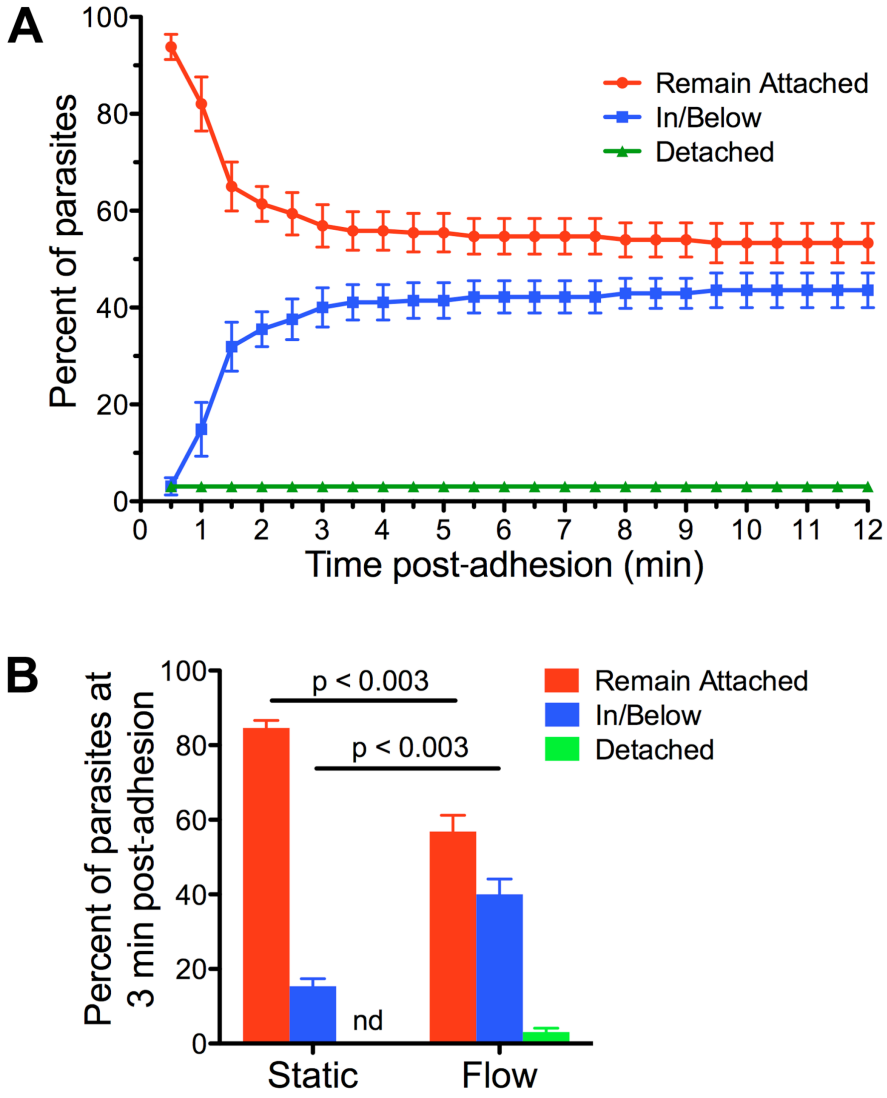

Figure 4.2: Influence of shear stress on *T. gondii* movement into and/or across the endothelium over time.
(A) *T. gondii* tachyzoites were flowed over HUVEC in the microfluidic channel for 12 min, and their interactions with the endothelium were analyzed. Parasites were considered adherent when they were in contact with the endothelial surface for a minimum of 4 sec. The location of each adherent parasite was assessed at 30 sec intervals post-adhesion. The percentages of parasites that remained attached (red circles), moved in/below (blue squares), or detached (green triangles) from the HUVEC are shown. Three independent experiments were performed, and the data were pooled. n=211. Bars represent the mean ± SEM. (B) *T. gondii* tachyzoites were added to HUVEC in either a chamber slide (static conditions) or in the microfluidic channel (flow conditions). At 3 min post-adhesion, the percentages of parasites that remained attached (red), moved in/below (blue), or in the flow condition, detached (green) from the HUVEC are shown (n_{Static}=431, n_{Flow}=211). For each condition, at least two independent experiments were performed, and the data were pooled. Bars represent the mean ± SEM. "nd" indicates no data. The Student's two-tailed *t*-test with Welch's correction was used for pairwise comparisons.

shear stress conditions on both HUVEC and FBS (Appendix B Movies 1 and 2, respectively). In both static and shear stress conditions, parasites that adhered to FBS moved at higher velocities than those that adhered to HUVEC. In addition, parasites that adhered to FBS traveled greater distances from where they initiated adhesion than those that adhered to HUVEC (Fig. 4.1 and Appendix B.1). The total pathlength is the total distance a parasite travels, whereas the maximum displacement is the greatest distance a parasite travels from the point where it initially adheres. Interestingly, the introduction of shear flow significantly increased the maximum displacement of tachyzoites on both substrates, without affecting their total pathlength (Fig. 4.1B). In either condition parasites are active and moving and produce similar pathlengths, however the influence of shear force on the direction of movement, tendency for movement in the direction of flow (Fig. 4.1A), could explain the enhanced displacement.

We next wanted to determine if shear force influenced the likelihood of parasites remaining attached to the endothelial surface or of invasion or migration across the endothelial barrier. To address this, we observed tachyzoites interacting with endothelium in flow conditions for 12 min and categorized their location every 30 sec after their adhesion to the monolayer. We found that parasites remained attached to the endothelial surface, moved into or below the endothelium (identified as dim by DIC illumination), or detached from the monolayer (Fig. 4.2A). Tachyzoite movement in the z-direction was most dynamic in the first four minutes immediately after adhesion: most of the parasites that entered the monolayer did so within 4 min, and beyond this time point, there were very few changes in parasite location in the z-direction. Since parasite motility is mediated by external exposure of adhesins that are finite, this timescale for active movement may be influenced by the availability of adhesins. To determine whether the addition of shear force influenced parasite invasion or migration across the monolayer, we compared parasite location in static and flow conditions within this dynamic period. In static conditions, 85% of the parasites remained on the surface of the HUVEC at 3 min post-adhesion, whereas 15% had entered the endothelium (Fig. 4.2B). Notably, we observed a nearly 2.5-fold

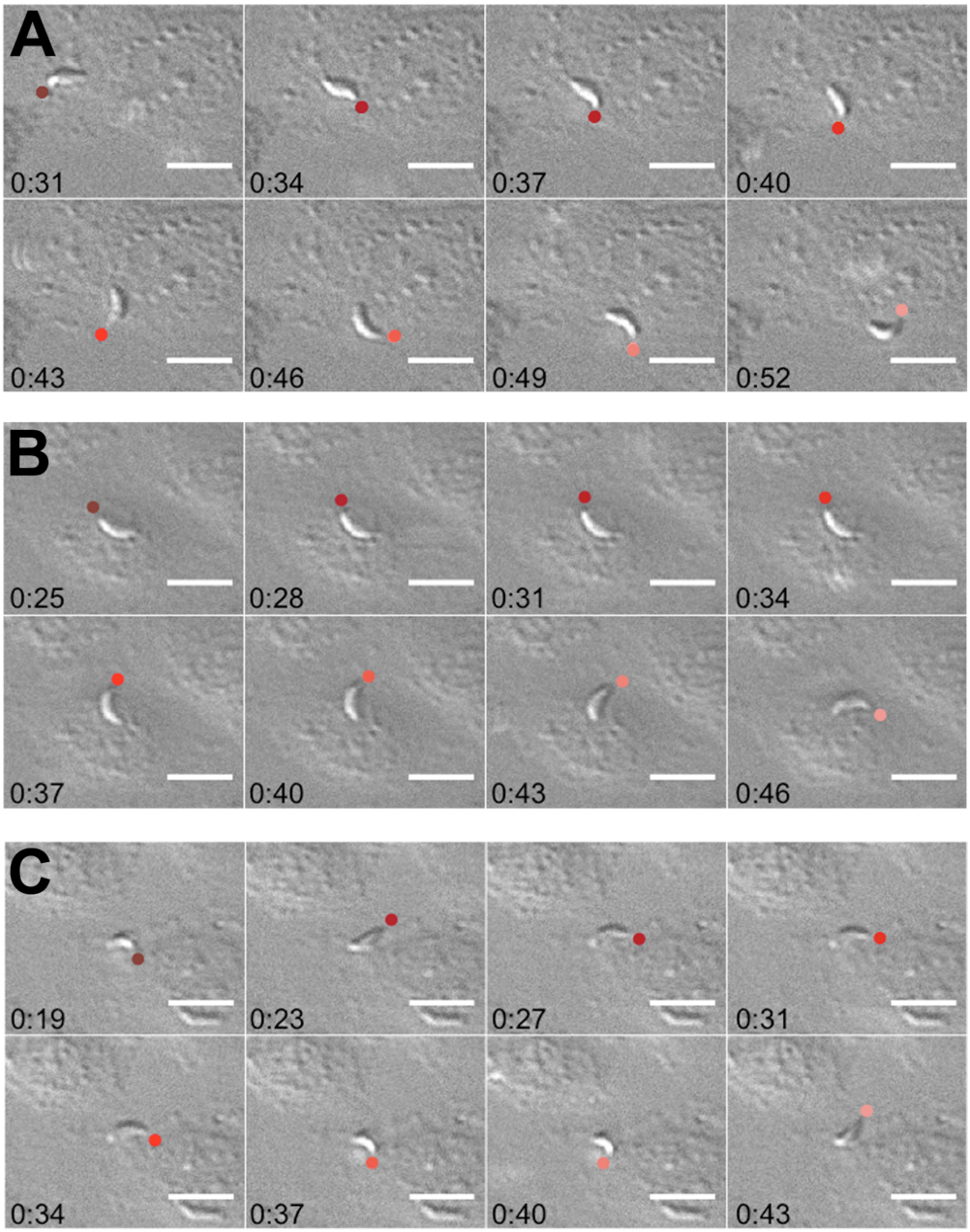

Figure 4.3: Modes of T. gondii motility on HUVEC in shear stress conditions.
T. gondii tachyzoites were flowed over HUVEC at 0.5 dyn/cm2. Cell tracking software was used to track the movements at the apical end of the parasite (designated with a colored circle). Representative time-lapse images of parasites performing (A) helical gliding, (B) circular gliding, or (C) twirling are shown.

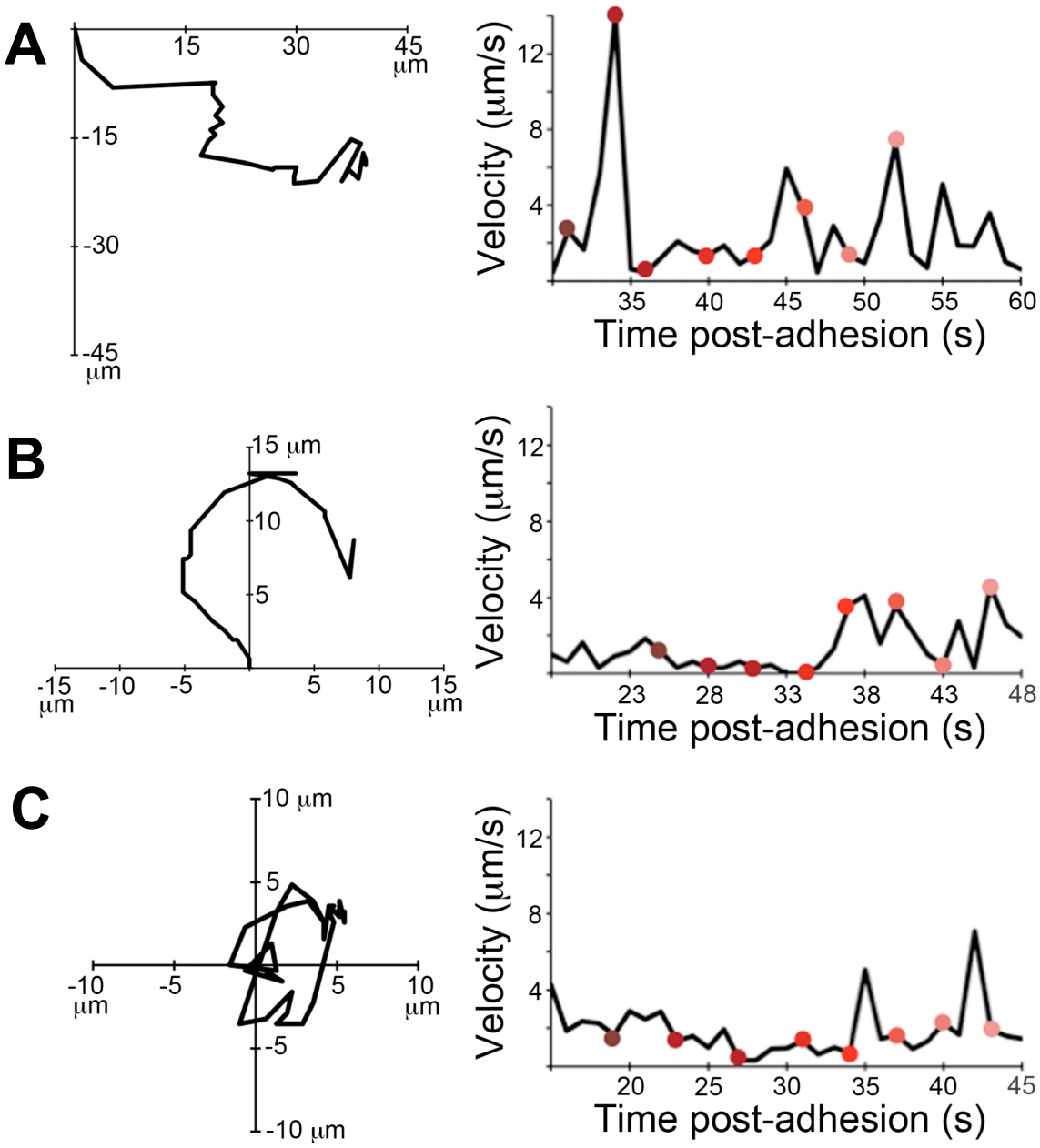

Figure 4.3: Modes of T. gondii motility on HUVEC in shear stress conditions (cont.). The path of the apical end of the parasite and the instantaneous velocity at the apical end is shown for each mode of motility. The colored dots in the velocity vs. time plots correspond to those in the time-lapse images. The direction of flow is from left to right. The scale bars are 10 μm.

increase in the percentage of parasites that migrated into or below the HUVEC monolayer in conditions of shear stress (Fig. 4.2B). Collectively, these data suggest that shear forces significantly affect parasite movement and the outcome of tachyzoite interactions with endothelium.

Characterization of T. gondii motility on HUVEC in shear stress conditions

To qualitatively and quantitatively examine parasite migration in flow conditions, a detailed analysis of motility was performed. In conditions of shear stress, parasites performed all three types of *T. gondii* movement (78): helical gliding, circular gliding, and twirling. Tachyzoites also moved "non-productively", characterized by stretching and retracting along the longitudinal axis and oscillation, which did not produce net forward movement along the plane of the substrate. Motionless tachyzoites were also observed and were characterized as stationary. Time-lapse images and videos of representative parasites performing helical gliding, circular gliding, or twirling on endothelium in shear stress conditions were acquired (Fig. 4. 3 and Appendix B Movie 3-5). The path and velocity of each parasite, as determined by tracking at the apical end, are shown. Tracking was done at the apical end because this allowed for clear resolution of the transitions between the different modes of parasite motility. Moreover, apical end tracking allowed us to gain information about parasite movements that did not necessarily result in net forward motion. For instance, tracking twirling parasites at the apical end permitted an analysis of twirling "velocity," which varied for individual parasites. During helical gliding (Fig. 4.3A and Appendix B Movie 3), a characteristic 180° rotation around the longitudinal axis occurred between 0:31 and 0:34 sec, producing a spike in instantaneous velocity (Fig. 4.3A), as has been previously reported (78). Two additional helical turns occurred between 0:43 and 0:46 and between 0:49 and 0:52. After each turn, the parasite reoriented, moving at velocities of up to 2 μm/sec. During circular gliding, the counterclockwise circular motion of the parasite was

evident in the shape of the trace produced from tracking analysis (Fig. 4.3B). In contrast to helical gliding, circular gliding occurred at relatively low velocities (typically less than 4 μm/sec), and was characterized by momentary pauses (Appendix B Movie 4). During twirling, the parasites oriented vertically, with the posterior end anchored to the substrate, and a tilting rotation was observed (Fig. 4.3C and Appendix B Movie 5). On average, the apical end of parasites in shear stress conditions twirled at relatively low velocity (2-4 μm/sec) with sporadic peaks in instantaneous velocity indicative of a reorientation event similar to that of helical gliding, but without net forward movement parallel to the endothelial monolayer. A minority of the population was also observed performing higher velocity twirling (> 7 μm/sec).

We frequently observed tachyzoites performing multiple modes of motility over time (Fig. 4.4A, B and Appendix B Movie 6). To better understand these complex parasite movements and the effects of substrate and fluidic shear stress, parasite motility was classified at either 10 sec or 60 sec after adhesion to either FBS or HUVEC and in static or flow conditions (Fig. 4.4C-D). The percentages of parasites that were moving, non-productive, or stationary in each condition are shown (Fig. 4.4C). For those parasites that were moved productively in Fig. 4.4C, the absolute numbers of parasites performing helical or circular gliding, or twirling were graphed (Fig. 4.4D). For parasites on FBS, the percentage of the parasite population that was motile remained relatively constant over time (Fig 4.4C), but the addition of shear stress resulted in a significantly larger portion of parasites performing helical gliding (Fig 4.4D). In contrast, for parasites that adhered to HUVEC, shear stress conditions increased the proportion of motile parasites immediately following adhesion (10 sec) and specifically enhanced helical and circular gliding; however, these highly dynamic modes of motility declined over time (60 sec). When we examined the motility of a representative subset of 15 parasites during their entire first minute post-adhesion, we observed similar trends (Fig. 4.5). We also observed a fraction of parasites that reinitiated motility after prolonged stationary periods. These data indicate that flow

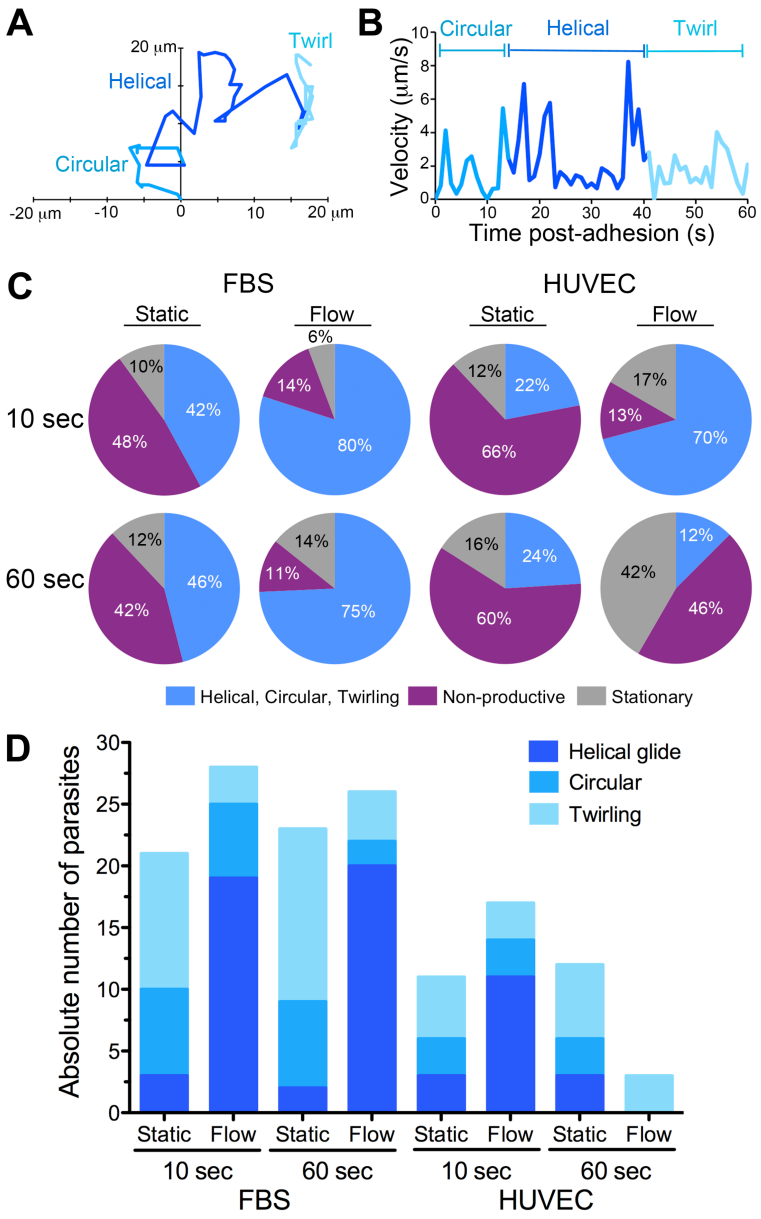

Figure 4.4: Characterization of parasite motility in static and shear stress conditions. *T. gondii* tachyzoites were added to FBS or HUVEC in either a chamber slide (static conditions) or in the microfluidic channel (flow conditions). (A) A tachyzoite performing three modes of motility within 1 min post-adhesion to HUVEC in flow conditions is shown. (B) A velocity plot over time is shown for the parasite in panel A. (C) The percentages of motile (blue), non-productive (purple), and stationary (grey) parasites at either 10 sec or 60 sec after adhesion to FBS or HUVEC in static or flow conditions are shown. ($n_{FBS, Static}$=50, $n_{FBS, Flow}$=35, $n_{HUVEC, Static}$=50, $n_{HUVEC, Flow}$=49). (D) The absolute numbers of motile parasites (from panel C) undergoing helical or circular gliding, or twirling at either 10 sec or 60 sec after adhesion to FBS or HUVEC in static or flow conditions are shown. ($n_{FBS, Static, 10\ sec}$=21, $n_{FBS, Flow, 10\ sec}$=28, $n_{FBS, Static, 60\ sec}$=23, $n_{FBS, Flow, 60\ sec}$=26, $n_{HUVEC, Static, 10\ sec}$=11, $n_{HUVEC, Flow, 10\ sec}$=17, $n_{HUVEC, Static, 60\ sec}$=12, $n_{HUVEC, Flow, 60\ sec}$=3. For (A, B and D), helical gliding (dark blue), circular gliding (medium blue), twirling (light blue).

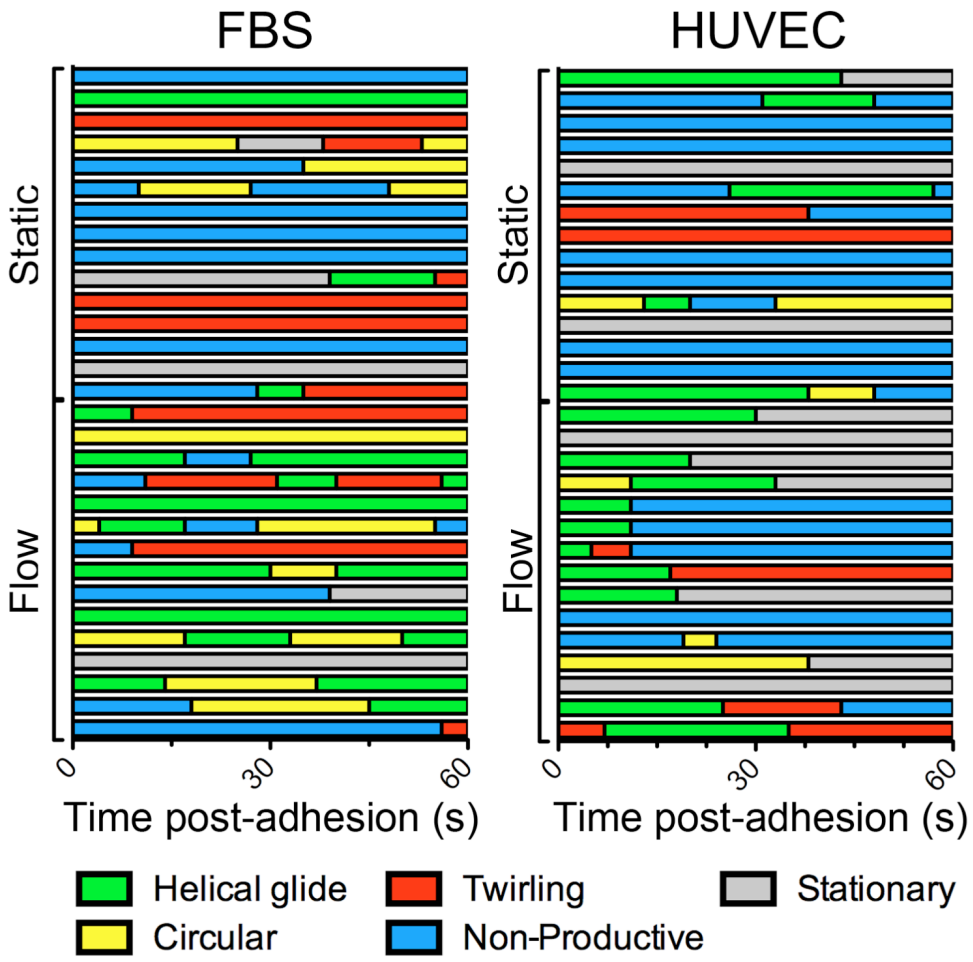

Figure 4.5: Parasite motility over time in static and shear stress conditions.
T. gondii tachyzoites were added to FBS or HUVEC in either a chamber slide (static conditions) or in the microfluidic channel (flow conditions). The motility of a representative subset of 15 parasites in each condition over time is shown, with each bar representing the motility of a single parasite. Helical gliding (green), circular gliding (yellow), twirling (red), non-productive movement (blue), stationary (grey).

conditions increased dynamic, productive motility (helical and circular gliding) immediately after attachment, which may contribute to the increased displacement observed for parasites under shear stress (Fig. 4.1).

Initial and sustained parasite adhesion at increasing shear force

The initial adhesion and in-depth motility analyses of extracellular tachyzoites were performed at 0.5 dyn/cm^2, a relatively low physiological shear stress (100). To address the effects of higher levels of shear stress on parasite adhesion, *T. gondii* tachyzoites were flowed over confluent monolayers of HUVEC at 0.5, 2, 5, or 10 dyn/cm^2 for 3 min, and adhesion events were counted. An adhesion event was defined as a parasite that appeared on the endothelial surface and remained attached in the plane of focus for a minimum of 4 sec. As shear force increased, we observed a decrease in the number of adhesion events (Fig. 4.6A and Appendix B.2).

We next investigated the adhesion strength of tachyzoites by examining their response to an increase in shear stress. This can be addressed by allowing adhesion to occur in static or low shear conditions and then increasing the flow rate (156). To do this, tachyzoites were flowed over HUVEC at 0.5 dyn/cm^2 for 3 min to allow for adhesion, and then the shear stress was maintained at 0.5 dyn/cm^2 or increased to 2, 5, or 10 dyn/cm^2 for an additional 3 min. Parasites could adhere at any point during the first 3 min of flow; however, only those that were attached to the HUVEC surface at the switch in shear force were analyzed. The percent of adherent tachyzoites that remained attached, entered the monolayer (in/below), or detached after the switch in shear stress was determined. We found that the percentage of adherent parasites that detached from the monolayer increased as shear stress increased (Fig. 4.6B). The increase in shear stress, however, did not affect the proportion of parasites that entered the monolayer (in/below category in Fig. 4.6B). These data indicate that the intensity of the shear stress influences the number of parasites that adhere to the endothelium and their ability to sustain

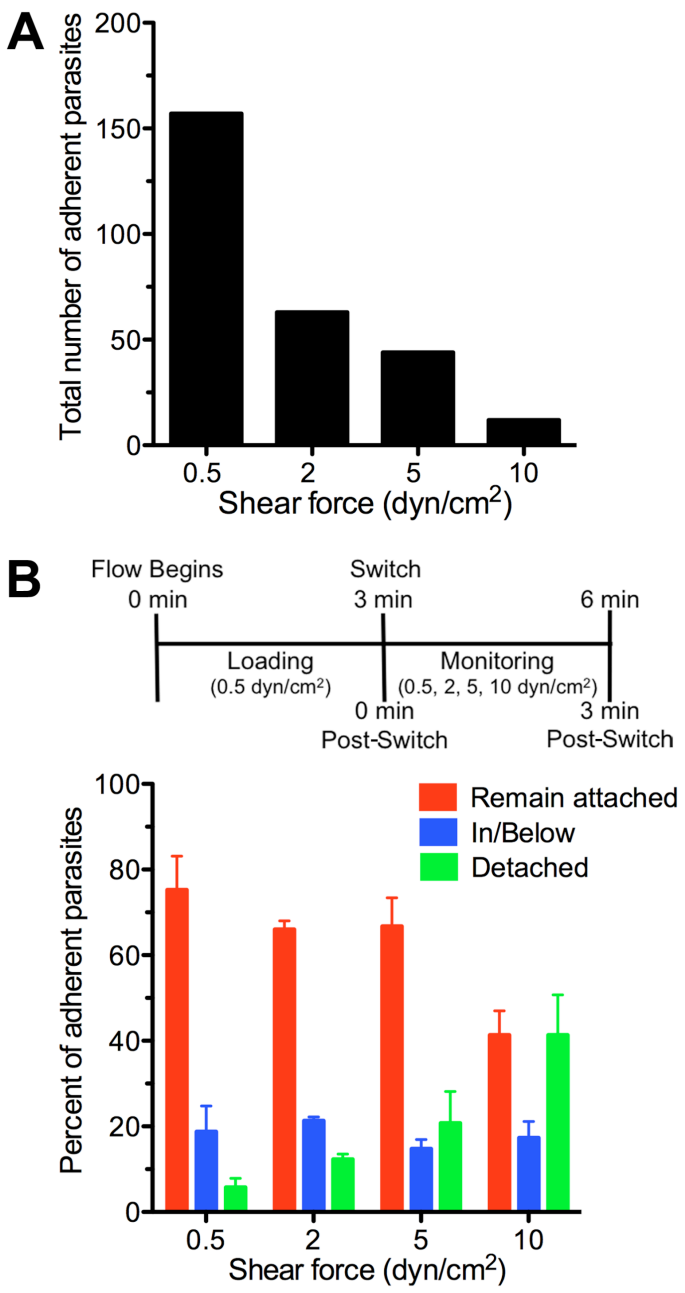

Figure 4.6: Initial and sustained adhesion at increasing shear force.
T. gondii tachyzoites were flowed over confluent monolayers of HUVEC in the microfluidic channel. (A) The total numbers of parasite adhesion events at shear forces of 0.5, 2, 5, and 10 dyn/cm^2 are shown. This graph represents aggregated data from 4 independent microfluidic experiments. n=468. (B) *T. gondii* were flowed over HUVEC at 0.5 dyn/cm^2 for a 3 min "loading" phase. The shear force was then maintained at 0.5 dyn/cm^2 or switched to 2, 5, or 10 dyn/cm^2. Those parasites that were attached to the endothelial surface at the switch were monitored for an additional 3 min. The percentage of adherent parasites that remained attached, moved inside/below, or detached from the HUVEC monolayer during the "monitoring" phase is shown. Bars represent the mean ± SEM. n=276 from 4 independent experiments.

adhesion; however, it does not appear to affect their likelihood of moving into or below the monolayer, at least at shear forces up to 10 dyn/cm^2.

Invasion or transmigration of T. gondii in shear stress conditions

We reasoned that parasites migrating into or below the monolayer may be invading the endothelium, as has been previously reported (157), or transmigrating across the endothelial barrier via a paracellular or transcellular route. We also wanted to determine if shear force influenced these possible outcomes of movement into the monolayer. For the static condition, tachyzoites were incubated on HUVEC monolayers for 20 min then washed and fixed. For shear stress conditions, *T. gondii* were flowed over the endothelium for 1-2 min, and a y-valve connector was used to flow media alone without disrupting flow for a total of 20 min. Fluidic channels were then perfused with fixative. In both conditions the cells were then stained with antibodies against the parasite dense granule protein GRA7, as a marker for invasion. In extracellular tachyzoites GRA7 is found in the dense granules, whereas in infected host cells GRA7 localizes to the parasitophorous vacuole (PV) lumen (158). In both static and flow conditions, we observed tachyzoites that appeared dim by DIC illumination (in/below) and were either surrounded by GRA7 staining or not (Fig. 4.7A). In static conditions 81% of DIC dim parasites localized to GRA7$^+$ vacuoles, whereas 19% were not associated with GRA7 staining. Interestingly, flow conditions significantly increased the percentage of DIC dim parasites that were GRA7$^-$ (35% of the population) (Fig. 4.7B). The DIC dim GRA7$^-$ population likely included parasites that had completed transmigration and were under the monolayer. Indeed, in live cell imaging experiments, we have observed tachyzoites that continued to migrate under the endothelium after entering the monolayer. We cannot exclude the possibility that some of the DIC dim GRA7$^-$tachyzoites were in the process of transcytosis at the time of analysis (in a vesicle that lacked GRA7) or had invaded immediately prior to fixation and had yet to secrete a sufficient amount of GRA7 into the PV to be detectable by immunofluorescence assay (IFA).

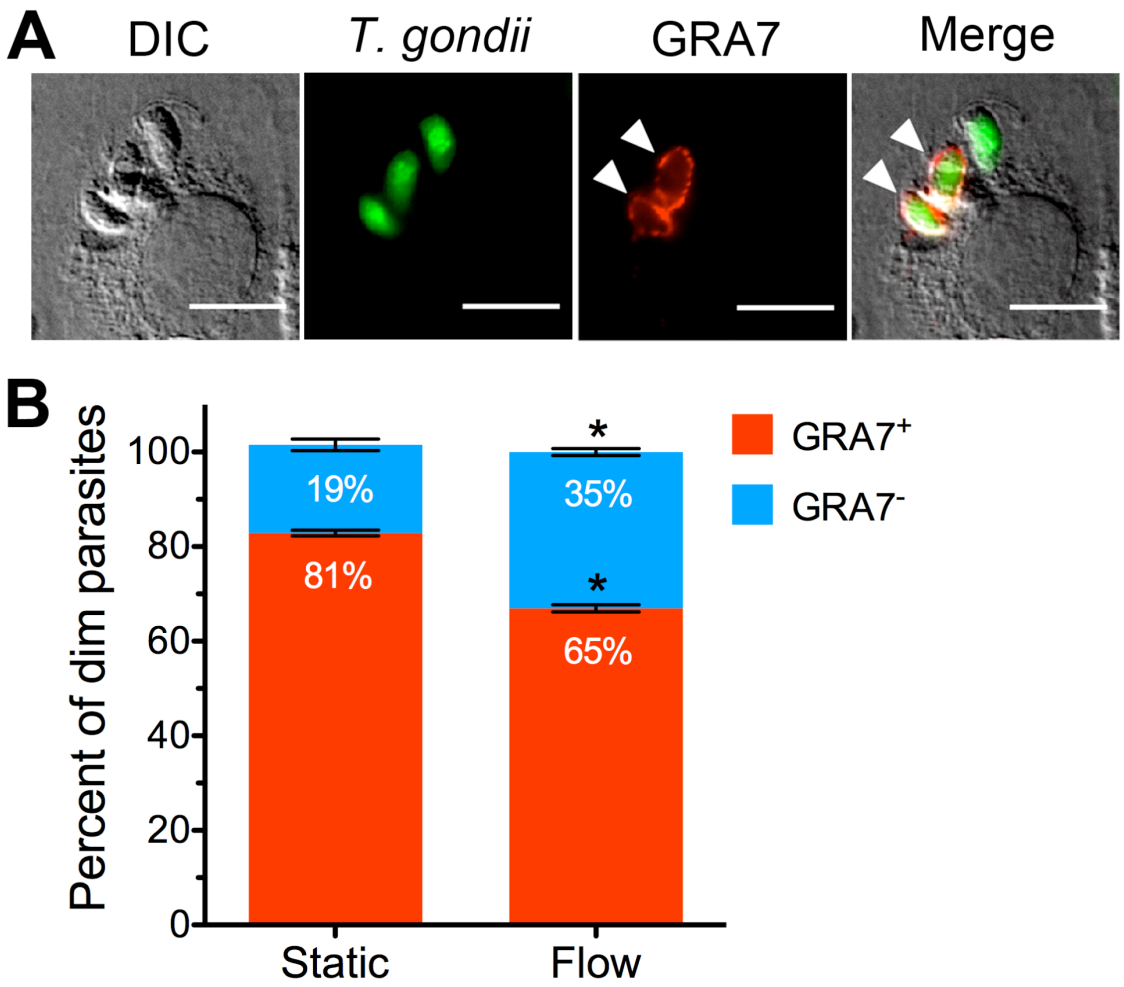

Figure 4.7: Invasion or transmigration of *T. gondii* in static and shear stress conditions. *T. gondii* were incubated for 20 min with a HUVEC monolayer in either static or shear stress conditions. Coverslips or fluidic channels were then fixed and stained with antibodies against GRA7. (A) Sample micrographs depict DIC dim parasites (previously categorized as in/below in **Fig 2 and 6B**) that are either GRA7$^+$ (white arrowheads) or GRA7$^-$. The scale bar is 10 μm. (B) The percentages of DIC dim parasites associated with GRA7 are shown. For each condition, two independent experiments were performed and the data were pooled, n_{Static}=499, n_{Flow}=309. Bars represent the mean ± SEM. The student's two-tailed *t*-test with Welch's correction was used for pairwise comparisons, * $p < 0.01$ for comparisons between the static and flow conditions.

Collectively, these data indicate that the majority of tachyzoites that adhere to the endothelium in shear stress and static conditions invade the endothelial cells of the monolayer and form a PV, and that flow conditions may result in a greater percentage of parasites that breach the barrier and undergo transmigration. The route of these transmigration events, through the junctions in a paracellular manner or through the cell body by transcytosis, remains to be determined, though our data does not exclude either possibility.

Role of MIC2 in adhesion to HUVEC in shear stress conditions

We next sought to address the role of parasite adhesion proteins in interactions with the endothelium under shear stress conditions and the possibility that different parasite adhesins may contribute to distinct stages of the *T. gondii* adhesion cascade in shear stress. One of the best characterized *T. gondii* surface proteins associated with adhesion and motility is the microneme protein MIC2 (72, 81, 82, 86, 159). In static assay conditions, MIC2 was found to be important for attachment to host cells, helical gliding, and invasion (81). However, a role for MIC2 has not yet been examined in adhesion to vascular endothelium or in conditions of shear stress. To address this possibility, we employed a conditional MIC2 knockdown system developed and generously provided by the Carruthers Lab (81). Parental tTA-dhfr parasites and the Δ*mic2e/mic2i* conditional MIC2 knockdown parasite line, which uses a tetracycline responsive promoter to control the expression of MIC2, were used. The addition of anhydrotetracycline (ATc) to these genetically modified cultures reduced the expression of MIC2 by both immunofluorescence assay (Fig. 4.8A) and Western blot (Fig. 4.8B). The tTA-dhfr and ATc-treated Δ*mic2e/mic2i* tachyzoites were fluorescently labeled, mixed 1:1 and perfused over a HUVEC monolayer, and adhesion events under flow conditions were counted along the entire length of the fluidic channel. A sample of the mixture was used to determine the input ratio (variable across experimental replicates, 40-60%:40-60%) of the two strains by both flow cytometry and by microscopy (data not shown). The ratio of tTA-dhfr and ATc-treated

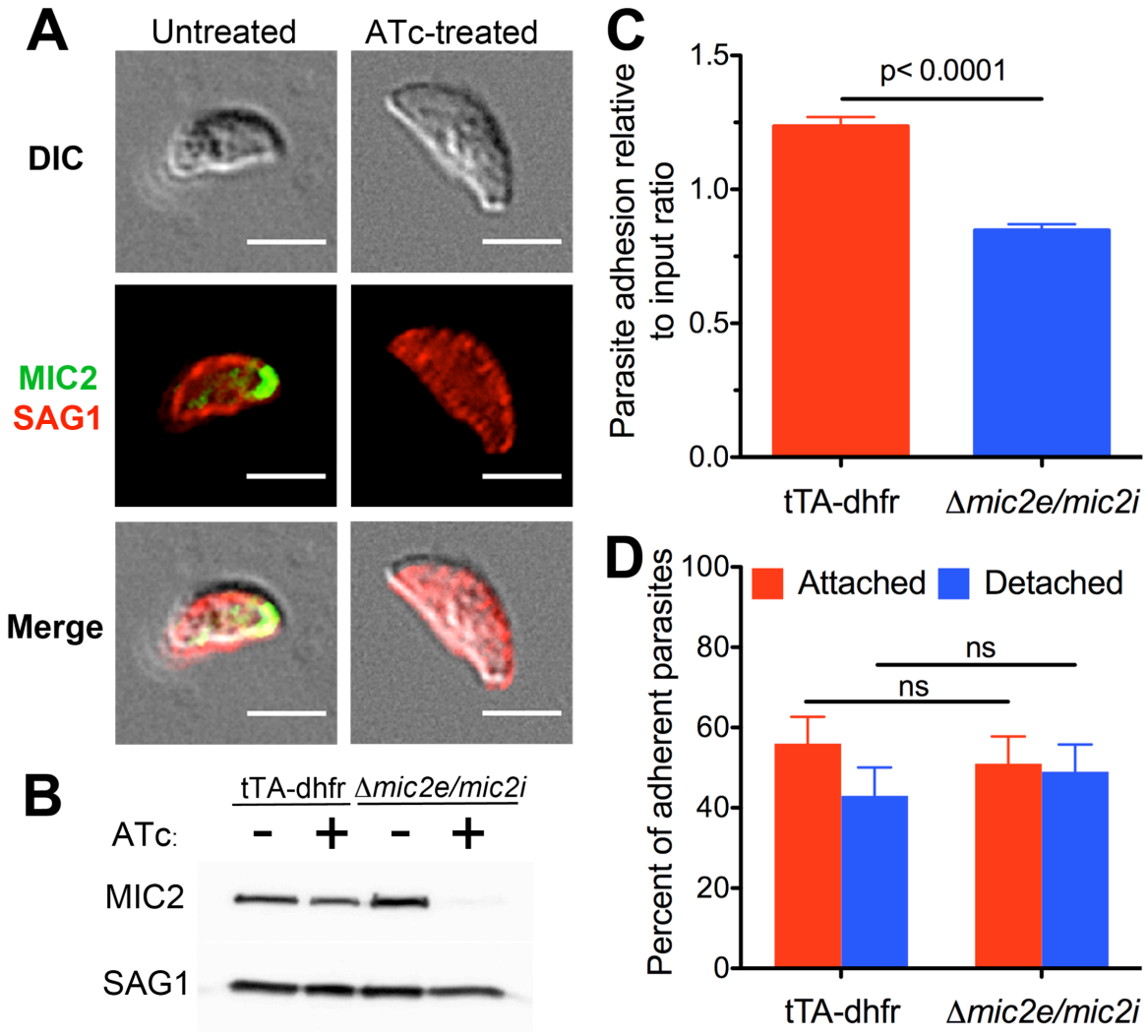

Figure 4.8: Role of MIC2 in adhesion to HUVEC in shear stress conditions.
(A) The Δ*mic2e/mic2i* parasites were treated with ATc for 2 days. Extracellular tachyzoites were stained with antibodies against MIC2 or SAG1 and imaged by DIC and fluorescence for MIC2 expression. (B) tTA-dhfr and Δ*mic2e/mic2i* parasites were untreated or treated with ATc for 2 days. Western blotting was performed to detect MIC2 or SAG1 in the parasite lysates. (C) tTA-dhfr tachyzoites were mixed 1:1 with ATc-treated Δ*mic2e/mic2i* tachyzoites and flowed over HUVEC. The parasites were allowed to adhere for 3 min, and DIC and fluorescence images were captured along the entire length of the channel while still under flow. Parasite adhesion relative to the input ratio is shown. A value of 1.0 would represent equivalent adhesion of the two populations. $n_{tTA\text{-}dhfr}$=1120, $n_{ATc\text{-}treated\ \Delta mic2e/mic2i}$=1073 from 3 independent experiments. (D) A mixture of tTA-dhfr and ATc-treated Δ*mic2e/mic2i* parasites were flowed over HUVEC in the microfluidic channel at 0.5 dyn/cm^2 for 3 min, and then the shear stress was increased to 10 dyn/cm^2 for an additional 3 min. The percent of adherent parasites that remained attached or detached after the increase in shear stress is shown. $n_{tTA\text{-}dhfr}$=70, $n_{ATc\text{-}treated\ \Delta mic2e/mic2i}$=88 from 2 independent experiments. For A, the scale bar is 5 μm. For C and D, error bars represent the mean ± SEM, and the Student's two-tailed *t*-test with Welch's correction was used for pairwise comparisons. "ns" indicates not significant.

Δ*mic2e/mic2i* tachyzoite adhesion events in the channel relative to the input ratio was calculated. A value of 1 indicates equivalent adhesion of the two populations. We observed a consistent underrepresentation of the ATc-treated Δ*mic2e/mic2i* parasites compared to the tTA-dhfr parasites (Fig. 4.8C). To control for the possiblity that treatment with ATc affected adhesion, we evaluated the adhesion of ATc-treated and untreated tTA-dhfr parasites in static conditions and found no significant difference in their adhesion (Appendix B.3A). In addition, when we examined adhesion in a static assay, we observed a similar underrepresentation of ATc-treated Δ*mic2e/mic2i* parasites compared to the tTA-dhfr parasites (Appendix B.3B). These data indicate that MIC2 contributes to *T. gondii* adhesion to endothelium in shear stress; however, a portion of ATc-treated Δ*mic2e/mic2i* parasites were still capable of adhesion in these conditions. Although we observed that MIC2 levels were substantially reduced in Atc-treated parasites, it is possible that a low level of MIC2 expression in these treated parasites contributed to this residual adhesion.

We next investigated a potential role for MIC2 in adhesion strengthening in conditions of increasing shear stress. To do this, a mixture of tTA-dhfr and ATc-treated Δ*mic2e/mic2i* tachyzoites were perfused over a HUVEC monolayer at 0.5 dyn/cm^2 to allow adhesion to occur. The shear stress was then increased to 10 dyn/cm^2. The percent of tachyzoites that remained attached or that detached from the monolayer after the increase in shear force was calculated. Interestingly, the tTA-dhfr and ATc-treated Δ*mic2e/mic2i* tachyzoites remained similarly attached to the endothelium after the increase in shear stress to 10 dyn/cm^2 (Fig. 4.8D): for both populations of parasites, approximately 50% of the tachyzoites detached after the transition to increased shear force. Collectively, these data suggest that MIC2 plays an important role in the initial phase of tachyzoite attachment to the endothelium but is not required for adhesion strengthening, and that other parasite adhesins may mediate these sustained interactions with the endothelium.

Discussion

Dissemination of *T. gondii* from the primary site of infection to secondary tissues is thought to occur through both intracellular and extracellular mechanisms (119). To leave the bloodstream, tachyzoites interacting with blood vessel walls must contend with the mechanical forces of shear stress. Live-cell microfluidic systems provide a highly tunable method for characterizing cellular adhesion and motility and analyzing the role of specific adhesins in attachment to human cellular substrates in flow conditions. Our current study shows that tachyzoites can adhere to and migrate on vascular endothelium in conditions of physiologic shear stress. In addition, we found that shear forces enhance dynamic motility and the likelihood of invasion and/or transmigration, both of which are critical components of pathogenesis. These findings support the relevance of including mechanical force as an additional experimental parameter in understanding patterns of parasite migration. In addition, recent work on *T. gondii* motility in a three-dimensional system revealed that tachyzoites move through matrigel in a corkscrew-like trajectory distinct from that observed in two-dimensional assays, further reinforcing the value of incorporating conditions that more closely mimic *in vivo* environments (160).

Multistep adhesion cascades are used by both circulating mammalian cells (123) and pathogens (76, 95) to exit the bloodstream. However the precise manner in which these interactions occur appears to vary. Initial adhesion interactions, often referred to as “tethering” or “capture,” are transient, occur at high velocities, and serve to decelerate the adhering cell. In *B. burgdorferi*, tethering is mediated by the fibronectin binding domain of the bacterial adhesin BBK32 and is the essential first interaction that decelerates the bacterium and brings it into close contact with the endothelial cell surface (76). For *P. berghei*, initial sporozoite adhesion to glass flow chambers required the parasite adhesins TRAP and S6 (95). Following initial adhesion, transient adhesion associated with a phase of rolling or active motility occurs. *P. berghei* sporozoites wave or glide (95), whereas *B. burgdorferi* perform dragging mediated by

the glycosaminoglycan binding domain of BBK32 (76). Subsequently, a transition to firm adhesion occurs. For *B. burgdorferi* a period of “stationary adhesion” near endothelial cell junctions immediately follows dragging and precedes transmigration and escape from the vasculature (75). A similar period of sustained firm adhesion prior to extravasation has been documented for *P. berghei* exiting blood vessels in the mouse dermis (161). We frequently observed that *T. gondii* gliding on endothelium was punctuated by periods of motionless activity, sometimes lasting several minutes, prior to reinitiation of migration. One potential explanation for these patterns is fluctuation in intracellular cation concentration. Intraparasitic calcium mobilization has been shown to coordinate microneme secretion (162) and influence motility (163). In addition, parasite egress is regulated by both potassium and calcium flux (164). As tachyzoites sense the dynamic chemical environment created by shear flow they may be responding to changes in local ion concentrations by fluxing cations. These changes in intracellular ion concentration could generate bursts of microneme secretion of parasite adhesins and result in the punctuated movement we observe in our system.

Our data suggest that *T. gondii* tachyzoite adhesion to endothelium in shear stress conditions could also be divided into a multistep cascade. It is likely that a combination of adhesion molecules, potentially with overlapping functions, mediate *T. gondii* adhesion in shear stress conditions. In our studies, MIC2 clearly played a role in this process. However, in conditions of increasing shear stress the MIC2-deficient parasites remained as adherent as the parental control parasites, implying a role for MIC2 in initial parasite adhesion that may be distinct from adhesion strengthening. One potential ligand for MIC2 on the endothelium is ICAM-1. MIC2 has been shown to interact with ICAM-1 to mediate *T. gondii* transepithelial migration (72), and ICAM-1 dependent transmigration across retinal endothelium has been observed (66). In our assays, a portion of the MIC2-deficient parasites was capable of adhesion to endothelium in shear stress conditions, indicating that other parasite factors may contribute to this process. *T. gondii* has been shown to use a broad range of sulfated glycosaminoglycans to bind to

substratum and host cells in static systems (165). Other microneme proteins are also known to contribute to parasite adhesion, invasion and virulence in mice (166). MIC1 binds host glycans, and a conserved microneme adhesive repeat (MAR) recognizes sialic acid and contributes to invasion (167, 168). The chitin binding-like domain of MIC3 is required for attachment to host cells (83, 169). Single gene disruptions of either MIC1 or MIC3 produce mild virulence defects; however double knock-outs produce a severe virulence defect *in vivo* (83). Also, the *T. gondii* surface antigen 3 (SAG3) can mediate the recognition of cell surface proteoglycans, such as heparin (170), and SAG3 deficient parasites have a 50-60% adhesion deficit in *in vitro* assays and an 80% reduction in virulence *in vivo* (171). Whether carbohydrate-mediated adhesion interactions contribute to tachyzoite capture, motility, sustained adhesion, or transmigration in shear stress conditions remains to be investigated.

Interestingly, *T. gondii* migrated farther and at higher velocities on FBS than on endothelial cells, suggesting that the endothelium itself may be a barrier to motility. This may be due to the varied topography of the endothelium and to the adhesion molecules expressed on the endothelial surface. In addition, vascular endothelium is heterogeneous in both structure and function (172), suggesting that the processes by which tachyzoites adhere to distinct endothelial cell types may also differ. Endothelial permeability is also highly modulated by acute and chronic inflammation. *T. gondii* infection induces an inflammatory response characterized by the expression of IL-12, TNF-α, and IL-6 (173). *T. gondii* infection of brain endothelial cells up-regulates the expression of ICAM-1 (48), and infection of human retinal epithelial cells up-regulates ICAM-1 and the inflammatory cytokines IL-1 and IL-6 (174). The stimulation of endothelial cells with proinflammatory mediators induces a pro-adhesive phenotype termed “endothelial cell activation” (175, 176). “Activated” endothelium expresses elevated levels of adhesion molecules and has decreased tight junction integrity, resulting in an increase in barrier permeability (177). The unique response of endothelium to infection-induced inflammatory mediators in a given tissue may impact the likelihood of parasite invasion of that tissue.

Ultimately, understanding how these interactions allow *T. gondii* dissemination out of the circulation will provide novel insight into mechanisms of parasite spread into tissues and the development of disease.

Acknowledgments

We thank all the members of the Morrissette, Prescher, Tenner and Nelson labs for thoughtful discussion of the project. We also thank Dr. Michael Buchmeier for the generous use of his microscope and Dr. Peter Bradley for sharing the GRA7 antibody. Lastly, we are grateful to Drs. Vern Carruthers and My-Hang Huynh for sharing parasite strains and antibodies and for their helpful discussion of the project.

CHAPTER 5

CONCLUSIONS AND FUTURE DIRECTIONS

Dissemination of *T. gondii* tachyzoites from the primary site of infection to secondary tissues is critical to pathogenesis and the establishment of chronic infection. To reach these secondary sites tachyzoites must contend with the dynamic environment of blood flow. Tachyzoites are thought to use both intracellular and extracellular routes to accomplish this migration. Our goal is to better understand the intricate interactions between the co-opted host cell and the extracellular tachyzoite with the endothelium in this dynamic environment. To address these types of questions we developed an *in vitro* fluidic microscopy system to observe and analyze the interactions of infected monocytes and extracellular tachyzoites with vascular endothelium. The aim of this system is to recapitulate the dynamic microenvironment of the vasculature *in vitro* using primary human cells. This system has allowed us to investigate the mechanisms by which parasites manipulate monocyte-endothelial cell interactions as well as how they interact directly with the endothelium in the context of fluidic shear stress.

We have shown that *T. gondii*-infected human monocytes can adhere to vascular endothelium in conditions of shear stress and that their adhesion dynamics are altered by infection. Infected monocytes rolled at significantly higher velocities and over greater distances (Fig. 3.2) and a subpopulation exhibited an extended crawling migration (Fig. 3.3). Our investigation of the molecular mechanism for these phenotypes revealed impaired integrin clustering and pseudopod extension in infected human monocytes (Fig. 3.5).

Using a further improved fluidics system we then examined the adhesion and motility of extracellular *T. gondii* tachyzoites to vascular endothelium in shear stress conditions. Tachyzoites adhered to endothelium and their migration was enhanced by shear flow. Compared to static conditions, tachyzoites in shear stress exhibited an increased displacement and more readily entered the monolayer (Fig. 4.1-2). Our evaluation of the contributions of the parasite adhesin MIC2 to these processes revealed a role for MIC2 in the initial adhesion of tachyzoites to endothelium in shear flow conditions (Fig. 4.8).

There are three predominant *T. gondii* strain types found throughout North America and Europe (149). These strain types differ in their virulence in mice and our investigations have used both the virulent type I and avirulent type II strains. It has been suggested that parasite strain type might influence dissemination strategy (119, 178). Infection with type I *T. gondii* is associated with high pathogenicity in mice (179) and the ability to rapidly reach a high parasite burden in distal tissues (37). Type I tachyzoites can transmigrate across mouse intestine *ex vivo* and exhibit an enhanced capacity for transmigration across polarized epithelium *in vitro* compared to the avirulent type II and type III strains. Additionally, a subpopulation of virulent type I *T. gondii* have been associated with a long-range migration phenotype (64).

Our data show that type I tachyzoites can adhere to vascular endothelium in shear stress conditions and retain motility. The presence of shear force influenced tachyzoite movement, significantly increasing displacement and movement into/below the endothelium. The majority of tachyzoites that moved into/below the monolayer in either static or shear stress conditions were invading the endothelial cells. However, the addition of shear flow also increased the number of tachyzoites not associated with the parasite vacuole marker GRA7, indicating that shear flow may increase the fraction of tachyzoites that undergo transmigration. Additionally, type I tachyzoites exhibited the classical modes of motility described for *T. gondii* in shear flow conditions, and fluidic shear stress increased the number of parasites found performing the most dynamic and productive modes of motility, namely helical gliding, immediately following adhesion. Collectively, these data suggest that the virulent type I strain may be employing an extracellular mode of migration as its primary means of dissemination, as has previously been proposed (42). Preliminary experiments examining the adhesion of type II tachyzoites to endothelium in shear flow conditions indicate that they can adhere under flow (data not shown), however an in-depth analysis of their movement has yet to be completed.

Since many studies provide evidence of successful dissemination of type II and III parasites *in vivo* (37, 38), these strain types may be relying on an intracellular mechanism. All

parasite strain types induce a hypermotility phenotype in DCs; however, the type II and III strains induced the greatest increase in transmigration capacity (39, 42). The adoptive transfer of infected DCs favors the dissemination of type II and type III parasites over type I (42). Similarly, when type II parasites are injected into the vasculature as extracellular parasites or in infected leukocytes they disseminate further when intracellular (180). An oral infection model has shown that the type II strain parasitizes neutrophils recruited to the intestine and appears to use them to facilitate spread throughout the host (45). Recently, a noncanonical and strain-specific pathway for *T. gondii* invasion of macrophages through the phagosome has been reported (181). The authors of this paper suggest that the strain-specific phagosome to vacuole invasion (PTVI) pathway maybe a mechanism by which the avirulent strains co-opt motile phagocytes and enhance their dissemination.

We have shown that type II *T. gondii*-infected human monocytes tether, roll, firmly adhere, and search/crawl on TNF-α activated endothelium in shear stress conditions, and that the dynamics of this adhesion are altered by infection. *T. gondii*-infected monocytes rolled at greater velocities and over greater distances than uninfected monocytes. Low velocity searching movement was found to be quite similar between infected and uninfected cells; however, a subset of the infected monocytes exhibited “wandering” searches that extended beyond 10μm from where searching was initiated. These data indicate that the avirulent type II *T. gondii* strain can co-opt multiple motile leukocyte populations and influence their migration as a means of intracellular dissemination. A preliminary examination of the adhesion of type I infected monocytes to endothelium in shear flow revealed no significant strain-specific differences in rolling adhesion compared to type II infected monocytes (data not shown), however a more extensive investigation of tethering, crawling and transmigration would be required to fully explore any strain-specific differences in the modulation of human monocyte adhesion and movement on endothelium.

Additionally, our data suggests that when compared to uninfected monocytes, infected monocytes are less adhesive. This is may seem counterintuitive when considering the invasive nature of infection and the pathogen's drive to disseminate in the host. However, it is not surprising that invasion by *T. gondii* is detrimental to the homeostatic interactions of monocytes with the endothelium, disrupting their ability to firmly adhere. Perhaps a more relevant comparison for dissemination is between intracellular versus extracellular routes. The advantages of intracellular transportation, co-opting a "professional migrator," may outweigh the transmigration capacity of an extracellular route, despite the impairment of adhesion relative to uninfected monocytes. This hypothesis could be directly tested using a competition assay in which the adhesion and transmigration capacity of infected leukocytes is compared directly to those of extracellular tachyzoites. This would allow us to determine which route allows the greatest number of parasites to breach the barrier. Moreover, this assay could be expanded to include an examination of multiple strain types to determine whether there are strain-specific preferences for particular routes.

In our effort to examine the dynamics of *T. gondii* adhesion and migration in the vasculature we aimed to recapitulate the vascular environment in a tunable *in vitro* system. Looking beyond the benefits of examining interactions in human cells and the addition of mechanical shear force, we can continue to improve our model by including many of the other factors present in the vasculature. Currently our experiments are conducted using cells in culture media; however, whole blood is a much more complex mixture, comprised of not only multiple cell types but also numerous soluble proteins, including antibodies and members of the complement family. There are a multitude of interactions that can occur among leukocytes, platelets, erythrocytes, and the vascular endothelium (182). How infected leukocytes and tachyzoites interact with this complex mixture and how that may facilitate adhesion is unknown.

In our investigation of *T. gondii*-infected human monocyte adhesion to vascular endothelium in shear flow we found that infection significantly altered the dynamics of monocyte

rolling and firm adhesion. To investigate the molecular basis for this we examined the expression of monocyte adhesion molecules. We found no significant changes in the expression of several selectin ligands. Additionally, the total levels of integrins LFA-1, VLA-4 and MAC-1 were not significantly affected by infection, and these integrins were capable of activation upon stimulation with a divalent cation. Interestingly, we found that *T. gondii* infection did alter integrin clustering and cell morphology. Infected monocytes failed to cluster LFA-1 or VLA-4 on the cell surface in response to contact with their respective ligands. Furthermore, infected cells retained a spherical shape and exhibited little to no pseudopod extension. The altered integrin clustering patterns and changes in cell morphology observed in *T. gondii*-infected monocytes could very well alter their ability to interact with other cells in circulation. Leukocyte-leukocyte interactions may prove particularly interesting to examine, since indirect capture has been shown to contribute significantly to the leukocyte accumulation in the presence of whole blood (183). In addition to leukocyte-leukocyte interactions, adhesion to activated platelets and platelet microparticles mediate leukocyte aggregation via integrins and selectins (112, 184). Platelet microparticles in particular can even bridge leukocyte-leukocyte adhesion using P-selectin (184). Beyond these direct adhesion interactions among cells in whole blood, the presence of red blood cells in the mixture can affect flow patterns and may help to push leukocytes toward vessel walls and facilitate their adhesion and accumulation (185).

Our investigation of extracellular tachyzoite adhesion revealed that tachyzoites can adhere to vascular endothelium in shear stress conditions and that the presence of shear stress influences motility. We were interested in the role of the parasite adhesion molecule MIC2 in these processes. Using a parasite strain with a conditional knockdown of MIC2, we found that MIC2 contributed to the initial phase of tachyzoite adhesion to endothelium, but is not required for sustained tachyzoite adhesion at increased shear stress. These data suggest that tachyzoite adhesion in shear stress conditions is most likely mediated by multiple parasite adhesins, each with different roles in distinct stages of adhesion. These parasite adhesins may have roles in

direct adhesion with the endothelium or could they could mediate attachment and accumulation to other tachyzoites or cells in the whole blood that are still in circulation or have already directly adhered to the endothelium. *T. gondii* adhesion to host cells is partially mediated by glycosaminoglycans, which are a common host cell determinant expressed on virtually all host cells. Binding via glycosaminoglycans is likely a means to initiate invasion (165); however, extracellular attachment may also serve to bring parasites into contact with the endothelium or to carry parasites through the circulation. This form of "hitchhiking" has been documented for *Neisseria gonorrhea* (52). Ultimately, understanding the multitude of interactions among tachyzoites and infected leukocytes with the cellular components of blood is critical to understanding how *T. gondii* disseminates through the circulation and reaches secondary tissues.

Looking beyond the complexity of blood itself, we can also consider the heterogeneity of the endothelial cell barriers at the many tissue sites parasites encounter during their dissemination. All of our work has focused on the interactions of infected cells and tachyzoites with vascular endothelium harvested from the human umbilical cord. The decision to use primary HUVEC was initially one of convenience and practicality. HUVEC are commonly used in the field of vascular biology; however, the heterogeneity of endothelium through out the vascular tree has become more and more appreciated (172, 186). The value of our *in vitro* microscopy system is that any endothelial cell that can be harvest and cultured in the lab can be put into the system and examined.

T. gondii disseminates to various tissues through out the body, but several of particular clinical interest include the brain and the eye. These tissues have unique endothelial cell barriers that are tightly regulated to maintain homeostasis (35, 187). Tachyzoites can cross retinal endothelium facilitated by ICAM-1 in static *in vitro* culture (66), and infected rat PBMCs have been shown to shuttle parasites across an *in vitro* blood brain barrier (BBB) model (48). How tachyzoites and infected leukocytes interact with these particular subsets of endothelium in

conditions of fluidic shear stress remains unknown. Our data indicates MIC2 mediates initial tachyzoite adhesion to HUVEC in shear stress conditions and suggests a potential role for altered integrin clustering in infected-monocyte adhesion; however, how generalizable these molecular mechanisms are remains unclear. It is tempting to speculate that the unique microenvironment of particular tissue barriers may require distinct adhesion and migration mechanisms on the part of both the tachyzoite and the infected leukocyte.

Beyond the inherent heterogeneity of vascular endothelium, infection itself can alter the state of the endothelium, providing an additional layer of complexity. During *in vivo* infection, ICAM-1, VCAM-1, and ALCAM-1 expression are increased at the BBB (188), and direct infection of brain endothelial cells alters gene expression patterns of cytokines, cell adhesion molecules and junction molecules (48). *Plasmodium*-infected red blood cells (IRBCs) undergo a very close association with brain endothelial cells and the transfer of IRBC material and malarial antigens to the endothelium results in the loosening of intracellular junctions (189). How these types of changes may ultimately affect barrier integrity and subsequently how “waves” of disseminating *T. gondii* may breach those barriers as infection progresses is not clear.

Through this dissertation work we have established an *in vitro* system to examine the dynamic interactions of extracellular *T. gondii* and infected human monocytes with endothelium in conditions of shear flow. Our system allows us to model the conditions in the vasculature using human primary cells and examine pathogen adhesion under conditions of physiological shear stress. We have shown that infection modulates human monocyte adhesion in shear stress conditions and revealed a previously unappreciated effect of *T. gondii* infection on ligand-dependent integrin clustering. Using this system we also established that extracellular tachyzoites can adhere to and glide on vascular endothelium in shear flow conditions. These conditions enhanced tachyzoite motility and movement into the endothelium. Lastly, we have shown that the parasite adhesin MIC2 contributes to the initial attachment of tachyzoites to the endothelium in shear flow conditions, but does not contribute to sustained parasite adhesion.

This suggests that tachyzoite adhesion to endothelium may be mediated by a multistep cascade of interactions, during which MIC2 plays a role early, in initial attachment, while other parasite adhesins mediate the subsequent, more sustained, interactions with the endothelium. Using this system we will continue to examine the dynamic interactions of both extracellular and intracellular parasites with endothelium and further our understanding of how *T. gondii* breach endothelial barriers and reach tissues where they cause disease.

CHAPTER 6

MATERIALS AND METHODS

Cell and Parasite Culture

THP-1 cells and primary human monocytes were cultured in RPMI 1640 (Hyclone, Logan, UT) with 10% heat-inactivated FBS (Omega Scientific, Tarzana, CA), 2 mM L-glutamine, 100 U/ml penicillin, and 100 ug/ml streptomycin. Primary monocytes were isolated from human PBMC by counter-flow elutriation (190). HUVEC were cultured in EGM-2 medium with EGM-2 SingleQuot supplements and growth factors (Lonza, Allendale, NJ). GFP-expressing type I *T. gondii* (*RH*) and type II *T. gondii* (*Prugniaud*) tachyzoites were maintained in HFFs in DMEM with 10% FBS, 2 mM L-glutamine, 100 U/ml penicillin, and 100 μg/ml streptomycin (D-10%) as previously described (191).

For extracellular adhesion and motility assays parasites were syringe-lysed, washed, and processed in a high potassium Endo buffer and then immediately transferred into D-10% for experimentation to prevent microneme exhaustion prior to adhesion and motility assays (192). For intracellular parasite adhesion and motility assays monocytes were infected at a multiplicity of infection (MOI) of one to three. Uninfected monocytes were cultured in parallel for comparison. All parasite and human cell lines were tested monthly for *Mycoplasma* contamination and were confirmed to be negative.

Fluidic Device Fabrication

Fluidic channels (H 1.5 mm, W 3 mm, 20 mm) were fabricated by laser cutting a PMMA, (MacMaster-Carr, Santa Fe Springs, CA) negative relief pattern. A 40 watt CO2 laser cutting system providing a 0.2 mm laser beam spot (VersaLaser VLS-2.30) was used. The laser cut PMMA master shape was treated with trichlorosilane by vapor deposition prior to use for replica molding of PDMS (Sylgard 184; DowCorning Corp, Midland, MI). PDMS was mixed at a 10:1 (w/w) ratio of elastomer base to curing agent and degassed in a vacuum desiccator for 30 min to remove residual air bubbles. The PDMS was poured on the PMMA master to achieve approximately 0.8 mm thickness and cured thermally at 65˚C for at least two hr. Cured PDMS

was peeled off from the PMMA master and cut to size using surgical steel blades. Fluidic access ports were punched using 14 gauge blunt needles for inlet and outlet tubing inputs. The PDMS slab was permanently bonded to a clean glass microscope slide after either ultraviolet-ozone (Jelight, Irvine, CA) surface activation for 15 min or by plasma bonding.

Microfluidic channels (H 0.1 mm, W 1.5 mm, L 10 mm) were fabricated using standard soft lithographic techniques (193). Briefly, a photomask containing arrays of a 1.5 mm by 10 mm pattern was generated by high-resolution laser-printing on a transparency (CAD/Art Services Inc. Bandon, OR). A 100 μm-thick layer of negative SU-8 photoresist (MicroChem Corp. Newton, MA) was deposited onto a silicon wafer and exposed to UV through the photomask to polymerize. Unpolymerized SU-8 was removed to create relief structures of the channels on the master. PDMS was then cast from the master, oxygen-plasma cleaned (Harrick O_2, Harrick Plasma, Ithaca, NY), and permanently bonded to glass slides.

Fabricated devices were sterilized by autoclaving before use for cell experiments.

Fluidics Experiments

For intracellular parasite adhesion assays monocytes were infected for 4 hr or 18 hr and stained with Hoechst dye. Uninfected cells were cultured in parallel for 4 hr or 18 hr and stained with CFSE. HUVEC were stained with 1 μM CellTracker CMTPX, seeded in fluidic devices coated with 20 μg/ml fibronectin, and activated with 25 ng/ml of TNF-α for 4 hr. All cell labeling dyes were obtained from Life Technologies (Carlsbad, CA). Immediately following staining both uninfected and infected cells were counted, combined 1:1, and loaded into a 10 ml syringe, which was mounted on the syringe pump. The device was connected to an open-loop flow system (Fig. 3.1D), with the flow rate controlled by a Model '11' Plus dual syringe pump (Harvard Apparatus, Holliston, MA). The device was placed in a UNO environmental chamber (OkoLab, Ottaviano, NA, Italy) that was maintained at 37°C and 5% CO_2 throughout imaging.

Approximately $4x10^6$ THP-1 cells or $5x10^6$ primary monocytes were flowed into the device. Time-lapse fluorescence images were acquired over ~5 min using 150-200 ms exposures for each channel (resulting in a composite image every ~3-5 sec).

For extracellular parasite adhesion and motility assays fluidic channels were coated with 20 μg/ml fibronectin and seeded with HUVEC overnight. Microfluidic channels were either coated with a 1:1 mixture of FBS in PBS for a minimum of 1 hr or with 20 μg/ml fibronectin and seeded with HUVEC for a minimum of 7 hr prior to experimentation. Channels were connected to an open-loop flow system and maintained in an environmental chamber on the microscope stage as described above. Tachyzoites were loaded into the syringe pump and perfused through the channels, and live time-lapse imaging was started immediately after flow was initiated.

The shear stress in the device is determined by the flow rate and channel dimensions. In the fluidic channels (H 0.8 mm, W 3 mm, L 20 mm) a flow rate of 1 ml/min is expected to yield a 0.5 dyn/cm^2 shear stress at the surface of the channel. In the microfluidic channels (H 0.1 mm, W 1.5 mm, L 10 mm) a flow rate of 12 μl/min is expected to yield a 0.5 dyn/cm^2 shear stress. Fluidic assays were performed at a shear force of 0.5 dyn/cm^2 unless otherwise noted. Imaging was performed on a Nikon Eclipse Ti inverted fluorescent microscope using NIS Elements acquisition software (Nikon Instruments Inc., Melville, NY).

Static experiments

Wells of an 8-well chamber slide were either coated with a 1:1 mixture of FBS in PBS for a minimum of 1 hr or were coated with 20 μg/ml fibronectin and seeded with HUVEC 1 day prior to experimentation. The chamber slide was maintained at 37°C and 5% CO_2 in an UNO environmental chamber (102), and the wells were inoculated with tachyzoites. Time-lapse DIC imaging was initiated immediately after the addition of parasites. For the MIC2 adhesion assays

in static conditions, the parasites were allowed to adhere to HUVEC for 15 min at 37°C, and the cells were washed 3 times with PBS to remove any unadhered parasites. Monolayers were then fixed with 4% paraformaldehyde (PFA, Electron Microscopy Sciences, Hatfield, PA) for 20 min at room temperature. DIC and fluorescence images were acquired in 6 random fields of view per well using a 20X objective.

Leukocyte Tracking and Analysis

The positions and instantaneous velocities of uninfected and infected monocytes were tracked in every frame the cells were within the field of view using the automated tracking module of the Nikon NIS Elements AR 3.22.11 software. Although the parasites expressed GFP, fluorescent dyes were used to distinguish the cells during cell tracking, since the parasite vacuole moved in and out of the plane of focus as the cells rolled, and the GFP signal alone was unreliable for tracking. All $CFSE^+$ cells were categorized as uninfected cells; only those cells that were both $Hoechst^+$ and GFP^+ (containing intracellular parasites) were categorized as infected cells. Cells were typically tracked over 55-90 frames. Cells moving at greater than 0.05 μm/sec were defined as “rolling”. The transition to “searching” was defined by a change in instantaneous velocity to 0.05 μm/sec or lower. Prism (GraphPad Software, La Jolla, CA) was used to plot the average velocity, total pathlength (the total distance traveled by the cell), and maximum displacement (the distance from the point of origin to the farthest point traveled) of individual cells during rolling or searching. Because infected cells typically rolled for greater distances than uninfected cells, fewer infected cells than uninfected cells performed searching within the field of view. Cells whose maximum displacement exceeded 10 μm during their searching phase were defined as performing “wandering” searching.

Parasite tracking and analysis

The tracking module of the Nikon NIS Elements AR 3.22.11 software was used to manually track the movements of the apical end of individual tachyzoites. For assays in shear stress, every parasite that entered the field of view was tracked. For static assays, at least the same number of parasites that were tracked in flow conditions were chosen at random and tracked as they came into focus. For plotting the traces of individual parasites, the origin (0,0) was set to the parasite's apical end when it first came into contact with the endothelium. The x- and y-coordinates of the apical end in the following frames were then used to plot each parasite's path on the endothelium. The average velocity, total pathlength, and maximum displacement of individual parasites during their first 30 sec post-adhesion were plotted using Prism.

Motility and adhesion assays

To assess parasite adhesion and motility on HUVEC or FBS-coated glass, time-lapse DIC images were acquired using a 20X objective with 1.5X zoom. For the motility assays in Figures 4.1, 4.3, 4.4, 4.5, and Appendix B.1, images were acquired every sec for up to 10 min, and an adhesion event was defined as the presence of a tachyzoite on the endothelial surface for a minimum of 3 sec. Velocity was defined as the distance traveled from one frame to the next divided by the time lapse. For the sustained adhesion assays in Figure 4.2, images were acquired every 4 seconds for up to 15 min, and an adhesion event was defined as the presence of a tachyzoite on the endothelial surface for a minimum of 4 sec. Parasite location in the z-direction relative to the endothelium was determined by DIC illumination during live cell imaging. In the initial interactions of tachyzoites with the surface of the endothelium, they appeared bright. Migration into or below the HUVEC monolayer was characterized by the dimming of DIC illumination. By using this change in DIC illumination, the parasites were categorized as remaining attached, migrating in/below, or detaching from the endothelium. For the adhesion

strengthening assays in Figure 4.6 and Appendix B.2, perfusion was initiated at 0.5 dyn/cm^2. 3 min later, the shear stress in the channel was either maintained or increased to 2, 5, or 10 dyn/cm^2. Parasites that adhered during the initial 3 min and remained attached at the surface at the change in shear stress were monitored and categorized as adherent, detached, or in/below the endothelium at the conclusion of 6 min of imaging. De novo adhesion events that occurred after the switch in shear force were also quantified.

MIC2 assays

Δ*mic2e/mic2i* and tTA-dhfr parasites (81) were a generous gift from V. Carruthers (University of Michigan, Ann Arbor). For the MIC2 knock-down experiments, Δ*mic2e/mic2i* tachyzoites were cultured in the presence of 2 mg/ml of ATc (Clontech, Mountain View, CA) for 2 days and the tTA-dhfr tachyzoites were cultured in parallel. Parasites were syringe-lysed from the HFF cultures, washed in Endo buffer, and stained with either 20 μM CellTracker CMPTX (Life Technologies, Carlsbad, CA) or 10 μM CFSE (Life Technologies) in Endo buffer. In control experiments, we confirmed that these dyes do not have an effect on tachyzoite adhesion or motility. Nonetheless, we alternated the dyes on the parental and knock-down parasites in each experimental run to control for this possibility. A 1:1 mixture of parasites at 5-10 x 10^6/ml was perfused at 0.5 dyn/cm^2 into the microfluidic channel. For adhesion assays (Fig. 4.8C), the parasites were perfused for 3 min, and live images were acquired along the entire length of the channel using a 10X objective. The total number of adherent parasites in both populations was then quantified and normalized to the input ratio, as determined by flow cytometry and fluorescence microscopy. The sustained adhesion assays (Fig. 4.8D) were performed as described above except that a mixture of dyed tTA-dhfr and ATc-treated Δ*mic2e/mic2i* tachyzoites were used.

Flow Cytometry

HUVEC were left unstimulated or were stimulated with 25 ng/ml of TNF-α (eBioscience, San Diego, CA) for 4 hr, collected in Hank's Buffered Salt Solution with 5 mM EDTA (Sigma-Aldrich, St. Louis, MO), and resuspended in PBS with 1% FBS for antibody staining. Monocytes were blocked with human Fc receptor binding inhibitor (eBioscience, San Diego, CA) prior to resuspension in PBS with 1% FBS for staining.

Uninfected monocytes, *T. gondii*-infected monocytes, or HUVEC were stained for 30 minutes with biotinylated or PE-conjugated anti-human mAbs: anti-ICAM-1 (HCD54), anti-VCAM-1 (STA), anti-E-Selectin (hCD62E), anti-LFA-1/α_L (HI111), anti-LFA-1/α_L (TS2/4), anti-MAC-1/α_M (ICRF44), anti-VLA-4/α_4 (9F10), or isotype control mouse IgG1κ (MOPC-21 or P3, eBioscience, San Diego, CA). All mAbs listed above were obtained from Biolegend (San Diego, CA), unless otherwise indicated. For biotinylated primary mAbs, streptavidin-PE (BD Biosciences, San Jose, CA) was used as a secondary stain for 15 min. All samples were stained with the 7-AAD viability dye (Biolegend, San Diego, CA) and acquired on a BD FACSCalibur using CellQuest Pro software (BD Biosciences, San Jose, CA). Data were analyzed using FlowJo software (Tree Star, Ashland, OR).

For measuring integrin activation, THP-1 cells at 18 hpi were stimulated either with HBSS, 1 mM $CaCl_2$, 1mM $MgCl_2$, and 3 mM $MnCl_2$ or with PBS as a control for five min at 37 C°. Cells were put on ice, blocked with PBS with 5% normal goat serum (NGS, Life Technologies, Carlsbad, CA) and 1% BSA, and stained with the following mAbs: anti-LFA-1/α_L (TS2/4), anti-active b_2 integrin (24), anti-VLA-4/α_4 (9F10), anti-active β_1 integrin (12G10), PE-conjugated anti-MAC-1/α_M (ICRF44), PE-conjugated anti-active α_M integrin (CBRM1/5), isotype control mouse IgG1κ (P3), or PE-conjugated control IgG1κ (MOPC-21). All mAbs listed above were obtained from Biolegend (San Diego, CA) except for 24 and 12G10, which were obtained from Abcam (Cambridge, MA). PE-conjugated goat anti-mouse IgG (Life Technologies,

Carlsbad, CA) was used as a secondary stain for unconjugated primary mAbs. Samples were fixed with 4% PFA and resuspended in PBS with 1% FBS for analysis by flow cytometry.

Quantitative real-time PCR (qPCR)

Total RNA was harvested from $1x10^6$ uninfected or *T. gondii*-infected THP-1 cells using a QiaShredder homogenizer and an RNeasy kit (Qiagen, Valencia, CA). cDNA was synthesized as previously described (191) and added to iQ SYBR Green SuperMix (BioRad Laboratories, Hercules, CA). qPCR was performed on a iCycler iQ (BioRad Laboratories, Hercules, CA) using the following primers: talin-1 (sense) 5' TCTCCCAAAATGCCAAGAAC 3', talin-1 (antisense) 5' CTCCACTAGCCCTTGCTGTC 3' (194), GAPDH (sense) 5' GAAGGTGAAGGTCGGAGT 3', GAPDH (antisense) 5' GAAGATGGTGATGGGATTTC 3'. The data from the qPCR were analyzed using the ΔΔcomparative threshold method (128). The values obtained for talin-1 expression were normalized to those of GAPDH, and the data are expressed as a ratio of mRNA levels. Error bars reflect the standard error of the mean from three independent experiments. No signals were detected when water or samples generated without reverse transcriptase were used as template.

Immunoblotting

For detection of talin, $1x10^6$ uninfected or *T. gondii*-infected THP-1 cells were lysed in 2X Laemmli buffer, separated on 10% SDS-PAGE, and transferred to PVDF membrane, as previously described (191). Membranes were blocked with 5% nonfat milk, blotted with anti-human talin mAb TA205 (EMD Millipore, Billerica, MA) or anti-human β-actin mAb AC-15 (Sigma-Aldrich, St. Louis, MO), stained with HRP-conjugated anti-mouse IgG (Jackson Immuno Research, West Grove, PA), developed using ECL (GE Healthcare Life Sciences, Pittsburgh, PA), and detected using a Nikon camera as previously described (195).

For detection of MIC2 and SAG1, parasite cell lysates were separated and transferred as described above, and immuno-blotted with mouse anti-MIC2 (6D10) and rabbit anti-SAG1 (196). The membranes were then stained with HRP-conjugated anti-mouse and anti-rabbit IgG and developed as described above.

Immunofluorescence microscopy

For integrin clustering assays coverslips were coated with 400 ng/ml recombinant human ICAM-1/Fc or VCAM-1/Fc (R&D Systems, Minneapolis, MN) and blocked with SuperBlock and StartingBlock buffers (Thermo Scientific, Rockford, IL). Uninfected or *T. gondii*-infected monocytes at 18 hpi were settled onto coated coverslips for 10 min at 37°C, fixed with 4% PFA, blocked with PBS containing 5% NGS and 1% BSA, and stained with anti-LFA-1/α_L (TS2/4) or anti-VLA-4/α_4 (9F10) and Alexa Fluor 594-conjugated goat anti-mouse IgG (Life Technologies, Carlsbad, CA). Coverslips were mounted using VectaShield with DAPI (Vector Laboratories, Burlingame, CA). Fluorescence and DIC confocal micrographs were acquired on a Nikon Eclipse Ti inverted microscope using a 60x objective and the EZ.C1 3.91 software module. Z-sections were captured at intervals of 0.5 µm. Micrographs were analyzed using ImageJ software. Fluorescence intensities across the z-sections of each cell were calculated as follows: corrected total cell fluorescence (CTCF) = *(mean fluorescence intensity (MFI) x surface area) – (background MFI x surface area).* The ratio of the CTCF at the cell base to the cell center and the ratio of the surface area at the cell base to the cell center were plotted using Prism software.

For GRA7 staining of parasites in static conditions, 5 x 10^5 RHgfp tachyzoites were added to confluent HUVEC monolayers on coverslips and incubated for 20 min. Coverslips were then washed with PBS and fixed with 4% PFA. HUVEC were permeabilized and stained for vacuolar GRA7 as previously described (197). Anti-GRA7 antibody (12B6) was a generous gift

from P. Bradley (University of California, Los Angeles). For shear stress conditions (Fig. 4.7), 5-10 x 10^6/ml tachyzoites were flowed at 0.5 dyn/cm^2 into fluidic channels over HUVEC. After 1-2 min, a y-valve connector was used to perfuse D-10% through the device, without disrupting flow, for an additional 18-20 min. The channels were then perfused with PBS, followed by 4% PFA, and permeabilized and stained as described above. Fluorescence and DIC micrographs were acquired using a 40X or 60X objective.

For the analysis of MIC2 expression, HFF infected with tTA-dhfr or Δ*mic2e/mic2i* tachyzoites were cultured in the presence or absence of ATc for 2 days. Tachyzoites were harvested by syringe-lysis, added to polylysine-coated coverslips, and fixed with 4% PFA. Samples were stained with anti-MIC2 (6D10) and rabbit anti-SAG1 polyclonal serum (196), followed by Alexa Fluor 305-conjugated goat anti-mouse IgG and Alexa Fluor 594-conjugated goat anti-rabbit IgG (Life Technologies) in PBS containing 3% FBS. Coverslips were mounted as described above. Anti-MIC2 (6D10) was kindly provided by V. Carruthers (University of Michigan, Ann Arbor). To determine the input ratio of fluorescently dyed Δ*mic2e/mic2i* and tTA-dhfr parasites, a wet mount of each mixture was analyzed. Images were acquired using a 10X objective with 1.5 X zoom and counted manually.

Statistics

Prism software was used to perform all statistical analyses. The Student's two-tailed t-test with Welch's correction was used for pairwise comparisons in Figures 3.2C, 3.3A, 3.5C, 3.5D, 4.2B, 4.7B, 4.8C and D, and Appendices A.1 A and B, A.3C, and B.3. The Student's unpaired, two-tailed t-test was used for statistical analyses in Figures 3.4B and 3.4C. A $\log_{10}$ transformation of data was used to correct for a non-normal distribution for data in Figures 3.2D, 3.3B, and Appendix A.1C. A one-way analysis of variance (ANOVA) with a Tukey comparison of all means was used to compare multiple means in Figures 3.2D, 3.3B, 3.6B, 3.6C, 4.1B, and Appendix A.1

REFERENCES

1. **Montoya JG**, **Liesenfeld O**. 2004. Toxoplasmosis. Lancet. **363**:1965–1976.
2. **Howe DK**, **Sibley LD**. 1995. *Toxoplasma gondii* comprises three clonal lineages: correlation of parasite genotype with human disease. J. Infect. Dis. **172**:1561–1566.
3. **Ajzenberg D**, **Bañuls AL**, **Su C**, **Dumètre A**, **Demar M**, **Carme B**, **Dardé ML**. 2004. Genetic diversity, clonality and sexuality in *Toxoplasma gondii*. Int. J. Parasitol. **34**:1185–1196.
4. **Cornelissena AWCA**, **Overdulvea JP**, **Van Der Ploega M**. 1984. Determination of nuclear DNA of five Eucoccidian parasites, *Isospora (Toxoplasma) gondii*, *Sarcocystis cruzi*, *Eimeria tenella*, *E. acervulina* and *Plasmodium berghei*, with special reference to gamontogenesis and meiosis in *I. (T.) gondii*. Parasitology. **88**:531–553.
5. **Boothroyd JC**, **Grigg ME**. 2002. Population biology of *Toxoplasma gondii* and its relevance to human infection: do different strains cause different disease? Curr. Opin. Microbiol. **5**:438–442.
6. **Dubey JP**, **Miller NL**, **Frenkel JK**. 1970. The *Toxoplasma gondii* oocyst from cat feces. J. Exp. Med. **132**:636–662.
7. **Sibley LD**. 2010. How apicomplexan parasites move in and out of cells. Curr. Opin. Biotechnol. **21**:592–598.
8. **Dobrowolski JM**, **Sibley LD**. 1996. *Toxoplasma* invasion of mammalian cells is powered by the actin cytoskeleton of the parasite. Cell. **84**:933–939.
9. **Mordue DG**, **Håkansson S**, **Niesman I**, **David Sibley L**. 1999. *Toxoplasma gondii* resides in a vacuole that avoids fusion with host cell endocytic and exocytic vesicular trafficking pathways. Exp. Parasitol. **92**:87–99.
10. **Yarovinsky F**. 2014. Innate immunity to *Toxoplasma gondii* infection. Nat. Rev. Immunol. **14**:109–121.
11. **Lyons RE**, **McLeod R**, **Roberts CW**. 2002. *Toxoplasma gondii* tachyzoite-bradyzoite interconversion. Trends Parasitol. **18**:198–201.
12. **Tomavo S**, **Fortier B**, **Soete M**, **Ansel C**, **Camus D**, **Dubremetz JF**. 1991. Characterization of bradyzoite-specific antigens of *Toxoplasma gondii*. Infect. Immun. **59**:3750–3753.
13. **Scanga CA**, **Aliberti J**, **Jankovic D**, **Tilloy F**, **Bennouna S**, **Denkers EY**, **Medzhitov R**, **Sher A**. 2002. Cutting edge: MyD88 is required for resistance to *Toxoplasma gondii* infection and regulates parasite-induced IL-12 production by dendritic cells. J. Immunol. **168**:5997–6001.
14. **Bliss SK**, **Marshall AJ**, **Zhang Y**, **Denkers EY**. 1999. Human polymorphonuclear leukocytes produce IL-12, TNF-alpha, and the chemokines macrophage-inflammatory protein-1 alpha and -1 beta in response to *Toxoplasma gondii* antigens. J. Immunol. **162**:7369–7375.
15. **Gazzinelli RT**, **Mendonça-Neto R**, **Lilue J**, **Howard J**, **Sher A**. 2014. Innate resistance against *Toxoplasma gondii*: an evolutionary tale of mice, cats, and men. Cell Host Microbe. **15**:132–138.
16. **Hunter CA**, **Subauste CS**, **Van Cleave VH**, **Remington JS**. 1994. Production of gamma interferon by natural killer cells from *Toxoplasma gondii*-infected SCID mice: regulation by interleukin-10, interleukin-12, and tumor necrosis factor alpha. Infect. Immun. **62**:2818–2824.
17. **Vercammen M**, **Scorza T**, **Bouhdidi El A**, **Van Beeck K**, **Carlier Y**, **Dubremetz JF**, **Verschueren H**. 1999. Opsonization of *Toxoplasma gondii* tachyzoites with nonspecific immunoglobulins promotes their phagocytosis by macrophages and inhibits their proliferation in nonphagocytic cells in tissue culture. Parasite. Immunol. **21**:555–563.

18. **Schreiber DRD**, **Feldman HA**. Identification of the activator system for antibody to *Toxoplasma* as the Classical Complement Pathway. J Infect. Dis. **141**:366–369.
19. **Robert-Gangneux F**, **Dardé ML**. 2012. Epidemiology of and diagnostic strategies for toxoplasmosis. Clin. Microbiol. Rev. **25**:264–296.
20. **McCabe RE**, **Brooks RG**, **Dorfman RF**, **Remington JS**. 1987. Clinical spectrum in 107 cases of toxoplasmic lymphadenopathy. Rev. Infect. Dis. **9**:754–774.
21. **Maenz M**, **Schlüter D**, **Liesenfeld O**, **Schares G**, **Gross U**, **Pleyer U**. 2014. Ocular toxoplasmosis past, present and new aspects of an old disease. Prog. Retin. Eye Res. **39**:77–106.
22. **Abbasi M**, **Kowalewska-Grochowska K**, **Bahar MA**, **Kilani RT**, **Winkler-Lowen B**, **Guilbert LJ**. 2003. Infection of placental trophoblasts by *Toxoplasma gondii*. J. Infect. Dis. **188**:608–616.
23. **Del Pizzo J**. 2011. Focus on Diagnosis: Congenital Infections (TORCH). Pediatr. Rev. **32**:537–542.
24. **Desmonts G**, **Daffos F**, **Forestier F**, **Capella-Pavlovsky M**, **Thulliez P**, **Chartier M**. 1985. Prenatal diagnosis of congenital toxoplasmosis. Lancet. **1**:500–504.
25. **Koppe JG**, **Loewer-Sieger DH**, **de Roever-Bonnet H**. 1986. Results of 20-year follow-up of congenital toxoplasmosis. Lancet. **1**:254–256.
26. **Talabani H**, **Mergey T**, **Yera H**, **Delair E**, **Brézin AP**, **Langsley G**, **Dupouy-Camet J**. 2010. Factors of occurrence of ocular toxoplasmosis. A review. Parasite. **17**:177–182.
27. **Roberts F**, **Mets MB**, **Ferguson DJ**, **O'Grady R**, **O'Grady C**, **Thulliez P**, **Brézin AP**, **McLeod R**. 2001. Histopathological features of ocular toxoplasmosis in the fetus and infant. Arch. Ophthalmol. **119**:51–58.
28. **Dutton GN**, **McMenamin PG**, **Hay J**, **Cameron S**. 1986. The ultrastructural pathology of congenital murine toxoplasmic retinochoroiditis. Part II: The morphology of the inflammatory changes. Exp. Eye Res. **43**:545–560.
29. **Phan L**, **Kasza K**, **Jalbrzikowski J**, **Noble AG**, **Latkany P**, **Kuo A**, **Mieler W**, **Meyers S**, **Rabiah P**, **Boyer K**, **Swisher C**, **Mets M**, **Roizen N**, **Cezar S**, **Sautter M**, **Remington J**, **Meier P**, **McLeod R**. 2008. Longitudinal study of new eye lesions in children with toxoplasmosis who were not treated during the first year of life. Am. J. Ophthalmol. **146**:375–384.e4.
30. **Melzer TC**, **Cranston HJ**, **Weiss LM**, **Halonen SK**. 2010. Host cell preference of Toxoplasma gondii cysts in murine brain: a confocal study. J. Neuroparasitolog. **1**:1–6.
31. **Flegr J**. 2007. Effects of *Toxoplasma* on human behavior. Schizophrenia Bull. **33**:757–760.
32. **Schlüter D**, **Löhler J**, **Deckert M**, **Hof H**, **Schwendemann G**. 1991. Toxoplasma encephalitis of immunocompetent and nude mice: immunohistochemical characterisation of *Toxoplasma* antigen, infiltrates and major histocompatibility complex gene products. J. Neuroimmunol. **31**:185–198.
33. **Suzuki Y**. 2002. Host resistance in the brain against *Toxoplasma gondii*. J. Infect. Dis. **185**:S58–S65.
34. **Grant IH**, **Gold JW**, **Rosenblum M**, **Niedzwiecki D**, **Armstrong D**. 1990. *Toxoplasma gondii* serology in HIV-infected patients: the development of central nervous system toxoplasmosis in AIDS. AIDS. **4**:519–521.
35. **Weiss N**, **Miller F**, **Cazaubon S**, **Couraud P-O**. 2009. The blood-brain barrier in brain homeostasis and neurological diseases**.** Biochim. Biophys. Acta. **1788**(4):842–857.
36. **Jones J**, **Lopez A**, **Wilson M**. 2003. Congenital toxoplasmosis. Am. Fam. Physician **67**:2131–2146.

37. **Hitziger N**, **Dellacasa I**, **Albiger B**, **Barragan A**. 2005. Dissemination of *Toxoplasma gondii* to immunoprivileged organs and role of Toll/interleukin-1 receptor signalling for host resistance assessed by in vivo bioluminescence imaging. Cell. Microbiol. **7**:837–848.
38. **Courret N**, **Darche S**, **Sonigo P**, **Milon G**, **Buzoni-Gâtel D**, **Tardieux I**. 2006. CD11c- and CD11b-expressing mouse leukocytes transport single *Toxoplasma gondii* tachyzoites to the brain. Blood. **107**:309–316.
39. **Lambert H**, **Hitziger N**, **Dellacasa I**, **Svensson M**, **Barragan A**. 2006. Induction of dendritic cell migration upon *Toxoplasma gondii* infection potentiates parasite dissemination. Cell. Microbiol. **8**:1611–1623.
40. **Lambert H**, **Dellacasa-Lindberg I**, **Barragan A**. 2011. Migratory responses of leukocytes infected with *Toxoplasma gondii*. Microbes Infect. **13**:96–102.
41. **Randall LM**, **Hunter CA**. 2011. Parasite dissemination and the pathogenesis of toxoplasmosis. Eur. J. Microbiol. Immunol. **1**:3–9.
42. **Lambert H**, **Vutova P**, **Adams W**. 2009. The *Toxoplasma gondii*-shuttling function of dendritic cells is linked to the parasite genotype. Infect. Immun. **77**(4):1679.
43. **Weidner JM**, **Kanatani S**, **Hernández-Castañeda MA**, **Fuks JM**, **Rethi B**, **Wallin RPA**, **Barragan A**. 2013. Rapid cytoskeleton remodelling in dendritic cells following invasion by *Toxoplasma gondii* coincides with the onset of a hypermigratory phenotype. Cell. Microbiol. **15**(10):1735-1752.
44. **Da Gama LM**, **Ribeiro-Gomes FL**, **Guimarães U**, **Arnholdt ACV**. 2004. Reduction in adhesiveness to extracellular matrix components, modulation of adhesion molecules and in vivo migration of murine macrophages infected with *Toxoplasma gondii*. Microbes Infect **6**:1287–1296.
45. **Coombes JL**, **Charsar BA**, **Han S-J**, **Halkias J**, **Chan SW**, **Koshy AA**, **Striepen B**, **Robey EA**. 2013. Motile invaded neutrophils in the small intestine of *Toxoplasma gondii*-infected mice reveal a potential mechanism for parasite spread. Proc Natl Acad Sci. **110**(21):E1913-22.
46. **Chtanova T**, **Han S-J**, **Schaeffer M**, **van Dooren GG**, **Herzmark P**, **Striepen B**, **Robey EA**. 2009. Dynamics of T cell, antigen-presenting cell, and pathogen interactions during recall responses in the lymph node. Immunity. **31**:342–355.
47. **Persson CM**, **Lambert H**, **Vutova PP**, **Dellacasa-Lindberg I**, **Nederby J**, **Yagita H**, **Ljunggren HG**, **Grandien A**, **Barragan A**, **Chambers BJ**. 2009. Transmission of Toxoplasma gondii from infected dendritic cells to natural killer cells. Infect. Immun. **77**:970–976.
48. **Lachenmaier SM**, **Deli MA**, **Meissner M**, **Liesenfeld O**. 2011. Intracellular transport of Toxoplasma gondii through the blood–brain barrier. J. Neuroimmunol. **232**:119–130.
49. **Forsyth LM**, **Minns FC**, **Kirvar E**, **Adamson RE**, **Hall FR**, **McOrist S**, **Brown CG**, **Preston PM**. 1999. Tissue damage in cattle infected with Theileria annulata accompanied by metastasis of cytokine-producing, schizont-infected mononuclear phagocytes. J. Comp. Pathol. **120**:39–57.
50. **Baumgartner M**. 2010. *Theileria annulata* promotes Src kinase-dependent host cell polarization by manipulating actin dynamics in podosomes and lamellipodia. Cell. Microbiol. **13**:538–553.
51. **Baumgartner M**. 2011. Enforcing host cell polarity: an apicomplexan parasite strategy towards dissemination. Curr. Opin. Microbiol. **14**(4):436-44
52. **Söderholm N**, **Vielfort K**, **Hultenby K**, **Aro H**. 2011. Pathogenic neisseria hitchhike on the uropod of human neutrophils. PLoS ONE. **6**:e24353.

53. **Drevets DA**, **Dillon MJ**, **Schawang JS**, **van Rooijen N**, **Ehrchen J**, **Sunderkotter C**, **Leenen PJM**. 2004. The Ly-6C^{high} monocyte subpopulation transports *Listeria monocytogenes* into the brain during systemic infection of mice. J. Immunol. **172**:4418–4424.
54. **Geissmann F**, **Manz MG**, **Jung S**, **Sieweke MH**, **Merad M**, **Ley K**. 2010. Development of monocytes, macrophages, and dendritic cells. Science. **327**:656–661.
55. **Strauss-Ayali D**, **Conrad SM**, **Mosser DM**. 2007. Monocyte subpopulations and their differentiation patterns during infection. J. Leukoc. Biol. **82**:244–252.
56. **Weber C**, **Belge KU**, **Hundelshausen von P**, **Draude G**, **Steppich B**, **Mack M**, **Frankenberger M**, **Weber KS**, **Ziegler-Heitbrock HW**. 2000. Differential chemokine receptor expression and function in human monocyte subpopulations. J. Leukoc. Biol. **67**:699–704.
57. **Geissmann F**, **Jung S**, **Littman DR**. 2003. Blood monocytes consist of two principal subsets with distinct migratory properties. Immunity **19**:71–82.
58. **Auffray C**, **Fogg D**, **Garfa M**, **Elain G**, **Join-Lambert O**, **Kayal S**, **Sarnacki S**, **Cumano A**, **Lauvau G**, **Geissmann F**. 2007. Monitoring of blood vessels and tissues by a population of monocytes with patrolling behavior. Science. **317**:666–670.
59. **Channon JY**, **Seguin RM**, **Kasper LH**. 2000. Differential infectivity and division of Toxoplasma gondii in human peripheral blood leukocytes. Infect. Immun. **68**:4822–4826.
60. **Abell C**, **Holland P**. 1969. Acute toxoplasmosis complicating leukemia. Diagnosis by bone marrow aspiration. Am. J. Dis. Child. **118**:782–787.
61. **Ley K**. 2003. The role of selectins in inflammation and disease. Trends Mol. Med. **9**:263–268.
62. **Johnston B**, **Butcher EC**. 2002. Chemokines in rapid leukocyte adhesion triggering and migration. Sem. Immunol. **14**:83–92.
63. **Abram CL**, **Lowell CA**. 2009. The ins and outs of leukocyte integrin signaling. Annu. Rev. Immunol. **27**:339–362.
64. **Barragan A**. 2002. Transepithelial migration of *Toxoplasma gondii* is linked to parasite motility and virulence. J. Ex. Med. **195**:1625–1633.
65. **Furtado JM**, **Bharadwaj AS**, **Ashander LM**, **Olivas A**, **Smith JR**. 2012. Migration of *Toxoplasma gondii*-infected dendritic cells across human retinal vascular endothelium. Invest. Ophthalmol. Vis. Sci. **53**:6856–6862.
66. **Furtado JM**, **Bharadwaj AS**, **Chipps TJ**, **Pan Y**, **Ashander LM**, **Smith JR**. 2012. *Toxoplasma gondii tachyzoites* cross retinal endothelium assisted by intercellular adhesion molecule-1 in vitro. Immunol. Cell. Biol. 90(9):912-5.
67. **Lawrence MB**, **Kansas GS**, **Kunkel EJ**, **Ley K**. 1997. Threshold levels of fluid shear promote leukocyte adhesion through selectins (CD62L, P, E). J. Cell. Biol. **136**:717–727.
68. **Schaff UY**, **Yamayoshi I**, **Tse T**, **Griffin D**, **Kibathi L**, **Simon SI**. 2008. Calcium flux in neutrophils synchronizes β2 integrin adhesive and signaling events that guide inflammatory recruitment. Ann. Biomed. Eng. **36**:632–646.
69. **Sigal A**, **Bleijs DA**, **Grabovsky V**, **van Vliet SJ**, **Dwir O**, **Figdor CG**, **van Kooyk Y**, **Alon R**. 2000. The LFA-1 integrin supports rolling adhesions on ICAM-1 under physiological shear flow in a permissive cellular environment. J. Immunol. **165**:442–452.
70. **Silveira C**, **Vallochi AL**, **Rodrigues da Silva U**, **Muccioli C**, **Holland GN**, **Nussenblatt RB**, **Belfort R**, **Rizzo LV**. 2011. *Toxoplasma gondii* in the peripheral blood of patients with acute and chronic toxoplasmosis. Brit. J. Ophthalmol. **95**:396–400.
71. **Furtado JM**, **Ashander LM**, **Mohs K**, **Chipps TJ**, **Appukuttan B**, **Smith JR**. 2013. *Toxoplasma gondii* migration within and infection of human retina. PLoS ONE. **8**:e54358.

72. **Barragan A**, **Brossier F**, **Sibley LD**. 2005. Transepithelial migration of *Toxoplasma gondii* involves an interaction of intercellular adhesion molecule 1 (ICAM-1) with the parasite adhesin MIC2. Cell. Microbiol. **7**:561–568.
73. **Amino R**, **Thiberge S**, **Martin B**, **Celli S**, **Shorte S**, **Frischknecht F**, **Ménard R**. 2006. Quantitative imaging of *Plasmodium* transmission from mosquito to mammal. Nat. Med. **12**:220–224.
74. **Shi M**, **Li SS**, **Zheng C**, **Jones GJ**, **Kim KS**, **Zhou H**, **Kubes P**, **Mody CH**. 2010. Real-time imaging of trapping and urease-dependent transmigration of *Cryptococcus neoformans* in mouse brain. J. Clin. Invest. **120**:1683–1693.
75. **Moriarty TJ**, **Norman MU**, **Colarusso P**, **Bankhead T**, **Kubes P**, **Chaconas G**. 2008. Real-time high resolution 3D imaging of the lyme disease spirochete adhering to and escaping from the vasculature of a living host. PLoS Pathog. **4**:e1000090.
76. **Moriarty TJ**, **Shi M**, **Lin Y-P**, **Ebady R**, **Zhou H**, **Odisho T**, **Hardy P-O**, **Salman-Dilgimen A**, **Wu J**, **Weening EH**, **Skare JT**, **Kubes P**, **Leong J**, **Chaconas G**. 2012. Vascular binding of a pathogen under shear force through mechanistically distinct sequential interactions with host macromolecules. Mol. Microbiol. **86**:1116–1131.
77. **Ménard R**. 2001. Gliding motility and cell invasion by Apicomplexa: insights from the *Plasmodium* sporozoite. Cell. Microbiol. **3**:63–73.
78. **Håkansson S**, **Morisaki H**, **Heuser J**, **Sibley LD**. 1999. Time-lapse video microscopy of gliding motility in *Toxoplasma gondii* reveals a novel, biphasic mechanism of cell locomotion. Mol. Biol. Cell. **10**:3539–3547.
79. **Asada M**, **Goto Y**, **Yahata K**, **Yokoyama N**, **Kawai S**, **Inoue N**, **Kaneko O**, **Kawazu S-I**. 2012. Gliding motility of *Babesia bovis* merozoites visualized by time-lapse video vicroscopy. PLoS ONE. **7**:e35227.
80. **Wetzel DM**, **Schmidt J**, **Kuhlenschmidt MS**, **Dubey JP**, **Sibley LD**. 2005. Gliding motility leads to active cellular invasion by *Cryptosporidium parvum* sporozoites. Infect. Immun. **73**:5379–5387.
81. **Huynh M-H**, **Carruthers VB**. 2006. *Toxoplasma* MIC2 Is a major determinant of invasion and virulence. PLoS Pathog. **2**(8):e84.
82. **Huynh M-H**, **Rabenau KE**, **Harper JM**, **Beatty WL**, **Sibley LD**, **Carruthers VB**. 2003. Rapid invasion of host cells by *Toxoplasma* requires secretion of the MIC2-M2AP adhesive protein complex. EMBO J. **22**:2082–2090.
83. **Cerede O**. 2005. Synergistic role of micronemal proteins in *Toxoplasma gondii* virulence. J. Ex. Med. **201**:453–463.
84. **Brossier F**, **David Sibley L**. 2005. *Toxoplasma gondii*: Microneme protein MIC2. Int. J. of Biochem. Cell B. **37**:2266–2272.
85. **Sultan AA**, **Thathy V**, **Frevert U**, **Robson KJ**, **Crisanti A**, **Nussenzweig V**, **Nussenzweig RS**, **Ménard R**. 1997. TRAP is necessary for gliding motility and infectivity of *Plasmodium* sporozoites. Cell **90**:511–522.
86. **Wan KL**, **Carruthers VB**, **Sibley LD**, **Ajioka JW**. 1997. Molecular characterization of an expressed sequence tag locus of *Toxoplasma gondii* encoding the micronemal protein MIC2. Mol. Biochem. Parasitol. **84**:203–214.
87. **Burrows MT**. 1912. A method of furnishing a continuous supply of new medium to a tissue culture in vitro. Anat. Rec. **6**:141–144.
88. **Forrester JV**, **Lackie JM**. 1984. Adhesion of neutrophil leukocytes under conditions of flow. J. Cell Sci. **70**:93–110.
89. **Lawrence MB**, **McIntire LV**, **Eskin SG**. 1987. Effect of flow on polymorphonuclear leukocyte/endothelial cell adhesion. Blood **70**:1284–1290.
90. **Lawrence MB**, **Springer TA**. 1991. Leukocytes roll on a selectin at physiologic flow rates: distinction from and prerequisite for adhesion through integrins. Cell. **65**:859–873.

91. **Luscinskas FW**, **Kansas GS**, **Ding H**, **Pizcueta P**, **Schleiffenbaum BE**, **Tedder TF**, **Gimbrone MA**. 1994. Monocyte rolling, arrest and spreading on IL-4-activated vascular endothelium under flow is mediated via sequential action of L-selectin, beta 1-integrins, and beta 2-integrins. J. Cell. Biol. **125**:1417–1427.
92. **Alon R**, **Feizi T**, **Yuen CT**, **Fuhlbrigge RC**, **Springer TA**. 1995. Glycolipid ligands for selectins support leukocyte tethering and rolling under physiologic flow conditions. J. Immunol. **154**:5356–5366.
93. **Simon SI**, **Hu Y**, **Vestweber D**, **Smith CW**. 2000. Neutrophil tethering on E-selectin activates beta 2 integrin binding to ICAM-1 through a mitogen-activated protein kinase signal transduction pathway. J. Immunol. **164**:4348–4358.
94. **Grubb SEW**, **Murdoch C**, **Sudbery PE**, **Saville SP**, **Lopez-Ribot JL**, **Thornhill MH**. 2009. Adhesion of *Candida albicans* to endothelial cells under physiological conditions of flow. Infect. Immun. **77**:3872–3878.
95. **Hegge S**, **Munter S**, **Steinbuchel M**, **Heiss K**, **Engel U**, **Matuschewski K**, **Frischknecht F**. 2010. Multistep adhesion of *Plasmodium sporozoites*. FASEB J. **24**:2222–2234.
96. **Brown DC**, **Larson RS**. 2001. Improvements to parallel plate flow chambers to reduce reagent and cellular requirements. BMC Immunol. **2**:9.
97. **Hanzlik J**, **Cretekos E**, **Lamkin-Kennard KA**. 2008. Biomimetic leukocyte adhesion: a review of microfluidic and computational approaches and applications. J. Bionic Eng. **5**:317–327.
98. **Herricks T**, **Seydel KB**, **Turner G**, **Molyneux M**, **Heyderman R**, **Taylor T**, **Rathod PK**. 2011. A microfluidic system to study cytoadhesion of *Plasmodium falciparum* infected erythrocytes to primary brain microvascularendothelial cells. Lab Chip. **11**:2994–3000.
99. **Shen Y**, **Siryaporn A**, **Lecuyer S**, **Gitai Z**, **Stone HA**. 2012. Flow directs surface-attached bacteria to twitch upstream. Biophys. J. **103**:146–151.
100. **Papaioannou TG**, **Stefanadis C**. 2005. Vascular wall shear stress: basic principles and methods. Hellenic. J. Cardiol. **46**:9–15.
101. **Wu C**, **Bauer JS**, **Juliano RL**, **McDonald JA**. 1993. The alpha 5 beta 1 integrin fibronectin receptor, but not the alpha 5 cytoplasmic domain, functions in an early and essential step in fibronectin matrix assembly. J Biol Chem. **268**:21883–21888.
102. **Ueno N**, **Harker KS**, **Clarke EV**, **McWhorter FY**, **Liu WF**, **Tenner AJ**, **Lodoen MB**. 2014. Real-time imaging of *Toxoplasma*-infected human monocytes under fluidic shear stress reveals rapid translocation of intracellular parasites across endothelial barriers. Cell. Microbiol. **16**:580–595.
103. **Harker KS**, **Jivan E**, **McWhorter FY**, **Liu WF**, **Lodoen MB**. 2014. Shear forces enhance *Toxoplasma gondii* tachyzoite motility on vascular endothelium. mBio **5**:e01111–13–e01111–13.
104. **Song JW**, **Cavnar SP**, **Walker AC**, **Luker KE**, **Gupta M**, **Tung Y-C**, **Luker GD**, **Takayama S**. 2009. Microfluidic endothelium for studying the intravascular adhesion of metastatic breast cancer cells. PLoS ONE. **4**:e5756.
105. **Lin F**, **Butcher EC**. 2006. T cell chemotaxis in a simple microfluidic device. Lab Chip. **6**:1462–1469.
106. **Barkefors I**, **Le Jan S**, **Jakobsson L**, **Hejll E**, **Carlson G**, **Johansson H**, **Jarvius J**, **Park JW**, **Li Jeon N**, **Kreuger J**. 2008. Endothelial cell migration in stable gradients of vascular endothelial gowth factor A and fibroblast growth factor 2: effects on chemotaxis and chemokinesis. J. Biol. Chem. **283**:13905–13912.
107. **Kim D**, **Haynes CL**. 2012. Neutrophil chemotaxis within a competing gradient of chemoattractants. Anal. Chem. **84**:6070–6078.
108. **Ricart BG**, **John B**, **Lee D**, **Hunter CA**, **Hammer DA**. 2010. Dendritic cells distinguish individual chemokine signals through CCR7 and CXCR4. J. Immunol. **186**:53–61.

109. **Yap B**. 2005. Mechanical deformation of neutrophils into narrow channels induces pseudopod projection and changes in biomechanical properties. J. Appl. Physiol. **98**:1930–1939.
110. **Antia M**, **Herricks T**, **Rathod PK**. 2007. Microfluidic modeling of cell-cell interactions in malaria pathogenesis. PLoS Pathog. **3**:1–10.
111. **Boyden S.** 1962. The chemotactic effect of mixtures of antibody and antigen on polymorphonuclear leucocytes. J. Exp. Med. **115**:453–466.
112. **Diacovo TG**, **Roth SJ**, **Buccola JM**, **Bainton DF**, **Springer TA**. 1996. Neutrophil rolling, arrest, and transmigration across activated, surface-adherent platelets via sequential action of P-selectin and the beta 2-integrin CD11b/CD18. Blood. **88**:146–157.
113. **Languino LR**, **Duperray A**, **Joganic KJ**, **Fornaro M**, **Thornton GB**, **Altieri DC**. 1995. Regulation of leukocyte-endothelium interaction and leukocyte transendothelial migration by intercellular adhesion molecule 1-fibrinogen recognition. Proc. Natl. Acad. Sci. **92**:1505–1509.
114. **Zocchi MR**, **Ferrero E**, **Leone BE**, **Rovere P**, **Bianchi E**, **Toninelli E**, **Pardi R**. 1996. CD31/PECAM-1-driven chemokine-independent transmigration of human T lymphocytes. Eur. J. Immunol. **26**:759–767.
115. **Schreiber TH**, **Shinder V**, **Cain DW**, **Alon R**, **Sackstein R**. 2007. Shear flow-dependent integration of apical and subendothelial chemokines in T-cell transmigration: implications for locomotion and the multistep paradigm. Blood. **109**:1381–1386.
116. **McGettrick HM**, **Buckley CD**, **Filer A**, **Ed Rainger G**, **Nash GB**. 2010. Stromal cells differentially regulate neutrophil and lymphocyte recruitment through the endothelium. Immunology. **131**:357–370.
117. **Serbina NV**, **Jia T**, **Hohl TM**, **Pamer EG**. 2008. Monocyte-mediated defense against microbial pathogens. Annu. Rev. Immunol. **26**:421–452.
118. **Krick JA**, **Remington JS**. 1978. Toxoplasmosis in the adult: an overview. N. Engl. J. Med. **298**:550–553.
119. **Lambert H**, **Barragan A**. 2010. Modelling parasite dissemination: host cell subversion and immune evasion by *Toxoplasma gondii*. Cell. Microbiol. **12**:292–300.
120. **Saeij JPJ**, **Boyle JP**, **Grigg ME**, **Arrizabalaga G**, **Boothroyd JC**. 2005. Bioluminescence imaging of *Toxoplasma gondii* infection in living mice reveals dramatic differences between strains. Infect. Immun. **73**:695–702.
121. **Dunay IR**, **DaMatta RA**, **Fux B**, **Presti R**, **Greco S**, **Colonna M**, **Sibley LD**. 2008. $Gr1^+$ inflammatory monocytes are required for mucosal resistance to the pathogen *Toxoplasma gondii*. Immunity. **29**:306–317.
122. **Goldszmid RS**, **Caspar P**, **Rivollier A**, **White S**, **Dzutsev A**, **Hieny S**, **Kelsall B**, **Trinchieri G**, **Sher A**. 2012. NK cell-derived interferon-γ orchestrates cellular dynamics and the differentiation of monocytes into dendritic cells at the site of infection. Immunity. **36**:1047–1059.
123. **Ley K**, **Laudanna C**, **Cybulsky MI**, **Nourshargh S**. 2007. Getting to the site of inflammation: the leukocyte adhesion cascade updated. Nat. Rev. Immunol. **7**:678–689.
124. **Vestweber D**, **Blanks JE**. 1999. Mechanisms that regulate the function of the selectins and their ligands. Physiol. Rev. **79**:181–213.
125. **Hidalgo A**, **Peired AJ**, **Wild MK**, **Vestweber D**, **Frenette PS**. 2007. Complete identification of E-selectin ligands on neutrophils reveals distinct functions of PSGL-1, ESL-1, and CD44. Immunity. **26**:477–489.
126. **Takagi J**, **Springer TA**. 2002. Integrin activation and structural rearrangement. Immunol. Rev. **186**:141–163.
127. **Schenkel AR**, **Mamdouh Z**, **Muller WA**. 2004. Locomotion of monocytes on endothelium is a critical step during extravasation. Nat. Immunol. **5**:393–400.

128. **Dransfield I**, **Cabañas C**, **Craig A**, **Hogg N**. 1992. Divalent cation regulation of the function of the leukocyte integrin LFA-1. J. Cell. Biol. **116**:219–226.
129. **Tadokoro S**. 2003. Talin binding to integrin tails: a final common step in integrin activation. Science. **302**:103–106.
130. **Cambi A**. 2006. Organization of the integrin LFA-1 in nanoclusters regulates its activity. Mol. Biol. Cell. **17**:4270–4281.
131. **Shaw SK**. 2004. Coordinated redistribution of leukocyte LFA-1 and endothelial cell ICAM-1 accompany neutrophil transmigration. J. Ex. Med. **200**:1571–1580.
132. **Green CE**. 2006. Dynamic shifts in LFA-1 affinity regulate neutrophil rolling, arrest, and transmigration on inflamed endothelium. Blood. **107**:2101–2111.
133. **Persat F**, **Mercier C**, **Ficheux D**, **Colomb E**, **Trouillet S**, **Bendridi N**, **Musset K**, **Loeuillet C**, **Cesbron-Delauw MF**, **Vincent C**. 2012. A synthetic peptide derived from the parasite *Toxoplasma gondii* triggers human dendritic cells' migration. J. Leukoc. Biol. 92(6):1241-50.
134. **Chtanova T**, **Schaeffer M**, **Han S-J**, **van Dooren GG**, **Nollmann M**, **Herzmark P**, **Chan SW**, **Satija H**, **Camfield K**, **Aaron H**, **Striepen B**, **Robey EA**. 2008. Dynamics of neutrophil migration in lymph nodes during infection. Immunity. **29**:487–496.
135. **Coombes JL**, **Han S-J**, **van Rooijen N**, **Raulet DH**, **Robey EA**. 2012. Infection-induced regulation of natural killer cells by macrophages and collagen at the lymph node subcapsular sinus. Cell Reports. **2**:124–135.
136. **Wilson EH**, **Harris TH**, **Mrass P**, **John B**, **Tait ED**, **Wu GF**, **Pepper M**, **Wherry EJ**, **Dzierzinski F**, **Roos D**. 2009. Behavior of parasite-specific effector $CD8^+$ T cells in the brain and visualization of a kinesis-associated system of reticular fibers. Immunity. **30**:300–311.
137. **John B**, **Ricart B**, **Tait Wojno ED**, **Harris TH**, **Randall LM**, **Christian DA**, **Gregg B**, **De Almeida DM**, **Weninger W**, **Hammer DA**, **Hunter CA**. 2011. Analysis of behavior and trafficking of dendritic cells within the brain during toxoplasmic encephalitis. PLoS Pathog. **7**:e1002246.
138. **Harris TH**, **Banigan EJ**, **Christian DA**, **Konradt C**, **Tait Wojno ED**, **Norose K**, **Wilson EH**, **John B**, **Weninger W**, **Luster AD**, **Liu AJ**, **Hunter CA**. 2012. Generalized Lévy walks and the role of chemokines in migration of effector $CD8^+$ T cells. Nature. **486**:545–548.
139. **Salas A**, **Shimaoka M**, **Kogan AN**, **Harwood C**, **Andrian Von UH**, **Springer TA**. 2004. Rolling adhesion through an extended conformation of integrin $\alpha L\beta 2$ and relation to α I and β I-like domain interaction. Immunity. **20**:393–406.
140. **Sumagin R**, **Prizant H**, **Lomakina E**, **Waugh RE**, **Sarelius IH**. 2010. LFA-1 and Mac-1 define characteristically different intralumenal crawling and emigration patterns for monocytes and neutrophils in situ. J. Immunol. **185**:7057–7066.
141. **Bakker GJ**, **Eich C**, **Torreno-Pina JA**, **Diez-Ahedo R**, **Perez-Samper G**, **van Zanten TS**, **Figdor CG**, **Cambi A**, **Garcia-Parajo MF**. 2012. Lateral mobility of individual integrin nanoclusters orchestrates the onset for leukocyte adhesion. Proc. Natl. Acad. Sci. **109**:4869–4874.
142. **Wabnitz GH**, **Lohneis P**, **Kirchgessner H**, **Jahraus B**, **Gottwald S**, **Konstandin M**, **Klemke M**, **Samstag Y**. 2010. Sustained LFA-1 cluster formation in the immune synapse requires the combined activities of L-plastin and calmodulin. Eur. J. Immunol. **40**:2437–2449.
143. **Rullo J**, **Becker H**, **Hyduk SJ**, **Wong JC**, **Digby G**, **Arora PD**, **Cano AP**, **Hartwig J**, **McCulloch CA**, **Cybulsky MI**. 2012. Actin polymerization stabilizes $\alpha 4\beta 1$ integrin anchors that mediate monocyte adhesion. J. Cell. Biol. **197**:115–129.
144. **Saeij JPJ**, **Boyle JP**, **Coller S**, **Taylor S**, **Sibley LD**, **Brooke-Powell ET**, **Ajioka JW**, **Boothroyd JC**. 2006. Polymorphic secreted kinases are key virulence factors in

Toxoplasmosis. Science. **314**:1780–1783.
145. **Saeij JPJ**, **Coller S**, **Boyle JP**, **Jerome ME**, **White MW**, **Boothroyd JC**. 2006. *Toxoplasma* co-opts host gene expression by injection of a polymorphic kinase homologue. Nature. **445**:324–327.
146. **Taylor S**, **Barragan A**, **Su C**, **Fux B**, **Fentress SJ**, **Tang K**, **Beatty WL**, **Hajj HE**, **Jerome M**, **Behnke MS**, **White M**, **Wootton JC**, **Sibley LD**. 2006. A secreted serine-threonine kinase determines virulence in the eukaryotic pathogen *Toxoplasma gondii*. Science. **314**:1776–1780.
147. **Reese ML**, **Zeiner GM**, **Saeij JPJ**, **Boothroyd JC**, **Boyle JP**. 2011. Polymorphic family of injected pseudokinases is paramount in *Toxoplasma* virulence. Proc. Natl. Acad. Sci. **108**:9625–9630.
148. **Berendt AR**, **Simmons DL**, **Tansey J**, **Newbold CI**, **Marsh K**. 1989. Intercellular adhesion molecule-1 is an endothelial cell adhesion receptor for *Plasmodium falciparum.* Nature. **341**:57–59.
149. **Dubey JP**, **Speer CA**, **Shen SK**, **Kwok OC**, **Blixt JA**. 1997. Oocyst-induced murine toxoplasmosis: life cycle, pathogenicity, and stage conversion in mice fed *Toxoplasma gondii* oocysts. J. Parasitol. **83**:870–882.
150. **Dubey JP**. 1997. Tissue cyst tropism in *Toxoplasma gondii:* a comparison of tissue cyst formation in organs of cats, and rodents fed oocysts. Parasitology. **115 (Pt 1)**:15–20.
151. **Harker KS**, **Ueno N**, **Wang T**, **Bonhomme C**, **Liu W**, **Lodoen MB**. 2013. *Toxoplasma gondii* modulates the dynamics of human monocyte adhesion to vascular endothelium under fluidic shear stress. J. Leukoc. Biol. **93**:789–800.
152. **Jewett TJ**, **Sibley LD**. 2003. Aldolase forms a bridge between cell surface adhesins and the actin cytoskeleton in apicomplexan parasites. Mol. Cell.**11**:885–894.
153. **Dobrowolski JM**, **Niesman IR**, **Sibley LD**. 1997. Actin in the parasite *Toxoplasma gondii* is encoded by a single copy gene, ACT1 and exists primarily in a globular form. Cell. Motil. Cytoskeleton. **37**:253–262.
154. **Frixione E**, **Mondragón R**, **Meza I**. 1996. Kinematic analysis of *Toxoplasma gondii* motility. Cell. Motil. Cytoskeleton. **34**:152–163.
155. **Wetzel DM**, **Håkansson S**, **Hu K**, **Roos D**, **Sibley LD**. 2003. Actin filament polymerization regulates gliding motility by apicomplexan parasites. Mol. Biol. Cell. **14**:396–406.
156. **Alon R**. 2005. $\alpha 4\beta 1$-dependent adhesion strengthening under mechanical strain is regulated by paxillin association with the $\alpha 4$-cytoplasmic domain. J. Cell. Biol. **171**:1073–1084.
157. **Taubert A**, **Krüll M**, **Zahner H**, **Hermosilla C**. 2006. *Toxoplasma gondi*i and *Neospora caninum* infections of bovine endothelial cells induce endothelial adhesion molecule gene transcription and subsequent PMN adhesion. Vet. Immunol. Immunopathol. **112**:272–283.
158. **Fischer HG**, **Stachelhaus S**, **Sahm M**, **Meyer HE**, **Reichmann G**. 1998. GRA7, an excretory 29 kDa *Toxoplasma gondii* dense granule antigen released by infected host cells. Mol. Biochem. Parasitol. **91**:251–262.
159. **Carruthers VB**, **Sherman GD**, **Sibley LD**. 2000. The *Toxoplasma* adhesive protein MIC2 is proteolytically processed at multiple sites by two parasite-derived proteases. J. Biol. Chem. **275**:14346–14353.
160. **Leung JM**, **Rould MA**, **Konradt C**, **Hunter CA**, **Ward GE**. 2014. Disruption of TgPHIL1 alters specific parameters of *Toxoplasma gondii* motility measured in a quantitative, three-dimensional live motility assay. PLoS ONE. **9**:e85763.
161. **Tardieux I**, **Ménard R**. 2008. Migration of apicomplexa across biological barriers: the *Toxoplasma* and *Plasmodium* rides. Traffic. **9**:627–635.
162. **Carruthers VB**, **Sibley LD**. 1999. Mobilization of intracellular calcium stimulates

microneme discharge in *Toxoplasma gondii*. Mol. Microbiol. **31**:421–428.
163. **Wetzel DM**. 2004. Calcium-mediated protein secretion potentiates motility in *Toxoplasma gondii*. J. Cell Sci. **117**:5739–5748.
164. **Fruth IA**, **Arrizabalaga G**. 2007. *Toxoplasma gondii*: induction of egress by the potassium ionophore nigericin. Int. J. Parasitol. **37**:1559–1567.
165. **Carruthers VB**, **Håkansson S**, **Giddings OK**, **Sibley LD**. 2000. *Toxoplasma gondii* uses sulfated proteoglycans for substrate and host cell attachment. Infect. Immun. **68**:4005–4011.
166. **Soldati D**, **Dubremetz JF**, **Lebrun M**. 2001. Microneme proteins: structural and functional requirements to promote adhesion and invasion by the apicomplexan parasite *Toxoplasma gondii*. Int. J. Parasitol. **31**:1293–1302.
167. **Friedrich N**, **Santos JM**, **Liu Y**, **Palma AS**, **Leon E**, **Saouros S**, **Kiso M**, **Blackman MJ**, **Matthews S**, **Feizi T**, **Soldati-Favre D**. 2010. Members of a novel protein family containing microneme adhesive repeat domains act as sialic acid-binding lectins during host cell invasion by apicomplexan parasites. J. Biol. Chem. **285**:2064–2076.
168. **Blumenschein TMA**, **Friedrich N**, **Childs RA**, **Saouros S**, **Carpenter EP**, **Campanero-Rhodes MA**, **Simpson P**, **Chai W**, **Koutroukides T**, **Blackman MJ**, **Feizi T**, **Soldati-Favre D**, **Matthews S**. 2007. Atomic resolution insight into host cell recognition by *Toxoplasma gondii*. EMBO J. **26**:2808–2820.
169. **Garcia-Réguet N**, **Lebrun M**, **Fourmaux MN**, **Mercereau-Puijalon O**, **Mann T**, **Beckers CJ**, **Samyn B**, **Van Beeumen J**, **Bout D**, **Dubremetz JF**. 2000. The microneme protein MIC3 of *Toxoplasma gondii* is a secretory adhesin that binds to both the surface of the host cells and the surface of the parasite. Cell. Microbiol. **2**:353–364.
170. **Jacquet A**, **Coulon L**, **De Nève J**, **Daminet V**, **Haumont M**, **Garcia L**, **Bollen A**, **Jurado M**, **Biemans R**. 2001. The surface antigen SAG3 mediates the attachment of *Toxoplasma gondii* to cell-surface proteoglycans. Mol. Biochem. Parasitol. **116**:35–44.
171. **Dzierszinski F**, **Mortuaire M**, **Cesbron-Delauw MF**, **Tomavo S**. 2000. Targeted disruption of the glycosylphosphatidylinositol-anchored surface antigen SAG3 gene in *Toxoplasma gondii* decreases host cell adhesion and drastically reduces virulence in mice. Mol. Microbiol. **37**:574–582.
172. **Aird WC**. 2007. Phenotypic heterogeneity of the endothelium: I. structure, function, and mechanisms. Circ. Res. **100**:158–173.
173. **Dupont CD**, **Christian DA**, **Hunter CA**. 2012. Immune response and immunopathology during toxoplasmosis. Semin. Immunopathol. **34**:793–813.
174. **Nagineni CN**, **Detrick B**, **Hooks JJ**. 2000. *Toxoplasma gondii* infection induces gene expression and secretion of interleukin 1 (IL-1), IL-6, granulocyte-macrophage colony-stimulating factor, and intercellular adhesion molecule 1 by human retinal pigment epithelial cells. Infect. Immun. **68**:407–410.
175. **Gamble JR**, **Harlan JM**, **Klebanoff SJ**, **Vadas MA**. 1985. Stimulation of the adherence of neutrophils to umbilical vein endothelium by human recombinant tumor necrosis factor. Proc. Natl. Acad. Sci. **82**:8667–8671.
176. **Schleimer RP**, **Rutledge BK**. 1986. Cultured human vascular endothelial cells acquire adhesiveness for neutrophils after stimulation with interleukin 1, endotoxin, and tumor-promoting phorbol diesters. J. Immunol. **136**:649–654.
177. **Dewi BE**, **Takasaki T**, **Kurane I**. 2004. In vitro assessment of human endothelial cell permeability: effects of inflammatory cytokines and dengue virus infection. J. Virol. Meth. **121**:171–180.
178. **Weidner JM**, **Barragan A**. 2013. Tightly regulated migratory subversion of immune cells promotes the dissemination of *Toxoplasma gondii*. Int. J. Parasitol. 44(2):85-90.
179. **Sibley LD**, **Boothroyd JC**. 1992. Virulent strains of *Toxoplasma gondii* comprise a single clonal lineage. Nature. **359**:82–85.

180. **Unno A**, **Suzuki K**, **Xuan X**, **Nishikawa Y**, **Kitoh K**, **Takashima Y**. 2008. Dissemination of extracellular and intracellular *Toxoplasma gondii* tachyzoites in the blood flow. Parasitol. Int. **57**:515–518.
181. **Zhao Y**, **Marple AH**, **Ferguson DJP**, **Bzik DJ**, **Yap GS**. 2014. Avirulent strains of *Toxoplasma gondii* infect macrophages by active invasion from the phagosome. Proc. Natl. Acad. Sci. **111**:6437–6442.
182. **McEver RP**. 2001. Adhesive interactions of leukocytes, platelets, and the vessel wall during hemostasis and inflammation. Thromb. Haemost. **86**:746–756.
183. **St Hill CA**. 2003. Indirect capture augments leukocyte accumulation on P-selectin in flowing whole blood. J. Leukoc. Biol. **73**:464–471.
184. **Forlow SB**, **McEver RP**, **Nollert MU**. 2000. Leukocyte-leukocyte interactions mediated by platelet microparticles under flow. Blood. **95**:1317–1323.
185. **Bagge U**, **Blixt A**, **Strid KG**. 1983. The initiation of post-capillary margination of leukocytes: studies in vitro on the influence of erythrocyte concentration and flow velocity. Int. J. Microcirc. Clin. Exp. **2**:215–227.
186. **Aird WC**. 2012. Endothelial cell heterogeneity. Cold Spring Harb. Perspect. Med. **2**:a006429–a006429.
187. **Cunha-Vaz J**, **Bernardes R**, **Lobo C**. 2010. Blood-retinal barrier. EJO. **21**:3–9.
188. **Silva NM**, **Manzan RM**, **Carneiro WP**, **Milanezi CM**, **Silva JS**, **Ferro EAV**, **Mineo JR**. 2010. *Toxoplasma gondi*: The severity of toxoplasmic encephalitis in C57BL/6 mice is associated with increased ALCAM and VCAM-1 expression in the central nervous system and higher blood brain barrier permeability. Exp. Parasitol. **126**:167–177.
189. **Jambou R**, **Combes V**, **Jambou M-J**, **Weksler BB**, **Couraud P-O**, **Grau GE**. 2010. *Plasmodium falciparum* adhesion on human brain microvascular endothelial cells involves transmigration-like cup formation and induces opening of intercellular junctions. PLoS. Pathog. **6**:e1001021.
190. **Bobak DA**, **Frank MM**, **Tenner AJ**. 1986. Characterization of C1q receptor expression on human phagocytic cells: effects of PDBu and fMLP. J. Immunol. **136**:4604–4610.
191. **Morgado P**, **Ong YC**, **Boothroyd JC**, **Lodoen MB**. 2011. *Toxoplasma gondii* induces B7-2 expression through activation of JNK signal transduction. Infect. Immun. **79**:4401–4412.
192. **Endo T**, **Tokuda H**, **Yagita K**, **Koyama T**. 1987. Effects of extracellular potassium on acid release and motility initiation in *Toxoplasma gondii*. J. Protozool. **34**:291–295.
193. **Kane RS**, **Takayama S**, **Ostuni E**, **Ingber DE**, **Whitesides GM**. 1999. Patterning proteins and cells using soft lithography. Biomaterials. **20**:2363–2376.
194. **Zhang L**, **Jia X**, **Zhang X**, **Sun J**, **Peng X**, **Qi T**, **Ma F**, **Yin L**, **Yao Y**, **Qiu C**, **Lu H**. 2010. Proteomic analysis of PBMCs: characterization of potential HIV-associated proteins. Proteome. Sci. **8**:12.
195. **Khoury MK**, **Parker I**, **Aswad DW**. 2010. Acquisition of chemiluminescent signals from immunoblots with a digital single-lens reflex camera. Anal. Biochem. **397**:129–131.
196. **Lodoen MB**, **Gerke C**, **Boothroyd JC**. 2010. A highly sensitive FRET-based approach reveals secretion of the actin-binding protein toxofilin during *Toxoplasma gondii* infection. Cell. Microbiol. **12**:55–66.
197. **Dunn JD**, **Ravindran S**, **Kim SK**, **Boothroyd JC**. 2008. The *Toxoplasma gondii* dense granule protein GRA7 is phosphorylated upon invasion and forms an unexpected association with the rhoptry proteins ROP2 and ROP4. Infect. Immun. **76**:5853–5861.

APPENDIX A

SUPPLEMENTAL MATERIAL FOR CHAPTER 3

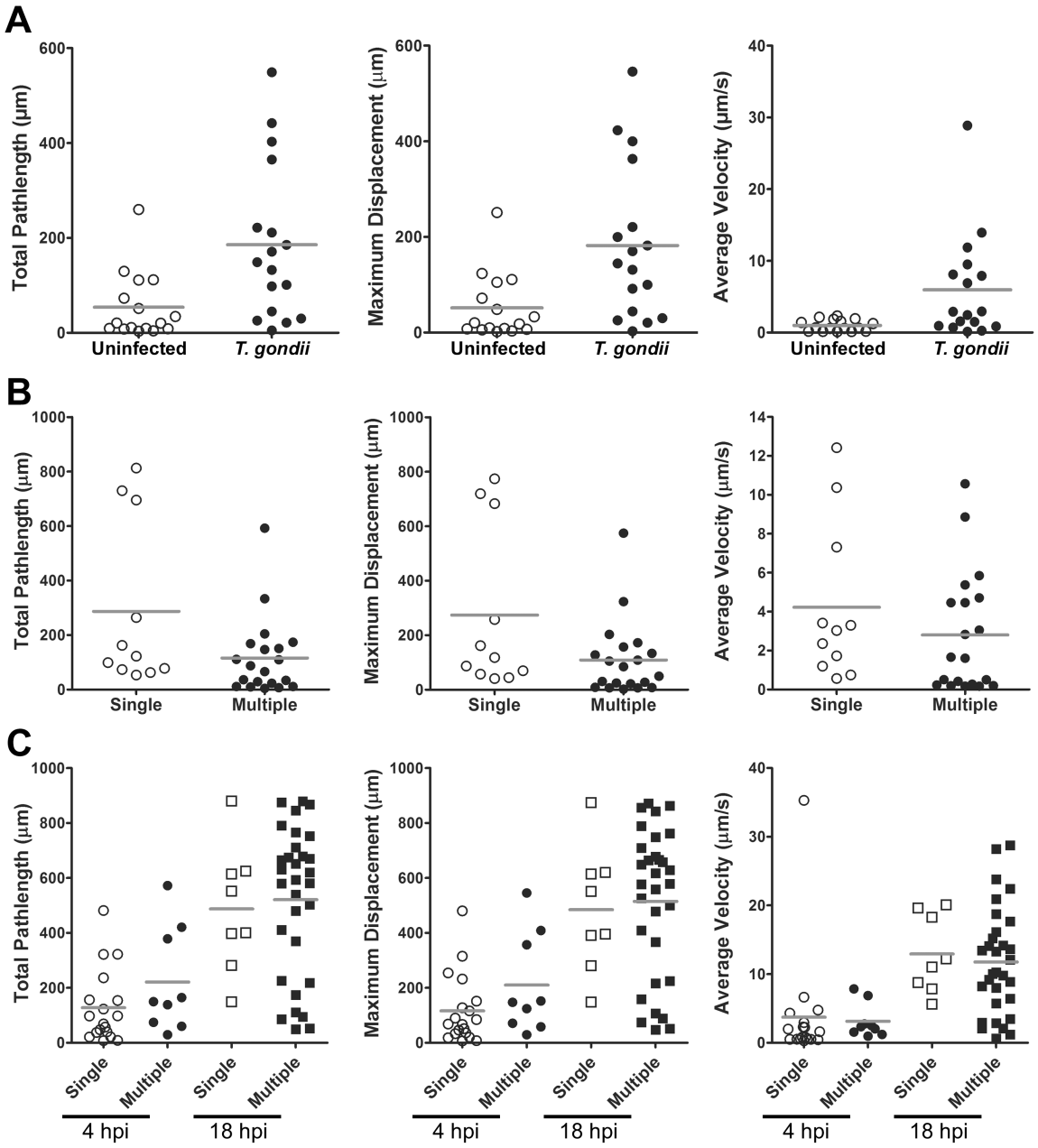

Appendix A.1: Analysis of infected and uninfected monocytes during rolling.
(A) The total pathlength, maximum displacement, and average velocity of uninfected THP-1 cells stained with Hoechst compared to THP-1 cells infected for 4 hr with CellTracker CMTPX-stained *T. gondii* and labeled with CFSE. Pooled data from two independent experiments ($n_{uninfected}$= 16, $n_{T.\ gondii}$=17). Total pathlength and maximum displacement, $p < 0.01$, average velocity, $p < 0.05$. (B-C) The total pathlength, maximum displacement, and average velocity of primary monocytes at 4 hpi (B) and THP-1 cells at 4 hpi and 18 hpi (C) are shown. "Single" refers to monocytes containing one intracellular parasite, and "multiple" refers to monocytes containing greater than one intracellular parasite. For A-C the horizontal line indicates the mean. The Student's two-tailed t-test with Welch's correction was used for statistical analyses in (A) and (B). A $\log_{10}$ transformation of data was used to correct for a non-normal distribution, and a one-way analysis of variance with a Tukey comparison of all means was used for statistical analysis in (C).

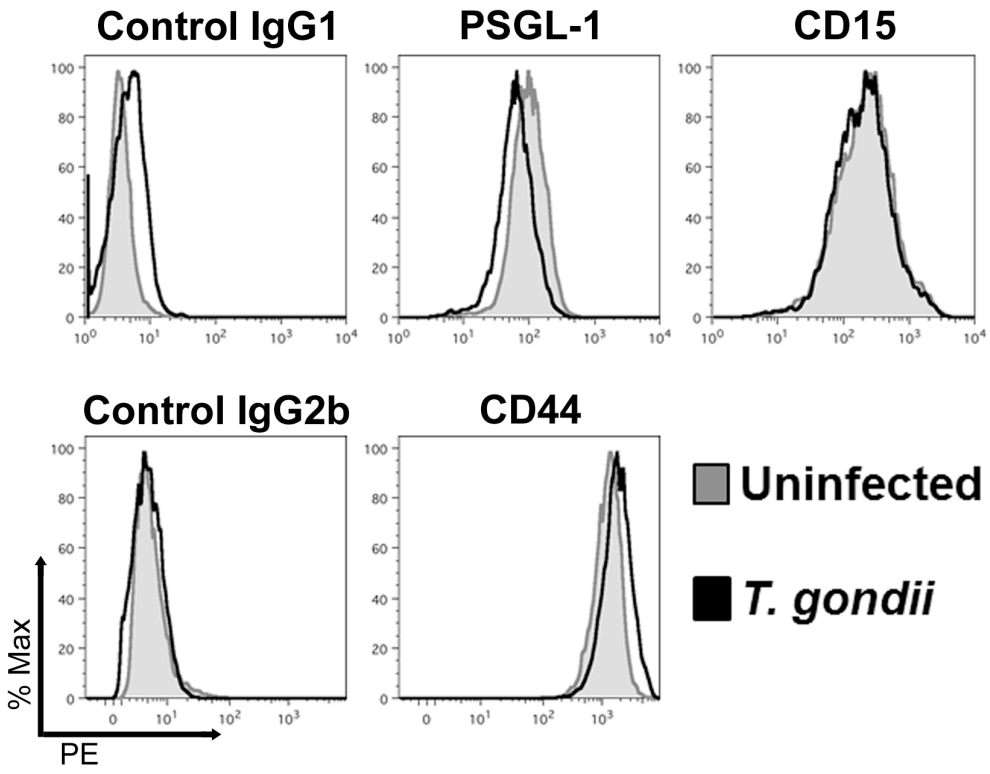

Appendix A.2. Selectin ligand expression on *T. gondii*-infected monocytes.
(A) THP-1 cells were uninfected (gray histograms) or infected with *T. gondii* for 18 hr (black histograms), stained with mAbs against PSGL-1, CD15, CD44 or their respective isotype controls and analyzed by flow cytometry. Shown are representative plots from one of 3 independent experiments.

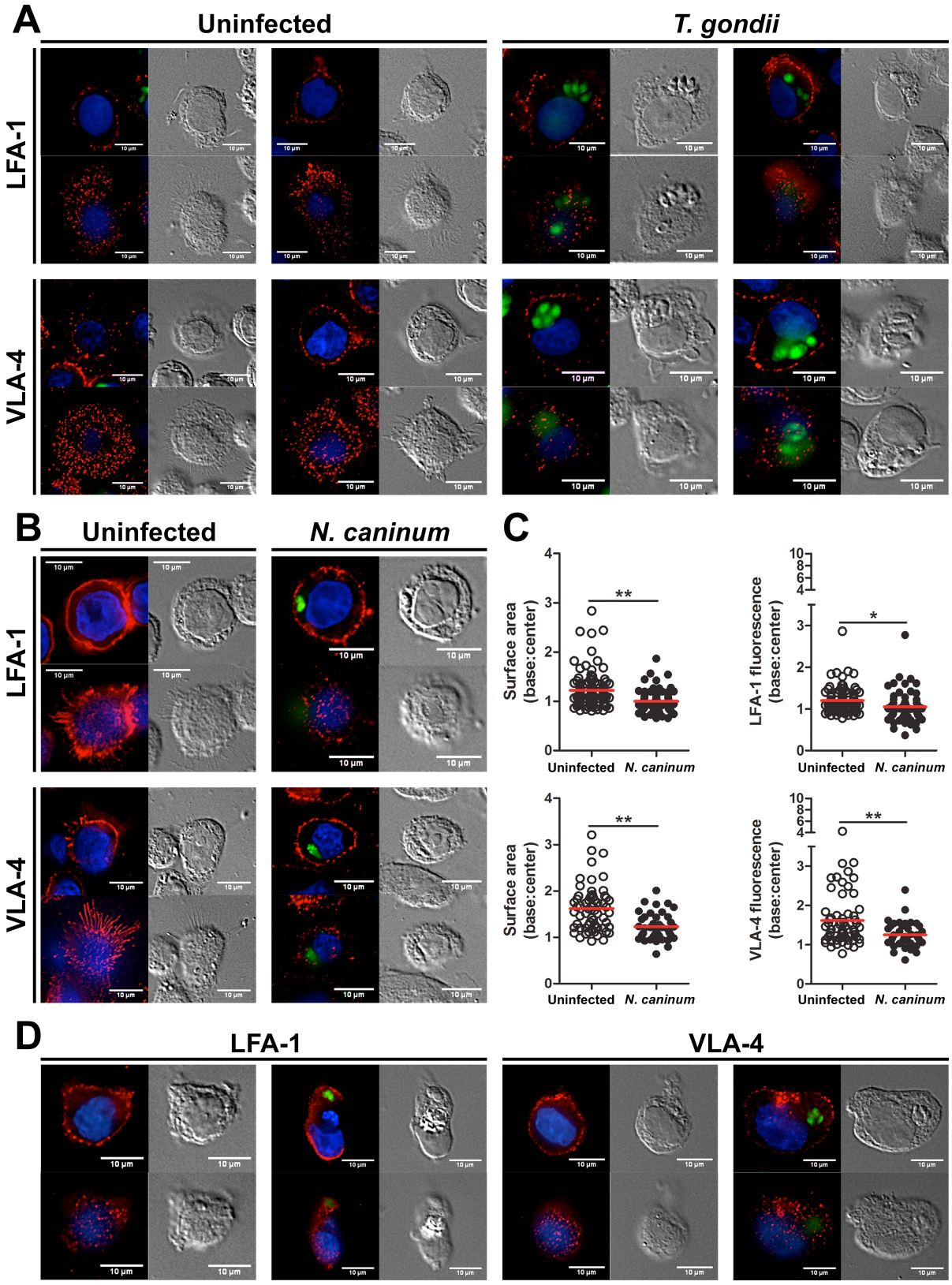
A
Uninfected
T. gondii
LFA-1
VLA-4
B
Uninfected
N. caninum
LFA-1
VLA-4
C
Surface area (base:center)
Uninfected
N. caninum
**
LFA-1 fluorescence (base:center)
*
Surface area (base:center)
**
VLA-4 fluorescence (base:center)
**
D
LFA-1
VLA-4

Appendix A.3. Micrographs of monocytes settled onto ICAM-1, VCAM-1 or human IgG. THP-1 cells were infected with GFP^+ *T. gondii* (A) or CFSE-labeled *N. caninum* (B) for 18 hr and settled onto immobilized recombinant human ICAM-1/Fc (top rows) or VCAM-1/Fc (bottom rows). Samples were fixed and stained with mAbs against LFA-1 or VLA-4 and Alexa Fluor 594-conjugated secondary antibody. Fluorescent and DIC z-sections from the cell base and cell center are shown for each cell. Parasites are shown in green, LFA-1 or VLA-4 in red, and nuclei in blue. (C) Differences in surface area and LFA-1 or VLA-4 distribution on uninfected or *N. caninum*-infected monocytes when settled onto ICAM-1/Fc or VCAM-1/Fc were quantified as ratios of their respective values at the cell base to the cell center. For cells settled onto ICAM-1, $n_{uninfected}$=100, $n_{N.\ caninumi}$=67 from two independent experiments. For cells settled onto VCAM-1, $n_{uninfected}$=62, $n_{N.\ caninumi}$=39 from two independent experiments. The red bar shows the mean. *$p < 0.01$, **$p<0.0001$. (D) THP-1 cells were infected with GFP^+ *T. gondii* and settled onto immobilized human IgG (R&D systems). Staining for LFA-1 or VLA-4 was performed as described above.

Appendix A Movie 1. Representative movie of THP-1 monocytes flowing over endothelium. THP-1 cells were uninfected or infected with GFP^+ *T. gondii* for 18 hr and stained with CFSE or Hoechst, respectively. Monocytes were flowed over TNF-a-activated endothelium that was stained with CellTracker CMTPX (red). The direction of flow is from left to right. The video shows time-lapse images at seven frames per second.

Appendix A Movie 2. 3-D projection of monocytes settled onto ICAM-1. The 3-D projection was reconstructed from z-sections of an uninfected (left) and *T. gondii*-infected THP-1 cell (right). Z-sections were compiled into a stack at intervals of 0.5 μm per section, fluorescent signals were interpolated, and the resulting projection was rotated along the x-axis at 15 frames per second. The parasite is shown in green, LFA-1 in red, and the nuclei in blue.

APPENDIX B

SUPPLEMENTAL MATERIAL FOR CHAPTER 4

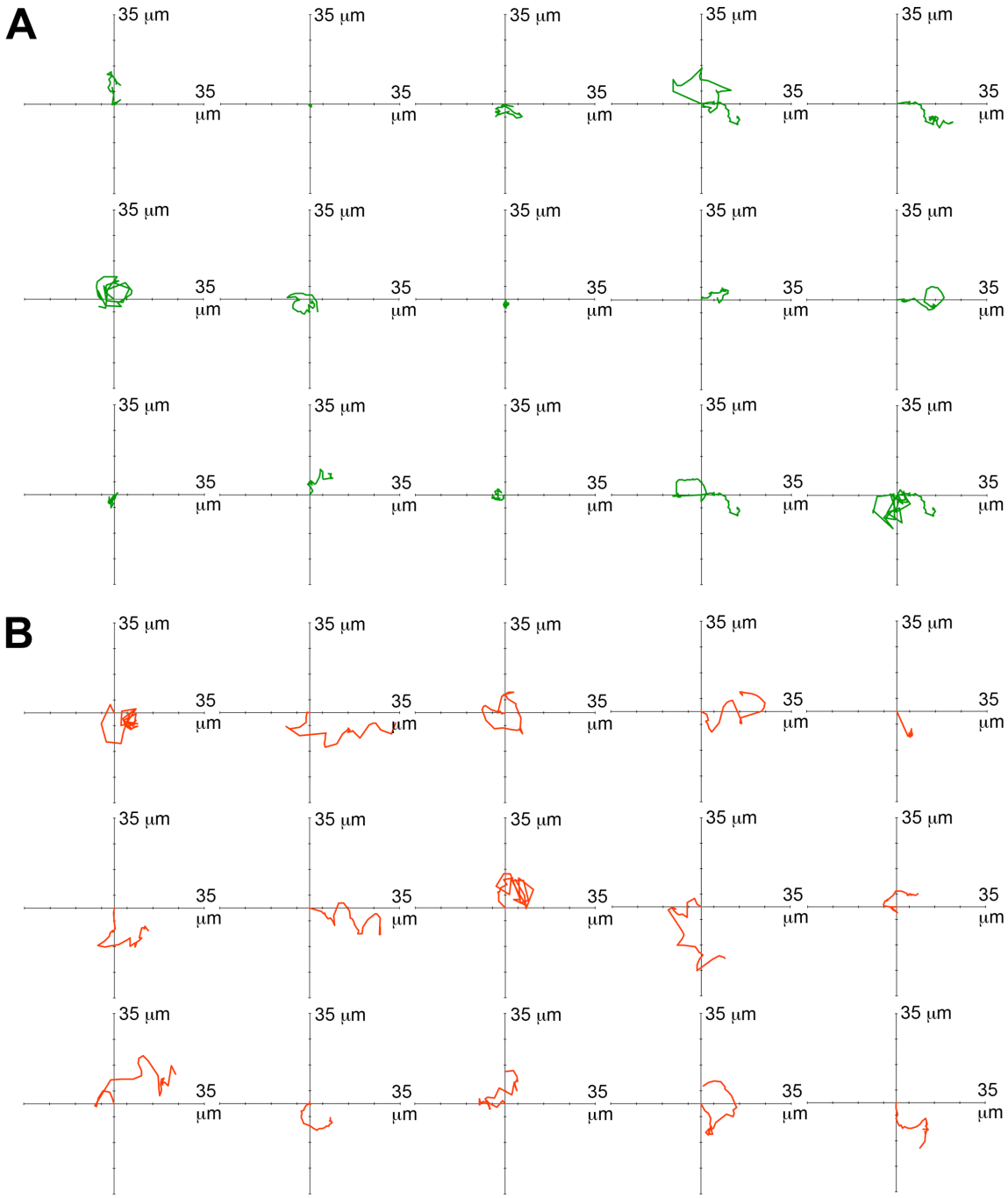

Appendix B.1: Individual traces of tachyzoite movement. Traces of extracellular tachyzoites on FBS in (A) static conditions or (B) flow conditions and on HUVEC in (C) static conditions or (D) flow conditions are shown. Each trace begins at the origin and shows the path of a single parasite per plot. These traces are grouped by condition and shown as combined data in Figure 1A.

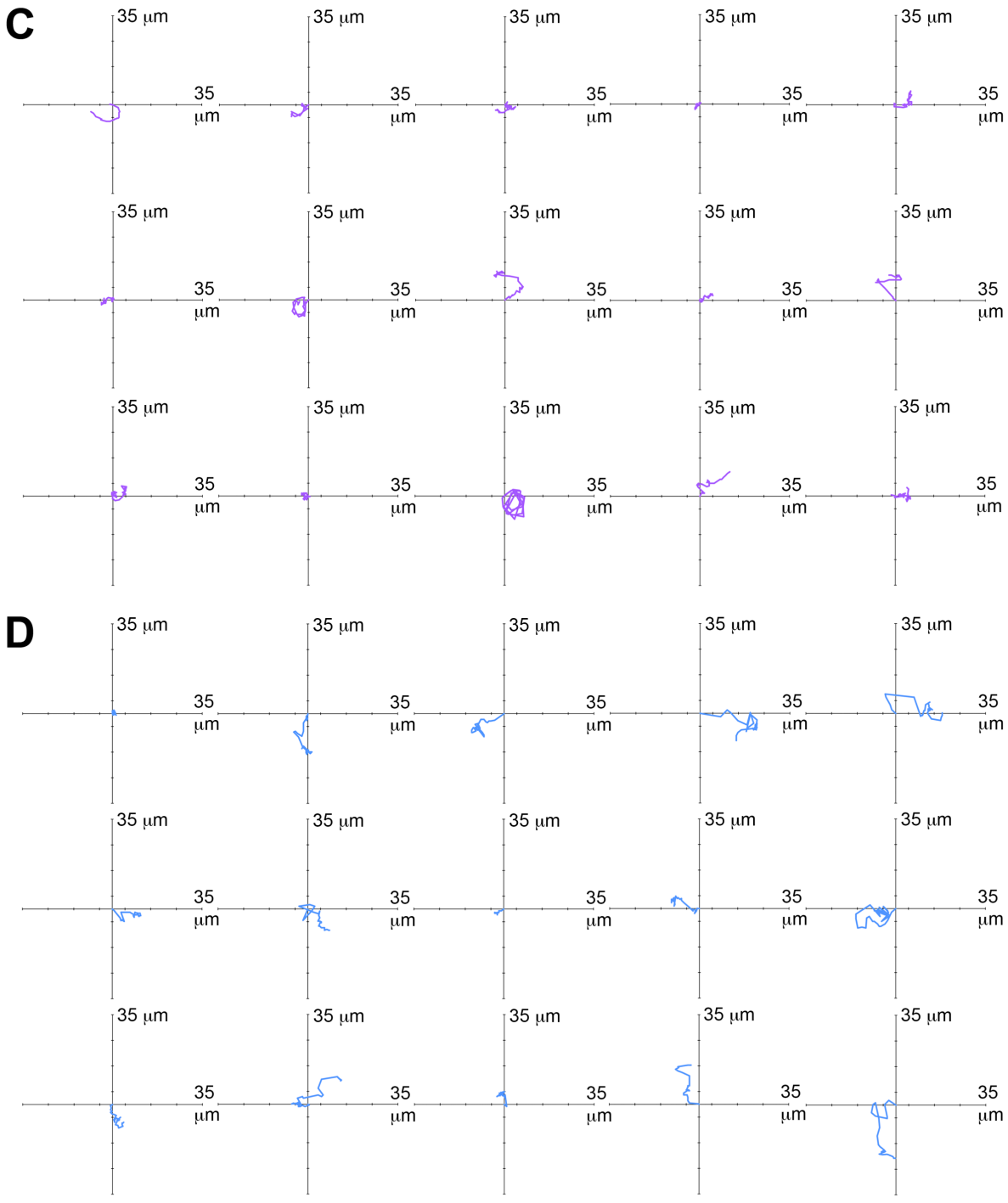

Appendix B.1: Individual traces of tachyzoite movement (cont.). Traces of extracellular tachyzoites on HUVEC in (C) static conditions or (D) flow conditions are shown. Each trace begins at the origin and shows the path of a single parasite per plot. These traces are grouped by condition and shown as combined data in Figure 1A.

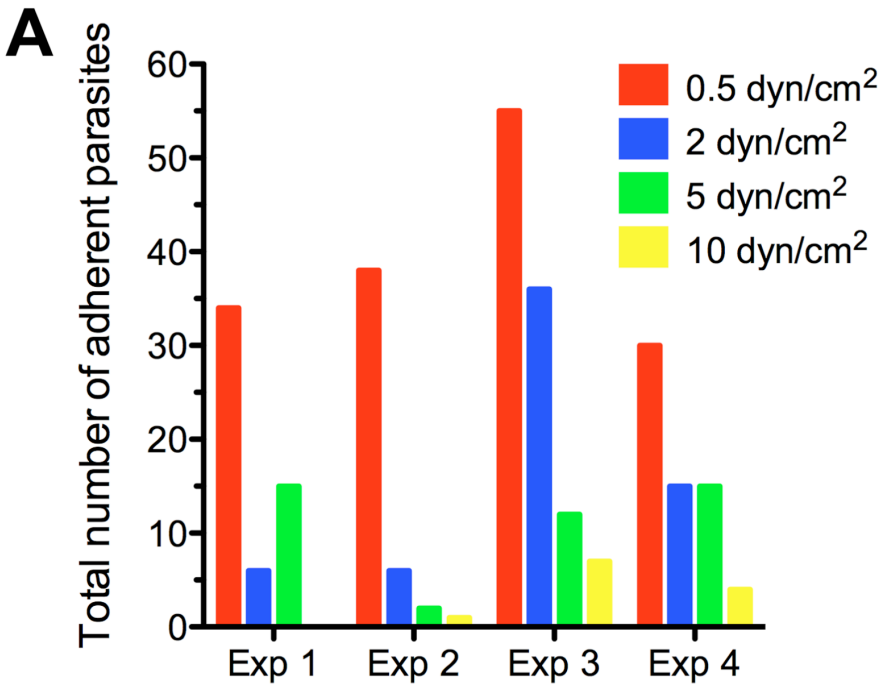

Appendix B.2. Adhesion events in increasing shear stress.
Data collected from 4 independent microfluidic experiments show the total number of adhesion events on HUVEC during flow at increasing shear stress. n=468.

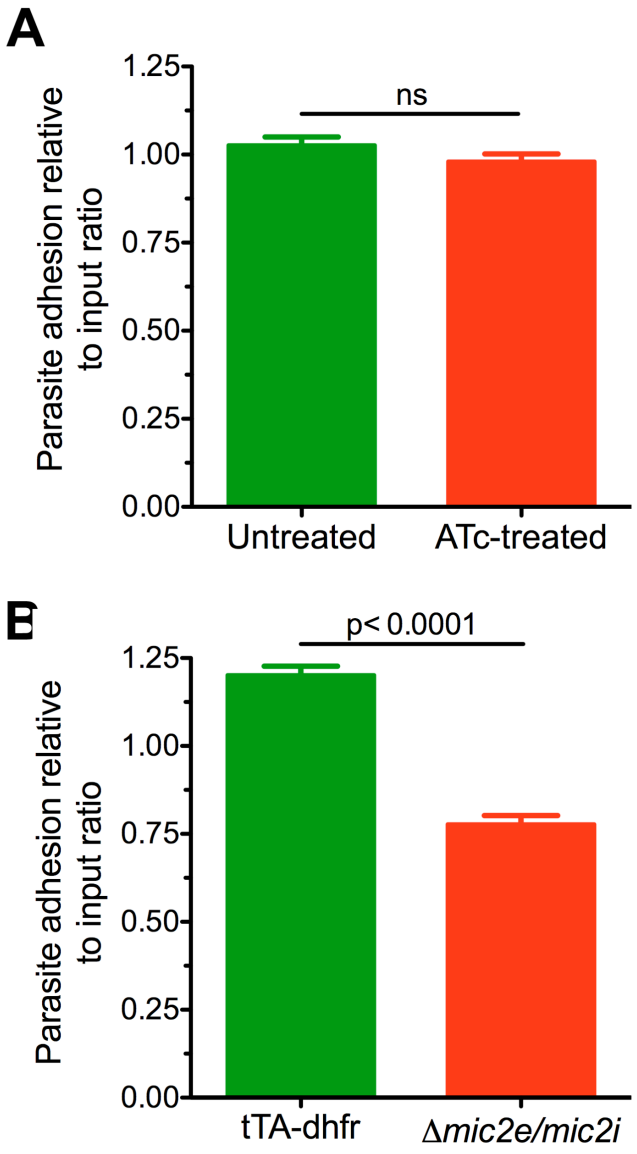

Appendix B.3. The effects of ATc treatment on adhesion and the adhesion of MIC2 conditional knockdown parasites in static conditions.
The indicated parasite populations were labeled with Celltracker dyes, mixed 1:1, and added to HUVEC in a chamber slide for 15 min. The cells were washed 3 times with PBS to remove non-adherent parasites, fixed, and imaged in DIC and fluorescence. Parasite adhesion relative to the input ratio is shown. A value of 1.0 would represent equivalent adhesion of the two populations. (A) tTA-dhfr parasites treated with ATc for 2 days were mixed 1:1 with untreated tTA-dhfr parasites. $n_{\text{Untreated tTA-dhfr}}$=1316, $n_{\text{ATc-treated tTAdhfr}}$=1278 from 2 independent experiments. (B) tTA-dhfr parasites were mixed 1:1 with ATc-treated Δ*mic2e/mic2i* parasites. $n_{\text{tTA-dhfr}}$=1598, $n_{\text{ATc-treated Δmic2e/mic2i}}$=932 from 2 independent experiments. Error bars represent the mean ± SEM and Student's two-tailed *t*-test with Welch's correction was used for pairwise comparisons. "ns" indicates not significant.

Appendix B Movie 1. Tachyzoite adhesion and gliding on HUVEC in shear stress conditions. DIC micrographs were acquired every 3 sec and played back at 10 frames/sec. The direction of flow is from left to right. The scale bar is 20 μm.

Appendix B Movie 2. Tachyzoite adhesion and gliding on FBS in shear stress conditions. DIC micrographs were acquired every sec and played back at 10 frames/sec. The direction of flow is from left to right. The scale bar is 20 μm.

Appendix B Movie 3. Tachyzoite performing helical gliding on HUVEC in shear stress conditions. DIC micrographs were acquired every sec and played back at 7 frames/sec. The red arrow indicates the apical end of the parasite. The direction of flow is from left to right. The scale bar is 10 μm.

Appendix B Movie 4. Tachyzoite performing circular gliding on HUVEC in shear stress conditions. DIC micrographs were acquired every sec and played back at 7 frames/sec. The red arrow indicates the apical end of parasite. The direction of flow is from left to right. The scale bar is 10 μm.

Appendix B Movie 5. Tachyzoite performing twirling on HUVEC in shear stress conditions. DIC micrographs were acquired every sec and played back at 7 frames/sec. The red arrow indicates the apical end of parasite. The direction of flow is from left to right. The scale bar is 10 μm.

Appendix B Movie 6. Tachyzoite performing complex motility on HUVEC in shear stress conditions. DIC micrographs were acquired every sec and played back at 7 frames/sec. The mode of motility is indicated in red in the bottom left corner throughout the duration of movement. The direction of flow is from left to right. The scale bar is 10 μm.